Preparation, Characterization and Electrochemical Applications of Modified Electrodes

By

Ruma Gupta

CHEM01201004014

Bhabha Atomic Research Centre, Mumbai

A thesis submitted to the

Board of Studies in Chemical Sciences

In partial fulfillment of requirements

For the Degree of

DOCTOR OF PHILOSOPHY

of

HOMI BHABHA NATIONAL INSTITUTE

March, 2014

HOMI BHABHA NATIONAL INSTITUTE

Recommendations of the Viva Voce Board

As members of the Viva Voce Board, we certify that we have read the dissertation prepared by **Ruma Gupta** entitled **"Prepartion, Characterization and Electrochemical Applications of Modified Electrodes"** and recommend that it may be accepted as fulfilling the dissertation requirement for the Degree of Doctor of Philosophy.

Goswami Date: 17.10.2014

Chairman: Prof. A. Goswami

S.K. Aggarwal Date: 17/10/14

Guide: Prof. S.K. Aggarwal

R.N. Goyal Date: 17.X.14

External Examiner: Prof. R.N. Goyal

Date:

Member 1: Prof. S.K. Mukerjee

Date: 17.10.14.

Member 2: Prof. S. Kannan

Final approval and acceptance of this dissertation is contingent upon the candidate's submission of the final copies of the dissertation to HBNI. I hereby certify that I have read this dissertation prepared under my direction and recommend that it may be accepted as fulfilling the dissertation requirement.

Date: 17/10/14

Place: Mumbai

<Signature> S.K. Aggarwal
Guide

STATEMENT BY AUTHOR

This dissertation has been submitted in partial fulfillment of requirements for an advanced degree at Homi Bhabha National Institute (HBNI) and is deposited in the Library to be made available to borrowers under rules of the HBNI.

Brief quotations from this dissertation are allowable without special permission, provided that accurate acknowledgement of source is made. Requests for permission for extended quotation from or reproduction of this manuscript in whole or in part may be granted by the Competent Authority of HBNI when in his or her judgment the proposed use of the material is in the interests of scholarship. In all other instances, however, permission must be obtained from the author.

Rumachandra

Ruma Gupta

DECLARATION

I, hereby declare that the investigations presented in the thesis have been carried out by me. The work is original and has not been submitted earlier as a whole or in part for a degree /diploma at this or any other Institution / University.

Ruma Gupta

Ruma Gupta

Dedicated to

My Father

List of Publications

REFFEREED JOURNALS

1. Influence of ionic speciation on electrocatalysis of fe(iii)/fe(ii) redox reaction at polyaniline (PANI) coated platinum electrode, Saurav Guin, **Ruma Chandra** and S.K. Aggarwal, Electrochimica Acta 55 (2010) 8402.
2. A mechanistic study on the electrocatalysis of the Pu(IV)/Pu(III) redox reaction at a platinum electrode modified with single-walled carbon nanotubes (SWCNTs) and polyaniline (PANI), **Ruma Gupta**, S.K Guin and S.K. Aggarwal, RSC Advances 2 (2012) 1810.
3. Electrochemical studies of U(VI)/U(IV) redox reaction in 1 M H2SO4 at single-walled carbon nanotubes (SWCNTs) modified gold (Au) electrode, **Ruma Gupta** and S.K. Aggarwal, Radiochimica Acta, 101 (2013) 399.
4. Single-walled carbon nanotubes (SWCNTs) modified gold (Au) electrode for simultaneous determination of plutonium and uranium, **Ruma Gupta**, Kavitha Jayachandran and S.K. Aggarwal, RSC Advances, 3 (2013) 13491.
5. Electrocrystallization of palladium (Pd) nanoparticles on platinum (Pt) electrode and its application for electro-oxidation of formic acid and methanol, **Ruma Gupta**, Saurav.K. Guin and Suresh K. Aggarwal, Electrochimica Acta 116 (2014) 314.
6. Electrochemical Investigations on Np(VI)/Np(V) redox couple using Single walled carbon nanotube modified glassy carbon electrode (SWCNT-GC), **Ruma Gupta**, J.V. Kamat and Suresh K. Aggarwal , Radiochimica Acta DOI: 10.1515/ract-2014-2273

SYMPOSIUM

1. Influence of Ionic Speciation on Electrocatalysis of Fe(III)/Fe(II) Redox Reaction at Polyaniline (PANI) Coated Platinum Electrode Saurav K. Guin, **Ruma Chandra**, H. S. Sharma and S. K. Aggarwal 4th ISEAC Triennial International Conference on ElectroAnalytical Chemistry and Allied Topics, edited by S. K. Aggarwal and S. K. Guin, p. 170 (2010).
2. A systematic study on the electrocatalysis mechanism of Fe(III)/Fe(II) redox reaction mediated by polyaniline coated platinum electrode **Ruma Chandra**, Saurav K. Guin and Suresh K. Aggarwal 4th ISEAC International Discussion Meet on Electrochemistry and its Applications (DM-ISEAC 2011), p 274.
3. Electrocatalytic Mechanism of Pu(IV)/Pu(III) Redox Couple at Single-walled Carbon Nanotubes (SWCNTs) and Polyaniline (PANI) Coated Platinum Electrode, **Ruma Gupta**, Saurav K. Guin and Suresh K. Aggarwal,ISEAC International Symposium cum Workshop on Electrochemistry (ISEAC-WS-2011), p 257.
4. Electrochemical studies on utilization of single walled carbon nanotube modified gold electrode for determination of uranium and plutonium **Ruma Gupta** and Suresh K. Aggarwal, 64th Annual Meeting of International Society of Electrochemistry (ISE), Sept. 8-13, 2013, Mexico.Poster Number: S-07-036.

ACKNOWLEDGEMENTS

This thesis would not have been accomplished without the support and encouragement of numerous people including my well wishers, my friends and colleagues who contributed in many ways to the successful completion of this thesis.

First and Foremost, I would like to express my sincere gratitude to my research guide ***Prof. S.K. Aggarwal*** for the continuous support, patience, motivation, and enthusiasm. His encouragement, immense knowledge and experience helped me in overcoming all the hurdles during the course of my Ph.D. Besides my advisor, I would like to thank members of my doctoral committee; ***Prof. A. Goswami, Prof. S.K. Mukerjee and Prof. S. Kannan,*** for their time, encouragement, thoughtful ideas and critical evaluation during the course of Ph.D.

I would like to express my sincere gratitude to ***Mr. Saurav Guin*** who has introduced me to this field. His calm demeanor, logical way of guidance, help in crucial experiments, monitoring the progress of work, teachings about the writing of manuscript has helped to bring out the proper shape of this work. My sincere thanks are due to ***Ms. Kavitha Jayachandran*** for her percious help and cooperation. I would also like to thank my colleagues from ***Dr. Jayshree Kamat, Ms. Jayashree Gamare, Mr. Arvind Ambolikar, Mr. Pranaw Kumar, Dr. Meera Keskar, Dr. K. Krishnan*** and all my labmates *f*or their help, encouragement and support during the course of the research work. My thanks are due to ***Dr.C.B Basak and Dr. A.K Debnath*** for experimental support. Special thanks to ***Sh. R. Shivaram*** and ***Mrs. Nilima Bhoir*** from FCD office for their help and support.

I am blessed to have friends who are constant source of laughter, joy and support. I would like to thank all my friends ***Manju, Sukanta, Sangita, Raj Kishore, Ankita, Shiny, Aishwarya, Deepak, Ashish, Niyanta, Neelam, Vinita, Priyanka and Amit*** who always stood by me and lend constant encouragement and support.

I would like to thank ***my parents*** for their unconditional love, support, faith, encouragement and confidence in me. I run short of words in expressing my gratitude towards my husband ***Santosh*** who always stood by me and encouraged me up at every step of life. I would like to express thanks to my ***son Avyaan*** who in his own way geared me up to reach the goal.

Ruma Gupta

CONTENTS

SYNOPSIS

Considering modification of an electrode, the following attributes are desirable (i) surface development, (ii) improved electrocatalysis and sensitivity, (iii) freedom from surface fouling, and (iv) exclusion of side reactions that might compete with the studied electrode process. All of the above mentioned are hard to come together when only bare electrodes are considered. To overcome these limitations, researchers started to experiment with new, often complex materials and dedicated catalysts. Using them, they started to create modified electrodes. The pioneering work in this field was presented by Lane and Hubbard in 1973 [1]. Since that time, the branch of electrochemistry studying these newly developed electrodes has seen remarkable growth, and numerous important results have been achieved. According to IUPAC, there are four main pathways for modifying electrode surfaces viz. chemisorption, covalent bonding, polymer film coating and composite [2].

With the advent of nanotechnology, various new materials such as, metal and metal oxide nanoparticles, carbon-based nanomaterials, have emerged as attractive modifiers. The uniqueness of nanomaterials for electrodes modification is based on their remarkable surface properties. Their surface to volume ratio increases with decrease in their size. Such outcome leads to a well developed surface area and significant enhancement of sensitivity, electrical conductivity, and selectivity of the modified electrode. A considerable effort has been made in the recent past in the use of tiny fuel cells as replacements for batteries in portable electronics. The advantages of using miniature fuel cells over conventional batteries are that the miniature fuel cells have a much higher stored energy density, and their ability to be immediately recharged by replacing the fuel cartridge [3]. The electrochemical oxidation of small organic molecules such as CH_3OH

and HCOOH has been the field of intensive research for the development of direct fuel cell [4-8]. In this thesis, uniform and monodispersed palladium (Pd) nanoparticles were prepared electrochemically over platinum electrode and were successfully employed for the electrooxidation of formic acid and methanol mitigating the effect of poisoning caused by adsorbed carbon monoxide (CO).

Nuclear Energy is one of the prominent sources for electricity generation all over the world. In a nuclear reactor, fuel, coolant, moderator and structural components are important materials. Among the above materials, uranium and plutonium bearing nuclear fuels are the basic elements for the production of nuclear energy and, therefore, have special importance. For the efficient as well as safe operation of the reactors, chemical quality assurance and characterization of starting materials and process intermediates is mandatory [9,10]. Moreover, in order to meet the stringent specifications, it is essential that the analytical method used should deliver results with high accuracy and reliability. Controlled potential coulometry is well technique for precise and accurate determination of uranium and plutonium [11-16]. Two different working electrodes viz. mercury (Hg) for U and platinum (Pt) for Pu are necessary for their determination because the couples U(VI)/U(IV) and Pu(IV)/Pu(III) have diverse redox potentials. However, the fouling of platinum electrode is encountered very often because of its passivation by oxide layer, [17-19]. Also the use of mercury as a working electrode needs to be eliminated as far as possible because of its associated toxicity and difficulties encountered while handling radioactive samples inside fumehood and glove-box.

There is a growing interest in the utilization of various kinds of conducting polymers to improve the physico-chemical properties of electrodes. Conducting electroactive polymers such as polypyrrole, polythiophene and polyaniline represent new class of

organic polymers that are capable of a range of interactions enabling them to interact with the species of interest. During the present work, polyaniline modified electrode was prepared and was used to study the mechanism of Electrocatalysis of Pu(IV)/Pu(III) redox couple in 1 M H_2SO_4.

Carbon nanotubes are interesting modifier offering unique mechanical and electrical properties combined with good chemical stability. Single-walled carbon nanotubes (SWCNTs) are well defined system in terms of their electronic properties. Even the impurities that may remain after synthesis, such as metallic compounds or nanoparticles, have a great impact on their electrocatalytic activity [20].

The present dissertation focuses on electrodes modified with single walled carbon nanotubes (SWCNTS) and electrochemical behaviour of actinides at the modified electrode in aqueous solution.

The main aim of this thesis is the preparation, characterization and applications of electrodes modified with metal nanoparticle, conducting polymer and carbon nanotubes. These are applied for electrocatalytic reactions such as formic acid and methanol oxidation and also for studying the redox behavior of actinides. The intention of these studies is to utilize the modified electrodes for determination of actinides in the nuclear fuel samples and to mitigate the effect of CO poisoning in direct formic acid fuel cells (DFAFC) and direct methanol fuel cells (DMFC).

Hence, the objectives of the present thesis are:

- Electrodeposition of palladium nanoparticles at platinum electrode and its applications for electrooxidation of formic acid and methanol.
- Electrocatalysis of plutonium at polyaniline modified Pt electrode

- Electrocatalytic performance of plutonium, uranium and neptunium at SWCNT modified electrode
- Simultaneous determination of U and Pu at SWCNT modified Au electrode.

The work described in this thesis is divided into five Chapters.

Chapter 1

This chapter details the need of modification of electrode. It includes the introduction to nanomaterials and their unique properties that make them ideal material for electrode modification. A brief description of fuel cells is given. The synthesis and applications of conducting polymers as electrode modifier are discussed. The importance of carbon nanotubes as electrode modifier and its applications are also included. This Chapter also gives an introduction to the various materials used in nuclear reactors and the significance of analytical characterization of these materials. The Chapter introduces the features of the Indian Nuclear Energy Program and the role of chemical quality assurance during the fabrication of high quality nuclear materials. Uranium and plutonium being the most important components of any nuclear reactor, it is mandatory to follow the chemical specifications stringently.

Chapter 2

This Chapter gives a brief introduction to electroanalytical chemistry, various electroanalytical techniques and the basic fundamental aspects of voltammetric and characterization techniques. Electrochemistry is the study of electron transfer reactions between electrodes and reactant molecules. In the present work, techniques used for the study of these reactions include cyclic voltammetry, differential pulse voltammetry, chronoamperometry and electrochemical impedance spectroscopy. The electrochemical experiments were all performed by the use of three electrode system, consisting of a

working electrode, a reference electrode and a counter electrode. This set up offers a great degree of control and repeatability as compared to a two electrode system.

Chapter 3

This Chapter comprises the synthesis of palladium nanoparticles (PdNPs) on platinum (Pt) electrode by employing a potentiostatic pulse method of electrodeposition. The mechanism of electrocrystallization of PdNPs on Pt was investigated in the system containing 1mM K_2PdCl_4 in 0.1M H_2SO_4. Experimental results showed that Pd electrodeposition follows the so-called Volmer–Weber growth mechanism. The nucleation and growth phenomena in the initial stages of Pd deposition were investigated by potentiostatic transient measurements. Experimental current transients for 0.28V and 0.15V in a non-dimensional $(i/i_{max})^2$ vs. t/t_{max} plot were compared with the theoretical curves. It was clearly seen that the experimental current transient at 0.28V corresponds to the model involving progressive nucleation. The transient at 0.15V fits relatively well with the theoretical curve for instantaneous nucleation. For further studies, PdNPs/Pt was prepared by potentiostatic deposition at 0.15 V and the time of deposition was varied. The electrodeposited PdNPs were characterized by X-ray photoelectron spectroscopy (XPS) and Field emmisision scanning electron microscopy (FESEM). The results obtained suggested the presence of chemisorbed oxygen on the surface of PdNPs. The influence of time of deposition on the size and monodispersity of the deposited PdNPs was investigated. The studies revealed that, the size of PdNPs increased with increase in the time of deposition. The effective catalytic surface area (ECSA) for the PdNPs/Pt was found to be 0.197 cm^2. This is a large real surface area for the platinum disk electrode with an initial geometric area of 0.031 cm^2 .The synthesized Pd nanoparticles modified Pt electrode displayed significantly different voltammetric behavior compared to bare Pt

electrode and also showed high catalytic activity towards the electrooxidation of formic acid and methanol.

Chapter 4

This Chapter deals with the electrocatalysis at polyaniline modified Pt electrode. At polyaniline modified electrode, two systems were studied. Initially Influence of ionic speciation on electrocatalytic performance of polyaniline coated platinum electrode for Fe(III)/Fe(II) redox reaction was studied. Porous-polyaniline coated Pt electrode (PANI/Pt) was electro-synthesized potentiodynamically in 0.1M aniline + 0.5M H_2SO_4 and was morphologically characterized by scanning electron microscopy (SEM). Nature of predominant Fe-species in HCl and H_2SO_4 was checked by UV–vis spectrophotometry. Electrocatalysis of Fe(III)/Fe(II) reaction was studied by cyclic voltammetry (CV) and electrochemical impedance spectroscopy (EIS) for three different solution compositions viz. (i) $FeCl_3/FeCl_2$ in 1M HCl, (ii) $FeCl_3/FeCl_2$ in 0.5M H_2SO_4 and (iii) $Fe_2(SO_4)_3/FeSO_4$ in 0.5M H_2SO_4. For different thicknesses of PANI, the peak current increased irrespective of the nature of the Fe-species, but the polarity of the charge on the Fe-species showed great influence on reversibility of electrocatalysis by PANI/Pt. The Donnan interaction of the polyaniline modified electrode for the three compositions was investigated with respect to $[Fe(CN)_6]^{3-}/H_2[Fe(CN)_6]^{2-}$ which are believed to be the predominant species present in $K_3[Fe(CN)_6]/K_4[Fe(CN)_6]$ solution in 0.5M H_2SO_4. The electrocatalytic performance of PANI/Pt for Fe(III)/Fe(II) redox reaction was found superior in HCl compared to that in H_2SO_4.

Further, a mechanistic study on the electrocatalysis of the Pu(IV)/Pu(III) redox reaction at a platinum electrode modified with polyaniline (PANI) was carried out. In this, electrochemistry of Pu(IV)/Pu(III) couple in 1 M H_2SO_4 was studied on bare and modified platinum electrode by cyclic voltammetry and electrochemical impedance

spectroscopy. The platinum electrode was modified with polyaniline (PANI-Pt). The modified electrode was characterized by scanning electron microscopy (SEM) and energy dispersive X-ray fluorescence (EDXRF). Electrocatalysis of Pu(IV)/Pu(III) redox reaction was observed on PANI-Pt. Pu(IV)/Pu(III) couple showed quasi-reversible electron transfer behavior on bare platinum electrode because of the PtO layer formation by Pu(IV) solution at the electrode-electrolyte interface. Electrocatalysis of Pu(IV)/Pu(III) couple on PANI-Pt was attributed to the cumulative effect of the Donnan interaction between PANI and Pu(IV) anionic complex, specific adsorption of Pu(IV) on the reactive centres, low charge transfer resistance across the electrode-electrolyte interface and a catalytic chemical reaction coupled with the electron transfer reaction.

Chapter 5

This Chapter explains the electrocatalytic performance of SWCNT modified electrode. Three redox couples were studied at SWCNT modified electrode. Firstly, mechanistic study on the electrocatalysis of Pu(IV)/Pu(III) redox reaction at platinum electrode modified with single-walled Carbon nanotubes (SWCNTs) was carried out. The stable colloidal dispersion of SWCNTs was prepared by sonicating ~1 mg of SWCNTs for one hour in a 1:4 mixture of nafion and water. The SWCNT-Pt electrode was prepared by dropping a known volume (1-20 μL) of the SWCNT suspension on the platinum electrode followed by drying. The preparation conditions were optimized by studying the cyclic voltammograms of 25 mM Pu(IV) in 1M H_2SO_4 at a scan rate of 20 mV/s recorded on each modified electrode. The redox peak currents of Pu(IV)/Pu(III) couple increased by increasing the volume of the SWCNT suspension on the platinum electrode, but maximum peak current was observed for 20 μL of SWCNT suspension. A part of the suspension fell down from the electrode surface for suspension volume higher than 20 μL. Therefore, the platinum electrode was modified with 20 μL of SWCNT suspension

for all further experiments. Electrocatalysis of Pu(IV)/Pu(III) redox reaction was observed on SWCNT-Pt. Pu(IV)/Pu(III) couple showed quasi-reversible electron transfer behavior on bare platinum electrode because of the PtO layer formation by Pu(IV) solution at the electrode-electrolyte interface. In SWCNT-Pt, the direct interaction between Pu(IV) and platinum was blocked by SWCNTs and it diminished the oxide layer formation at the interface. The lower charge transfer resistance at SWCNT-Pt also promoted the rate of electron transfer reaction of Pu(IV)/Pu(III) couple.

Electrochemical studies of U(VI)/U(IV) redox reaction in 1 M H_2SO_4 at single-walled carbon nanotubes (SWCNTs) modified gold (Au) electrode are also discussed in this chapter. Uranium (U) is one of the actinide elements used as a nuclear fuel in both the research and the power reactors. A simple analytical methodology which should be fast, accurate and precise is desirable for the purpose of quality assurance of nuclear fuels as well as for the nuclear materials accounting. Coulometry on a mercury pool electrode with the irreversible U(VI)/U(IV) couple in 1 M H_2SO_4 is the most frequently followed technique for the accurate determination of U . But the hazards associated with mercury demands the development of alternative working electrodes which can replace the use of mercury and give better performance than the mercury pool electrode. In this context, electrochemistry of U(VI)/U(IV) couple in 1 M H_2SO_4 was studied on bare and modified gold (Au) electrodes by cyclic voltammetry (CV), differential pulse voltammetry (DPV) and electrochemical impedance spectroscopy (EIS). The gold electrode modified with single-walled carbon nanotubes (SWCNTs-Au) was characterized by scanning electron microscopy (SEM). A detailed investigation was done to determine the kinetic parameters at the modified electrode. It was found that the electrocatalysis of U(VI)/U(IV) couple on SWCNT-Au is driven by an increase in the rate constant of the electron transfer reaction compared to that with the bare gold electrode. Electrochemical impedance spectroscopy

data confirmed the electrocatalytic activity of SWCNT-Au electrode. After a detailed study on electrocatalytic mechanism of U(VI)/U(IV) couple and Pu(IV)/Pu(III) redox couple, studies were carried out to simultaneously determine Pu and U at SWCNT-Au electrode in the fuel samples. In the differential pulse voltammetry technique (DPV), both Pu and U gave sensitive reduction peaks at 564 mV and -128 mV, respectively, versus saturated Ag/AgCl electrode. Under the optimized experimental conditions, Pu and U gave linear responses over ranges of 10 to 100 μM (R^2 = 0.990) and 3 to 10 μM (R^2 = 0.987), respectively. The detection limits were found to be 8.2 μM for Pu and 2.4 μM for U.

This Chapter also explains the electrochemical investigations on Np(VI)/Np(V) redox couple using single walled carbon nanotube modified glassy carbon electrode (SWCNT-GC). Neptunium (Np) is one of the actinides produced in nuclear reactors. It is located between U and Pu in the Periodic Table, suggesting that its chemical properties are qualitatively similar to those of U and Pu. Because of this chemical similarity as well as its considerable content in the spent nuclear fuels, the behavior of Np assumes importance in the fuel reprocessing process. Besides, the long half-life of ^{237}Np, 2.14×10^6 years and high solubility of Np under environmentally relevant conditions makes it problematic on the long-term repository of radioactive wastes. Electrochemistry of Np(VI)/Np(V) couple in 1 M H_2SO_4 was studied on bare and modified glassy carbon (GC) electrodes by cyclic voltammetry (CV), differential pulse voltammetry (DPV) and electrochemical impedance spectroscopy (EIS). The modified electrode (SWCNTs-GC) was characterized by scanning electron microscopy (SEM). The peak-to-peak potential separation (ΔE_p) was found to be 133 mV, which is much smaller than the ΔE_p value of 338 mV observed on bare glassy carbon electrode. It indicates that the Np(VI)/Np(V) couple still exhibits a quasi-reversible electron transfer behavior on SWCNT-GC. The increase of the redox

peak current along with the significant enhancement in the electrochemical reversibility suggest the electrocatalytic action of SWCNT-GC for the Np(VI)/Np(V) redox reaction. The charge transfer coefficient (α) and the heterogeneous rate constant (k_s) of Np(VI) reduction on SWCNT-GC in 1 M H_2SO_4 were calculated as 0.83 and 5.25×10^{-1}cm s^{-1}, respectively. This shows that the modification of glassy carbon surface with SWCNT catalyzed the Np(VI)/Np(V) redox reaction. Indeed, the SWCNT/GC electrode presents an interlinked highly mesoporous three-dimensional structure with a relatively higher electrochemically accessible surface area and easier charge transfer at the electrode/electrolyte interface. Therefore, the quasi-reversible redox reaction of Np(VI)/Np(V) couple on GC transformed to a more reversible redox reaction on SWCNT-GC. The impedance data on charge transfer resistance (R_{ct}) i.e. $R_{ct}^{SWCNT-GC} < R_{ct}^{GC}$ supported the trends of the heterogeneous rate constants calculated from the cyclic voltammetry experiments i.e. $k_s^{SWCNT-GC} > k_s^{GC}$. This confirms the electrocatalytic behavior of SWCNT-GC for the Np(VI)/Np(V) redox reaction.

In summary, the important highlights of the work are as follows:

1) The palladinized platinum electrode (PdNPs/Pt) was prepared by potentiostatic electrodeposition of Pd nanoparticles on Pt electrode. Mechanism of electrocrystallization of Pd nanoparticles was investigated. Highly monodispersed and homogeneous Pd nanoparticles were deposited under optimized conditions on the platinum electrode from the simple palladium salt solution. The new findings are of fundamental importance to understand electrochemical formation mechanism of palladium nanoparticles allowing a relatively narrow size distribution. The PdNPs-Pt demonstrated the enhanced electrocatalytic oxidation

of formic acid and methanol for promising performance as catalyst in direct methanol fuel cells and direct formic acid fuel cells.

2) Influence of ionic speciation in different electrolytic compositions on the performance

   of the electrocatalysis of PANI/Pt for Fe(III)/Fe(II) redox reaction was studied. It was concluded that the predominant ionic species of the redox couple is guided by the type of solvent or electrolyte composition. Thus, the behavior of PANI film for the same redox reaction e.g. Fe(III)/Fe(II) can be improved by the judicial choice of electrolyte composition for analysis.

3) PANI-Pt was prepared by optimized procedure and the modified electrode showed good electrocatalytic properties for the Pu(IV)/Pu(III) redox reaction in 1M H_2SO_4. PANI-Pt showed electrocatalytical performance because of the cumulative effect of the Donnan interaction between PANI and Pu(IV)-quadra sulphate complex (QSC), specific adsorption of the analyte on the electron transfer centre, higher electron transfer rate constant and catalytic chemical reaction coupled with the electron transfer reaction. This work provides a new opportunity to improve the quality of Pu analysis and shorten the analytical time for the electroanalysis of actinides and other elements.

4) SWCNT-Au prepared by the optimized procedure showed good electrocatalytic properties for the U(VI)/U(IV) redox reaction in 1M H_2SO_4. The electrocatalysis of U(VI)/U(IV) couple on SWCNT-Au was found to be driven by the increase in the rate constant of the electron transfer reaction compared to that with the bare gold electrode. Electrochemical impedance spectroscopy data confirmed the electrocatalytic activity of SWCNT-Au electrode. These studies were continued and an electrochemical method was developed and successfully applied for the

simultaneous determination of Pu and U using a SWCNT–Au electrode. The detection limits were found to be 8.2 mM for Pu and 2.4 mM for U. The proposed method could be applied to the determination of Pu and U in fuel samples.

5) SWCNT-GC prepared by the optimized procedure showed good electrocatalytic properties for the Np(VI)/Np(V) redox redox reaction in 1 M H_2SO_4. The electrocatalysis of Np(VI)/Np(V) redox couple on SWCNT-GC is driven by the increase in the rate constant of the electron transfer reaction compared to that with the bare glassy carbon electrode. Electrochemical impedance spectroscopy data confirmed the electrocatalytic activity of SWCNT-GC electrode. These studies will help in developing methodologies for the determination of Np using solid electrodes and will allow to shorten the time for the electroanalysis.

References

1. R.F. Lane, A.T. Hubbard, *J. Phys. Chem*., **77** (1973) 1411.
2. R.A. Durst, A.J. Baumner, R.W. Murray, R.P. Buck, C.P. Andrieux, *Pure Appl. Chem*., **69** (1997) 1317.
3. B.J. Feder, New York Times, New York, 2003.
4. C. Lamy, A. Lima, V. Lerhun, F. Delime, C. Coutanceau, J.M. Leger, *J. Power Sources*, **105,** (2002), 283.
5. J. Nordlund, G. Lindberbh, *J. Electrochem. Soc.* **149**, (2002) 1107.
6. T. Iwasita, *Electrochim. Acta,* **48,** (2002), 289.
7. R. Parson, Y. Vatsumura, *J. Electroanal. Chem*., **257,** (1988), 9.
8. H. Nonaka, Y. Matsumura, *J. Electroanal. Chem*., **520,** (2002), 101.
9. M.V. Ramaniah, Analytical chemistry of fast reactor fuels- A review, Pure and Appl. Chem., **54** (1982) 889.

10. C. Ganguly, R.N. Jayaraj, Characterization and quality control of nuclear fuels, Allied publishers: New Delhi (2002).

11. IAEA Document, Nuclear Fuel Technology, ISO/TC85/ SC5N12183, February 2004.

12. G. L. Booman, W. B. Holbrook and J. E. Rein, Anal. Chem., **29**, (1957), 219.

13. G. C. Goode and J. Herrington, Anal. Chim. Acta, **38**, (1967), 369.

14. J. J. Lingane, Anal. Chim. Acta, **50**, (1970), 1.

15. G. L. Booman and W. B. Holbrook, Anal. Chem., **31**, (1959), 10.

16. N. Gopinath, N. N. Mirashi, K. Chander and S. K. Aggarwal,J. Appl. Electrochem., **34**, (2004), 617.

17. F. Kodera, Y. Kuwahara, A. Nakazawa and M. Umeda, J.Power Sources, **172**, (2007), 698.

18. D. C. Johnson and S. Bruckenstein, Anal. Chem., **43**, (1971), 1313.

19. 9 M. W. Breiter, J. Electroanal. Chem., **8**, (1964), 230.

20. C.E. Banks, A. Crossley, C. Salter, S.J. Wilkins, R.G. Compton, Angew. Chem. Int. Ed., **45** (2006) 2533.

LIST OF FIGURES

Page No.

CHAPTER-1

CHAPTER-2

CHAPTER-3

CHAPTER-4

CHAPTER-V

LIST OF TABLES

Page No.

CHAPTER 1

Introduction

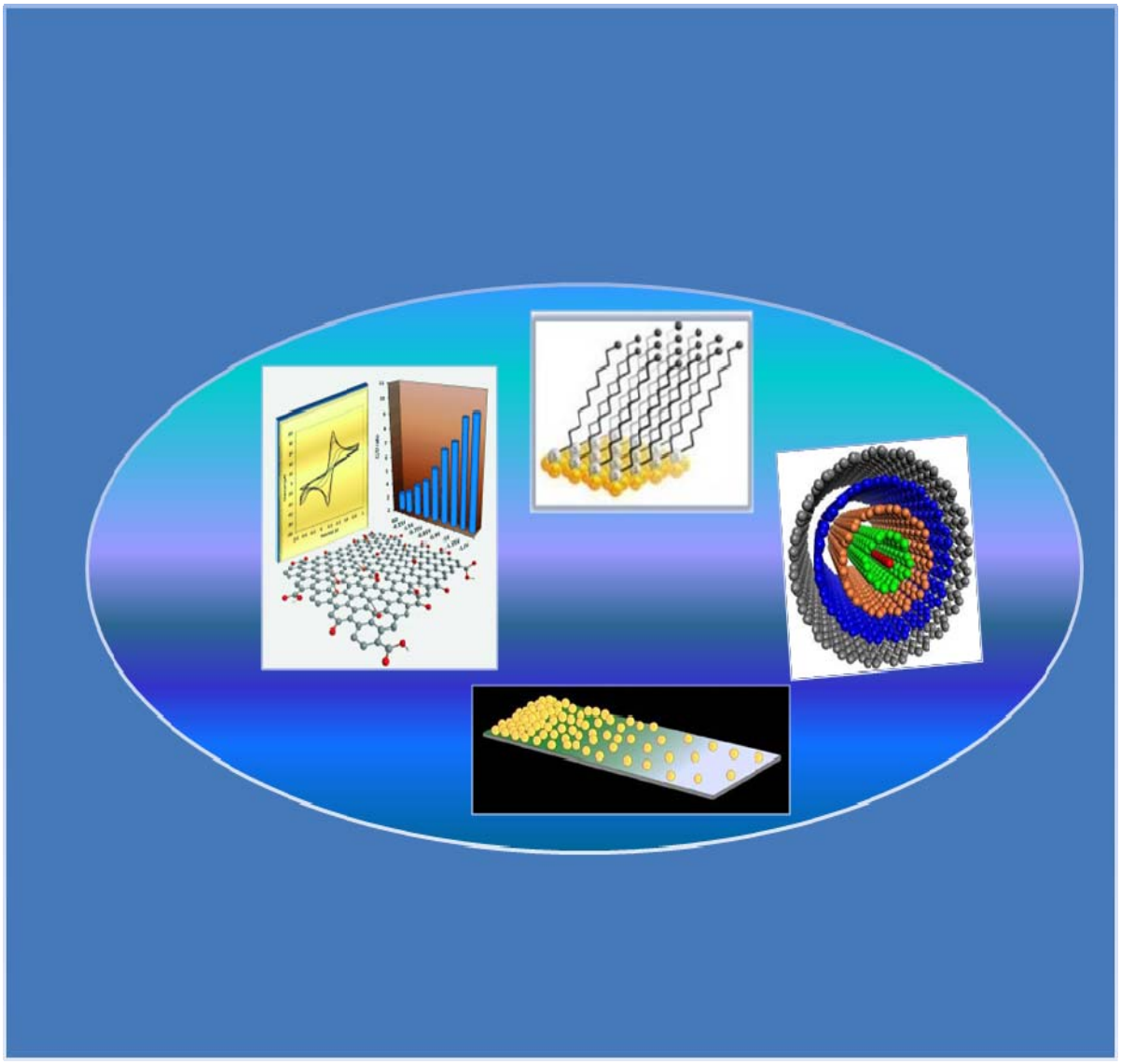

1.1 Modified electrodes

When considering an electrode designed for energy conversion or detection of analyte, one is interested in the following desired attributes: (i) surface development (ii) improved electrocatalysis and sensitivity (iii) freedom from surface fouling and (iv) exclusion of side reactions that might compete with the studied electrode process. All of above mentioned are difficult to achieve when only bare electrodes are taken into account. To overcome these limitations, researchers started to experiment with new, often complex materials and dedicated catalysts. Using them, they started to create so called modified electrodes. The pioneering work in that field was presented by Lane and Hubbard in 1973 [1]. Since that time the branch of electrochemistry studying these newly developed electrodes has seen remarkable growth, and numerous important results have been achieved. Modified electrodes are designed and implemented in the field of electroanalytical detection to improve the sensitivity and selectivity of the system. In this respect, the electrode material is tailored specifically in such a way as to promote desired electrochemical reaction [2,3]. The immobilization of different species on various electrode materials can be achieved by following techniques:

(i) Adsorption of electrode modifier on the bare electrode surface

(ii) Covalent bonding of the modifier on the electrode surface

(iii) Physical coating of preformed modifier on the electrode surface

(iv) Direct deposition of the modifier on the bare electrode surface

With the advent of nanotechnology, various new materials such as carbon-based nanomaterials, metals and metal oxide nanoparticles have emerged. The uniqueness of nanomaterials when applied for electrodes modification is based on their remarkable surface properties. Their surface to volume ratio increases with decrease in size. Such outcome leads to a well developed surface area and significant amelioration of sensitivity, electrical conductivity, and selectivity of the electrode modified with such materials.

There is a growing interest in the utilization of various kinds of conducting polymers to modify the physico-chemical properties of electrodes. Conducting electroactive polymers such as polyaniline, polypyrrole and polythiophene represent a new class of organic polymers that are capable of a range of interactions enabling them to interact with the species of interest.

The present dissertation focuses on electrodes modified with metal nanoparticles, conducting polymers and carbon nanotubes (CNTs). It presents diverse approaches for the modification of electrode surface, depositing metal nanoparticles and conducting polymer electrochemically studying their electrochemical behaviour in the absence and presence of analyte of interest. It also explains that modifying working electrodes are in enhancing the reversibility and kinetics of the electrode processes compared to unmodified working electrode.

1.2 Introduction to Metallic nanostructures

A nanoparticle is defined as a particle with atleast one dimension in the nanoscale size range. For transition metal nanoparticles, the decrease in size to the length scale increases the surface-to-volume ratio. This, together with the ability to make them in different sizes and shapes, makes them potentially useful for catalysis. Nanoparticles have been shown to possess structural, electronic, dielectric, magnetic, optical and chemical properties that are different from the corresponding bulk materials. These properties exhibit strong size variations. The systematic adjustment of the parameters used in synthesis can be employed to control the size and shape of the nanoparticles [4,5].

There are two principal approaches for the preparation of nanomaterials called the "top-down" approach and the "bottom-up" approach. The top-down approach involves reducing the dimension(s) of the large macroscopic materials to small-sized particles by the systematic breakdown of bulk material. The top down method involves some form of grinding (ball-milling), lithographic or laser ablation condensation techniques. The advantage of grinding mechanism is its simplicity and there is no requirement of various organic and inorganic compounds (sometimes volatile and toxic) during the preparation process. However, the quality of the nanoparticles produced by grinding is known to be poor in comparison with the materials produced by the bottom up methods. The main drawbacks include contamination problems from grinding equipment, low particle surface areas, irregular shape and size distributions and high energy requirements needed to produce relatively small particles. However, nanomaterials produced by top-down approach still find use for catalytic, magnetic and structural purposes. In bottom-up approach, the nanoparticles are prepared by assembling the individual atoms or

molecules in the presence of stabilizer or protecting agent e.g. reduction of metal ions to form metal nanoparticles. Stabilizer or protecting agents prevent the agglomeration by either steric repulsion or electrostatic repulsion among nanoparticles. A number of chemical, electrochemical and physical methods have been reported for the synthesis of nanomaterials via bottom-up approach. In the past few years, research articles on the microbial/biological synthesis of nanomaterials have also been published. The shape and size controlled nanoparticles are prepared by using either templates or controlling the ratio of metal ion to stabilizer.

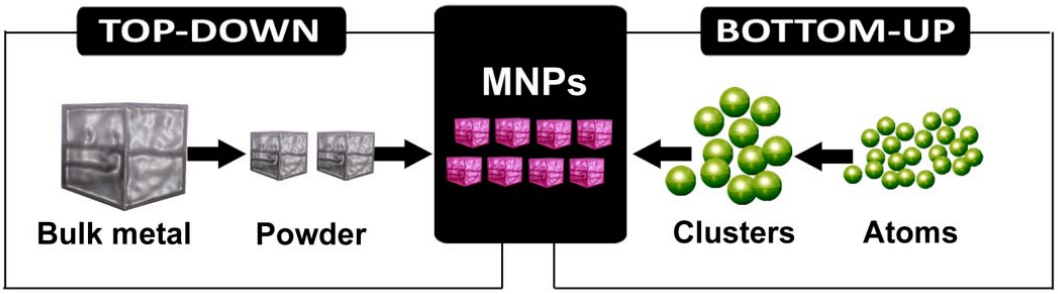

Fig.1.1 *Approaches for prepartion of metal nanomaterials(MNPs)*

Metal nanoparticles are usually prepared by the reduction of metal ions. The modes of reduction are chemical, electrochemical, microbial, radiation-assisted (UV light, electron beam, γ-radiation) etc. The medium for metal nanoparticles synthesis may be either aqueous or nonaqueous or sometimes both.

Electrodeposition provides an attractive method for the synthesis of metallic nanostructures. This involves the application of an appropriate electrochemical driving force to an electrode/electrolyte interface, resulting in the adherence of the metal species to the electrode surface. In the case of metal electrodeposition, this most commonly occurs by the

reduction of a metallic salt to its elemental state, although variations such as the electrochemically driven precipitation of certain metal oxides or hydroxides are known [6,7]. Electrodeposition is a widely studied field which is of keen interest in materials science applications as it can be used to synthesize a wide range of nanostructured materials[8,9]. Several benefits of this method of nanofabrication include the synthesis of materials of variable size, shape, crystallographic orientation, density and composition, which can be formed in the absence of capping agents [10-12]. This can be readily achieved through the electrochemical parameters employed such as the applied potential (or current density) and the duration of the electrodeposition, as well as the nature of the electrode surface and the composition of the electrodeposition solution [10,13,14]. A number of different electrochemical techniques also exist, including deposition at fixed, stepped or pulsed potentials or current densities, or by sweeping the applied deposition potential [15]. These techniques provide a level of control over the reduction process not available in other methods such as chemical synthesis of nanomaterials. Here, the reduction potential is carefully controlled through the use of a potentiostat rather than relying on the reduction potential supplied by the chemical reductant [9].

1.3 Conducting Polymers

Conducting polymers have attracted much interest in recent years. They contain π-electron backbones responsible for their unusual electronic properties such as electrical conductivity, low energy optical transitions, low ionisation potential and high electron affinity. The π conjugated system of these polymers have single and double bonds alternating along the polymer chain which make them capable of functioning as electron transfer mediators. With these materials, redox changes are not localised at a specific centre but rather delocalized over a number of conducting polymer groups. Polyacetylene was the first polymer that could be made electronically conductive and the conductivities range upto 10^3 S/cm for an iodine doped polymer [16]. This discovery unexpectedly started a great deal of research activity in conducting polymers [17,18]. Since then, a large number of conducting polymers have been synthesized. The most important polymers are polyacetylene [16,19,20], polyaniline[21], polypyrrole[22], polyphenylene[23], polythiophene[24] and poly (phenylene vinylidene)[25].

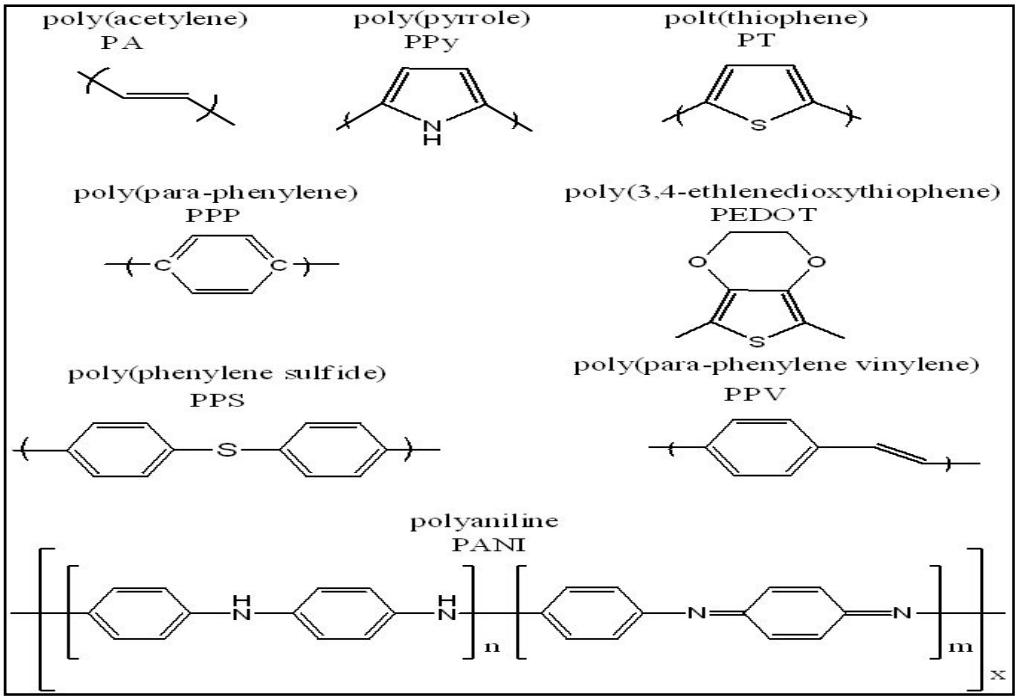

Fig.1.2 *Important conducting polymers known*

Among these, polyaniline has been the most extensively studied conducting polymer over the past due to its reversible redox and switching properties, ease of synthesis and wide range of potential applications. Its polymeric structure is different from other conducting polymers such as polythiophene and polypyrrole, and leads to three oxidation states each with its own distinctive colour [26]. The fully reduced leucoemeraldine base (LB) form is colourless or pale yellow, protonated emeraldine salt (ES) form is bright green and the fully oxidized pernigraniline base (PB) form is dark blue [27,28].Polyaniline has a very strong pH sensitivity, which is based on a reversible acid base reaction [28]. The only electrically conducting form of PANI, the ES form, can be obtained either by protonation of half oxidized emaraldine base (EB) or by oxidation of LB. It is noteworthy that the protonation does not effect the oxidation state of PANI. The structures and transition states of polyaniline are shown in Figure 1.3.

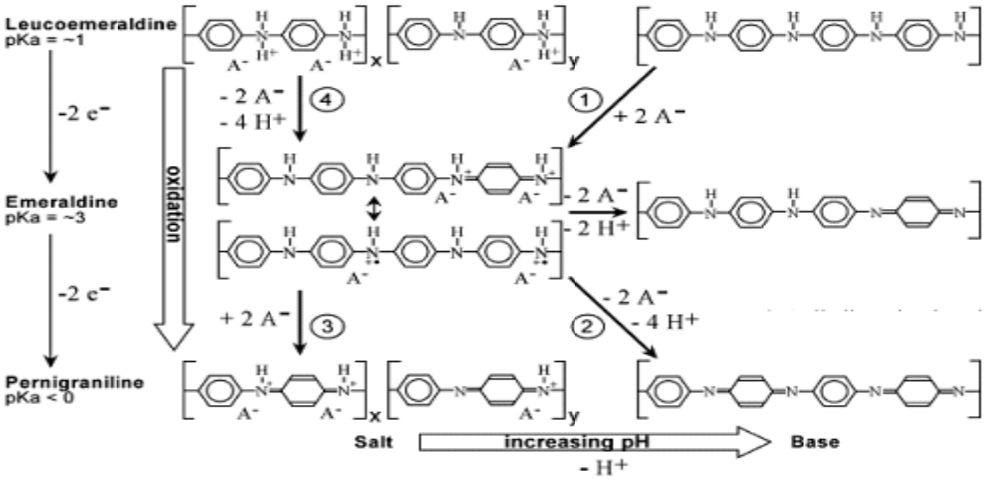

Fig.1.3 *Structures and transition states of Polyaniline*

Conducting polymers can be synthesized either by chemical or electrochemical polymerization from a monomer solution containing an electrolyte salt. Polyaniline is generally synthesized electrochemically because electrochemical methods allow the oxidation potential of polymerization to be controlled and thus the quality of the polymer can be optimized. Electrochemically synthesized polymers also possess adequate mechanical properties compared to chemical methods. The electrochemical polymerization can be performed in an electrochemical cell with three electrode system. The working electrode is usually platinum [29,30], glassy carbon [31,32], or ITO(indium tin oxide)[33]. The auxillary electrode can platinum gauze or reticulated vitreous carbon [34,35]. The selection of reference electrode is dependent on the solvent. In aqueous media, silver/ silver chloride (Ag/AgCl) or saturated calomel electrode (SCE) reference electrodes are suitable, while in organic solvents, psudo reference electrodes are commonly employed.

Electrochemical polymerization can be done by different methods of which the following three are the most common. (i) In galvanostatic method, a controlled anodic current is applied to the working electrode of the electrochemical cell to oxidize the monomer. As a

result of this, polymer film is produced on electrode surface. The rate of polymer synthesis can be controlled by the oxidation current density. The major advantage of the galvanostatic technique is that large surface area films can be synthesized on a batch or continuous basis, (ii) In the potentiostatic method, the potential of the electrode is maintained at a certain value where the polymerization reaction occurs. The potentiostatic technique has a major advantage of being able to selectively oxidize the monomer at a given potential, (iii) The third method is potentiodynamic where the potential is scanned over the range at which polymerization takes place. This technique has been employed for initial studies to obtain the optimum monomer oxidation potential for potentiostatic synthesis.

The oxidation of monomers and oligomers creates cation radicals which combine to form the polymer backbone. This polymer backbone is positively charged and the charge compensation is achieved by the incorporation of dopant anion. The amount of anion is related to the level of oxidation of polymer backbone and is characteristic of each polymer film. Generally, one dopant anion is incorporated for every two to three monomer units [36]. Properties like morphology, electroactivity and conductivity of the polymer are very much dependent on the conditions of polymerization such as electrolyte, solvent, monomer concentration, temperature, current, and potential applied [34,36,37-55].

The mechanism of polyaniline conductivity differs from other electroconducting polymers, owing to the fact that nitrogen atoms are involved in the formation of radical cation, unlike most of the electroconducting polymers whose radical cation is formed at carbon. On the other hand, nitrogen is also involved in the conjugated double bonds system. Therefore, electrical conductivity of polyaniline is dependent both on the oxidation and protonation degrees [56-59]. As mentioned before, polyaniline is characterized by existence of various

oxidation forms. Polyaniline in the form of emeraldine base can be doped (protonated) to conducting form of emeraldine salt. Emeraldine base, half oxidized form, is consisted of equal amounts of amine (-NH-) and imine (=NH-) sites. Imine sites are subjected to protonation to form bipolaron or dication (emeraldine salt form). Bipolaron is further dissociated by injection of two electrons both from electron pairs of two imine nitrogen, into quinodiimine ring, and the third double bond of benzenoid ring is formed [60]. Unpaired electrons at nitrogen atoms are cation radicals, but essentially they represent polarons. The polaron lattice, responible for high conductivity of polyaniline in the form of emeraldine salt, is formed by redistribution of polarons along polymer chain, according to shematic representation given in Fig.1.4 [59]. Although both bipolaron and polaron theoretical models of emeraldine salt conductivity were proposed [59, 61], it was lately confirmed that beside the fact that a few of spineless bipolarons exist in polyaniline, formation of polarons as charge carriers explained high conductivity of polyaniline [62,63]. As mentioned, unique property of polyaniline is conductivity dependence on the doping (proton) level [64,59]. The maximal conductivity of polyaniline is achieved at doping degree of 50%, which corresponds to polyaniline in the form of emeraldine salt [61]. For higher doping degrees, some of the amine sites are protonated, while lower doping degrees means that some of the imine sites are left unprotonated [59]. This explains in the light of the polaron conductivity model, reduction of emeraldine salt to leucoemeraldine and oxidation to perningraniline states leading to decrease in the conductivity. The order of magnitude for conductivity varies from 10^{-2} S cm^{-1}, for undoped emeraldine, up to 10^{3} S $cm^{-1}$for doped emeraldine salt [65]. Beside the fact that doping degree has a pronounced effect on the conductivity, various other factors

such as moisture amount [66], morphology [67], temperature [68] etc. were also found to have influence on the polyaniline conductivity.

Fig. 1.4 *Schematic presentation of polyaniline conductivity*

Both the mechanism and the kinetics of the electrochemical polymerization of aniline were extensively investigated [69]. Electrochemical, similarly to chemical polymerization of aniline is carried out only in acidic electrolyte, since higher pH leads to the formation of short conjugation oligomeric material with different nature. As stated before, it is generally accepted that the first step of the polymerization process of aniline involves formation of aniline cation radicals, by anodic oxidation on the electrode surface, which is considered to be the rate-determining step [70]. The existence of aniline radical cation was experimentally

confirmed, by introducing molecules, (resorcinol, hydroquinone, benzoquinine etc.), capable of retarding or even stopping the reaction, which evidenced a radical mechanism [71]. The oxidation of the aniline monomer is an irreversible process, occurring at higher positive potentials than redox potential of polyaniline. The following step is dependent on numerous factors such as electrolyte composition, deposition current density, or potential scan rate, nature and state of the anode material, temperature etc. [65]. There is a need for relatively high concentration of radical cations near the electrode surface. Radical cations can be involved, depending on reactivity, in different reactions. If it is quite stable, it may diffuse into the solution and react to form soluble products of low molecular weights. On the other hand, if is very unstable, it can react rapidly with anion or the solvent, in the vicinity of the electrode and form soluble products with low molecular weights [72]. In favorable case, coupling of the anilinium radicals would occur, followed by the elimination of two protons and rearomatization leading to the formation of dimer (lately oligomer). The aniline dimer, or oligomer, is further oxidized on the anode together with aniline. The chain propagation is achieved by coupling radical cations of the oligomer with anilinium radical cation. Finally, the counter anion originating from the acid, normally present in the electrolyte, dopes the polymer, meeting the requirement of electroneutrality. The mentioned mechanism of aniline electrochemical polymerization is schematically presented in Fig. 1.5 [59].

It was evidenced that electrochemical polymerization of aniline is an autocatalytic process. It was observed that the current increased over time, at constant potentials higher than 0.80 V and that anodic peak potentials shifted to more negative values upon increasing cycle number. Generally, it means the formation of more polymer formed on the anode with the highert rate of the electrochemical polymerization.

Step.1 *Oxidation o f monomer*

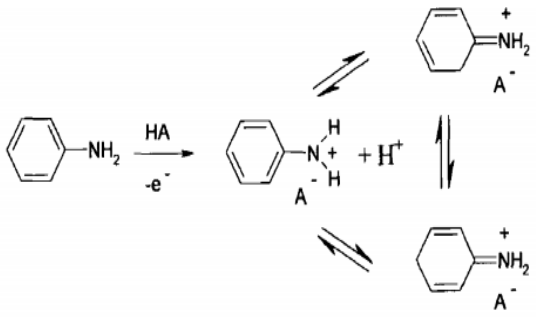

Step.3*Chain Propagation*

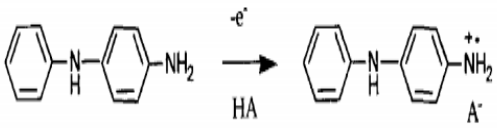

Step.2 *Radical coupling and rearomatisation*

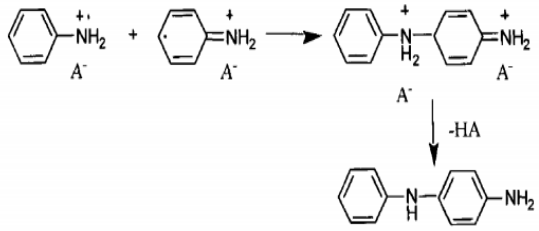

Step.4 *Doping of polymer*

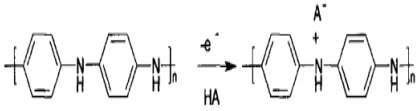

Fig.1.5*. Schematic presentation of mechanism of electrochemical polymerization of aniline*

1.4 Carbon Nanotubes

In order to understand the structure and properties of nanotubes, the bonding structure and properties of carbon atoms are briefly mentioned first. A carbon atom has six electrons with two of them filling the 1s orbitals. The remaining four electrons fill the sp^3 or sp^2 as well as the sp hybrid orbital, responsible for bonding structures of diamond, graphite, nanotubes, or fullerenes. Carbon nanotubes (CNTs) are allotropes of carbon with a cylindrical nanostructure. Nanotubes have been constructed with length-to-diameter ratio of up to 132,000,000:1 [73] which is significantly larger than any other material. A CNT can be viewed as a hollow cylinder formed by rolling graphite sheets. Their name is derived from their size, since the diameter of a nanotube is of the order of a few nanometers, while they can be up to several millimeters in length. Bonding in nanotubes consists essentially of sp^2 type. However, the circular curvature will cause quantum confinement and σ-π rehybridization in which three σ bonds are slightly out of plane; for compensation, the π orbital is more delocalized outside the tube. This makes nanotubes mechanically stronger, electrically and thermally more conductive, and chemically and biologically more active than graphite. In addition, they allow topological defects such as pentagons and heptagons to be incorporated into the hexagonal network to form capped, bent, toroidal, and helical nanotubes whereas electrons will be localized in pentagons and heptagons because of redistribution of π electrons. For convention, we call a nanotube defect free if it is of only hexagonal network and defective if it also contains topological defects such as pentagon and heptagon or other chemical and structural defects.

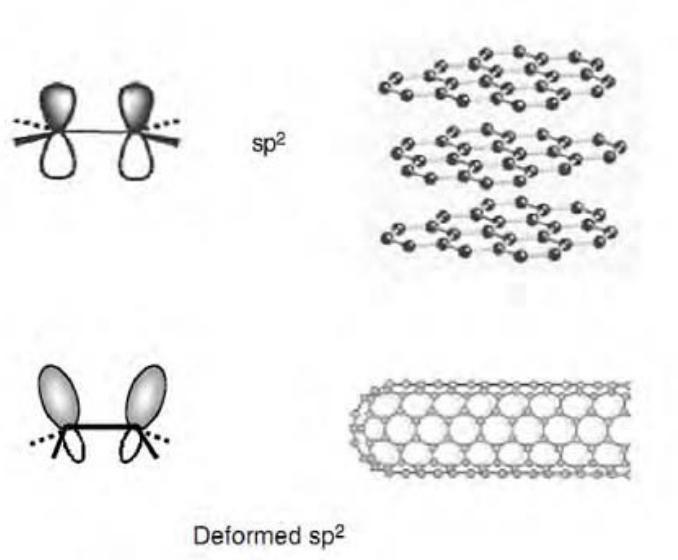

Fig1.6. *Bonding structures of graphite and nanotubes: when a graphite sheet is rolled over to form a nanotube, the sp^2 hybrid orbital is deformed for rehybridization of sp^2 toward sp^3 orbital or σ-π bond mixing. This rehybridization structural feature, together with π electron confinement, gives nanotubes unique, extraordinary electronic, mechanical, chemical, thermal, magnetic, and optical properties*

Nanotubes are categorized as single-walled nanotubes (SWNTs) and multi-walled nanotubes (MWNTs).

Single-walled

Single-walled nanotubes (SWNT) have a diameter approximately close to 1 nanometer, with a tube length that can be many millions of times longer. The structure of a SWNT can be viewed as wrapping a one-atom-thick layer of graphite called graphene into a seamless cylinder [75,75].

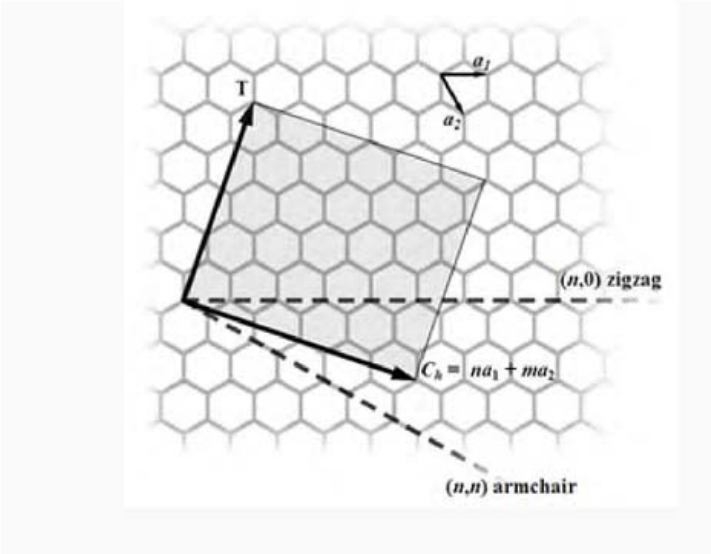

Fig.1.7. *(n,m) nanotube naming scheme*

The nanotube can be uniquely characterized by a vector C in terms of a set of two integers (n,m) corresponding to graphite vectors a_1 and a_2 (Fig.1.7) [76].

$$C = na_1 + ma_2$$

that describes how to "roll up" the graphene sheet to make the nanotube. T denotes the tube axis, and a_1 and a_2 are the unit vectors of graphene in real space.

The way the graphene sheet is wrapped is represented by a pair of indices (n,m) called the chiral vector. The integers n and m denote the number of unit vectors along two directions in the honeycomb crystal lattice of graphene. If m = 0, the nanotubes are called "zigzag". If n = m, the nanotubes are called "armchair". Otherwise, they are called "chiral". Single-walled nanotubes are an important variety of carbon nanotubes because they exhibit electric properties that are not shared by the multi-walled carbon nanotube (MWNT) variants.

Multi-walled

Multi-walled nanotubes (MWNT) consist of multiple rolled layers (concentric tubes) of graphite [77]. Two models are used to describe the structures of multi-walled nanotubes. First is the Russian Doll model, sheets of graphite are arranged in concentric cylinders, e.g. a (0,8) single-walled nanotube (SWNT) within a larger (0,10) single-walled nanotube. Whereas in the Parchment model, a single sheet of graphite is rolled in around itself, resembling a scroll of parchment or a rolled newspaper. The interlayer distance in multi-walled nanotubes is close to the distance between graphene layers in graphite, approximately 3.3 Å. Multi-walled carbon nanotubes are very important when functionalization is required (this means grafting of chemical functions at the surface of the nanotubes) to add new properties to the CNT. In the case of SWNT, covalent functionalization will break some C=C double bonds, leaving "holes" in the structure on the nanotube and thus modifying both its mechanical and electrical properties.

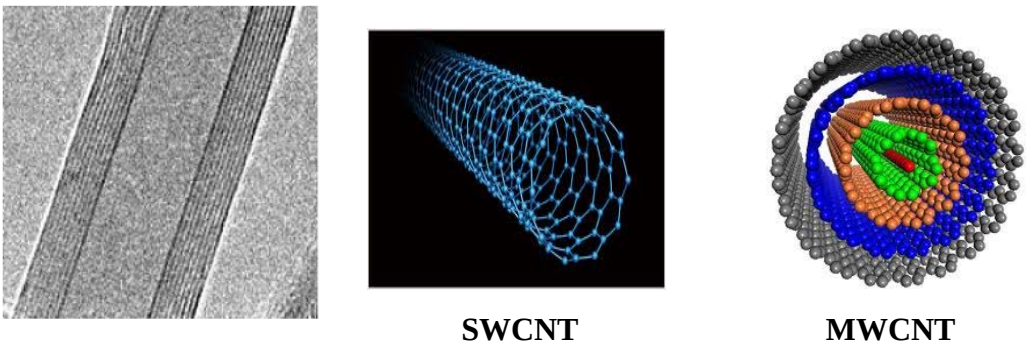

Fig.1.8. *On the left: TEM image of MWCNT, On the right: Schematic representation of single and multiwalled nanotube structure*

Due to their unique structure, nanotubes exhibit extraordinary electronic, mechanical, chemical, thermal, magnetic, and optical properties explained below.

• Electrical Properties

Electronic properties of nanotubes have received the greatest attention in nanotube research and applications [78-80]. Because of the symmetry and unique electronic structure of graphene, the structure of a nanotube strongly affects its electrical properties [81-83]. When graphite is rolled over to form a nanotube, a periodic boundary condition is imposed along the tube circumference or the C direction. This leads to the following condition at which metallic conductance occurs:

$$n\text{-}m = 3q$$

From the above equation, we can see that one third of the tubes are metallic and two thirds are semiconducting. For example, for a given (n,m) nanotube, if n = m, the nanotube is metallic. When (n – m) is a multiple of 3, then the nanotube is semiconducting with a very small band gap, otherwise the nanotube is a moderate semiconductor [84]. Thus, in principle, all armchair (n = m) nanotubes are metallic. In theory, as it has been calculated from numerous models, metallic nanotubes can carry an electrical current density of 4 $\times 10^9 A/cm^2$ which is more than 1,000 times greater than metals such as copper [85]. Intertube coupling also affects the electrical properties of the nanotubes and, therefore, needs to be considered, when discussing about conductivity of the nanotubes. It was observed that, the intertube coupling induces a small band gap for certain metallic tubes but a reduced band gap by 40% for semiconducting tubes in a SWNT rope [86,87].

The same observations were expected for a MWNT. Although due to the fact that MWNT have bigger diameteres, they showed a smaller intertube coupling as compared with sinlge walled nanotubes. Taking this into consideration, all semiconducting tubes in a MWNT tend to be semi-metallic just like graphite because of reduced band gap for large tubes and hole-electron pairing for multiwall coupling. A lot of research groups confirmed that individual MWNT samples showed the dominating metallic or semimetallic nature of a MWNT while small band gap was reported and attributed to presence of defects or an electric contact barrier. A MWNT basically behaves like metal or semimetal because of the dominating larger outer tube.

Multiwalled carbon nanotubes with interconnected inner shells show superconductivity with a relatively high transition temperature Tc= 12 K. In contrast, the Tc value is an order of magnitude lower for ropes of single-walled carbon nanotubes or for MWNTs with usual, non-interconnected shells [88]. As mentioned previously, the π electron is more delocalized in a defectfree nanotube because of σ-π rehybridization and thus should give rise to higher conductivity than that of graphite. In Figure 1.6, when curved, π orbitals become rich or more delocalized outside the tube, this leads to increased conductivity. Many recent studies show decreasing behaviour of resistivity with temperature.

• Optical and Thermal Properties

Carbon nanotubes are of great interest for their thermal properties. Measurements show that single-wall carbon nanotubes (SWNTs) room temperature thermal conductivity is about 3500 W/(m·K) [89] and over 3000 W/(m·K) for individual multiwalled carbon nanotubes (MWNTs)[90]. The low temperature specific heat and thermal conductivity show

direct evidence of 1-D quantization of the phonon band structure. Lot of studies have been focused on the optical and optoelectronic properties of nanotubes. The one-dimensional band structure makes nanotubes ideal for optical applications with wavelength ranging from 300 to 3000 nm.

• Mechanical and Electromechanical properties

σ bonding is the strongest in nature, and because a nanotube is structured with mainly σ bonds, this constitutes the ultimate fiber with the strength in its tube axis. Experimental measurements and theoretical calculations conclude that a nanotube has one of the highest Young's modulus and tensile strength [91-93]. In general, it has been proved that various types of defect-free nanotubes are stronger than graphite. This is due to the fact that the axial component of σ bonding is greatly increased when a graphite sheet is rolled over to form a cylinderical structure or a SWNT. Young's modulus is independent of tube chirality, but dependent on tube diameter. From calculation, the highest value for tube diameter between 1 and 2 nm is about 1 TPa. Thus the larger the diameter of the tube, the more it is approaching the graphite properties. When different diameters of SWNTs consist in a coaxial MWNT, the Young's modulus will take the highest value of a SWNT plus contributions from coaxial intertube coupling or van der Waals force. Thus, it is obvious that the Young's modulus for MWNT is higher than a SWNT. Although, when SWNTs are held together in a bundle, the weak van der Waal force will induce a strong shearing among the packed SWNTs. As a result, this will decrease the Young's modulus. It is shown experimentally that the Young's modulus decreases from 1 TPa to 100 GPa when the diameter of a SWNT bundle increases from 3 nm to 20 nm [94]. The elastic response of a nanotube to deformation was also examined and was found very

remarkable. In most hard materials, a fall was observed with a strain of 1% or less due to propagation of dislocations and defects. From experiments conducted, results showed that CNTs can sustain up to 15% tensile strain before fracture [95]. This behaviour was attributed to an elastic buckling through which high stress is released. This is another unique property of nanotubes, and such a high elastic strain for several deformation modes is originated from sp^2 rehybridization in nanotubes through which the high strain gets released. However, sp^2 rehybridization will lead to change in electronic properties of a nanotube when the tubes are being reformatted. Many models [96] predict that chiral nanotubes will experience change in electronic properties for either tensile or torsional strain whereas symmetric armchair or zigzag tubes may or may not change their electronic properties. In asymmetric tubes, either strain will cause asymmetric σ-π rehybridization, and therefore, change in electronic properties. However, effect of strain on a symmetric tube is not so straightforward. The above theory can also be extended to tube bending. Many experiments have confirmed the predicted remarkable electromechanical properties of nanotubes or electronic response to mechanical deformation. There has not been much effort to study the electromechanical properties of SWNT bundles and MWNTs. Intertube coupling may play a larger role in electromechanical properties as it does for Young's modulus and tensile strength.

• Magnetic and Electromagnetic properties

Magnetic and electromagnetic properties of CNTs have also attracted a great interest. Magnetic properties such as anisotropic g-factor and susceptibility of nanotubes are expected to be similar to those for graphite while some unusual properties may exist for nanotubes [97]. It can also be expected from a lot of models that CNTs would have interesting

electrical response to a magnetic field. Experiment and theory confirm the metal-insulator transition and band gap change whereas transport again is an intriguing issue. There are some relations that predict a metal insulator transition and band gap change for semiconductor tubes under magnetic field parallel to tube axis [98]. These are similar to electrical response of nanotubes to mechanical deformation, as mentioned in the above section. As reported, when driven by magnetic or strain field, the Fermi level will move away from the original position, and this results in the band gap change pattern [99].

• Chemical Properties

The high specific surface and σ-π rehybridization of the nanotubes, facilitate molecular adsorption, doping, and charge transfer , which, in turn, modulate electronic properties. Carbon nanotubes surface makes the nanotubes ideal for many applications as they interact strongly chemically resulting in a change in its properties.

Why CNTs can be suitable for use in catalysis and electrocatalysis ?

Carbon nanotube has been proposed as a promising support material for catalyst due to its unique characteristics, including high aspect ratio, high electron conductivity, and enhanced mass transport capability as mentioned in the above Section. A typical CNT sample contains both residual catalyst metallic impurities and carbon-based impurities. Even with extensive purification, it is impossible to entirely remove the impurities contained within CNTs [100-102]. This is a major concern for electrochemists, as it is well known that heterogeneous electron-transfer is very sensitive to the presence of impurities on the electrode surface. Metallic impurities within CNTs have received a substantial amountof

attention as a result of the pioneering work of Compton et al.in this field. Compton et al.have reported that metallic impurities are responsible for the ‘‘electrocatalytic’’ performance of CNT’s. Metallic impurities at concentrations of 0.01% wt are still able to dominate the electrochemistry of CNTs. It is only recently that the idea of nanographite impurities governing the electrochemistry of CNTs has come to light. Compton et al.stressed the need for electrochemists to perform suitable control experiments before concluding that CNTs possess inherent electrocatalytic properties, as it was observed that graphite powder-modified electrodes produce similar effects to electrodes modified with nanotubes[103]. Recently, It was proved that the observed heterogeneous electron-transfer (HET) rate of CNTs only resembles that of graphite because of the graphitic impurities contained within CNTs [104]. It was also demonstrated that it is the nanographite impurities, rather than metallic impurities, within CNTs that are responsible for the observed ‘‘electrocatalytic’’ reduction of the azo group in methyl orange, hydroquinone, NADH and amino acids [105]. Also Within the layered structure of graphite we can identify two types of graphitic plane: the basal plane, containing all the atoms of a particular graphite layer, and the edge-plane, perpendicular to the basal plane. Due to the nature of the chemical bonding in graphite, the two planes display noticeably different electrochemical properties. For example, for most redox couples the electrode kinetics at edge-plane graphite is considerably faster than at basal plane graphite [106]. Structurally, SWCNTs consist of a single tube of ‘‘rolled up’’ graphite sheet where as MWCNTs consist of several concentric tubes of graphite fitted one inside the other. There is some morphological variation possible in MWCNTs which is dependant on the conditions and the chosen method of CNT formation e.g.chemical vapour deposition or the high voltage arc method. They can be produced in ‘‘hollow-tube’’ form where the axis of the graphite

planes is parallel to the axis of the nanotube, ‘‘herringbone’’ form where the graphite planes are formed at an angle to the axis of the tube or finally in a ‘‘bamboo-like’’ form which is similar to the herringbone form except that the nanotubes are periodically closed along the length of the tube into compartments rather like bamboo or a ‘‘stack of paper cups fitted one inside the other’’. In the latter two cases, as the axis of the graphite planes are at an angle to the nanotube itself, a high proportion of the graphite sheets must terminate at the surface of the tube giving rise to a large number of edge-plane or edge-plane-like defect sites along the surface of the tube. It is believed that, it is these edge-plane-like defects that are responsible for much of the electrochemical activity of the CNTs compared to the smooth, more basal plane like regions along the CNT surface [107]. During the present work, single-walled carbon nanotubes (SWNTs) are selected as the electrocatalyst for studying the electrochemistry of actinides.

1.5 Fuel Cells

The extensive use of fossil fuels has resulted in severe pollutant emissions, including SOx, NOx, CO, and particulates which pose severe threat to the health of human beings [108]. In addition, a steady depletion of world’s limited fossil fuel reserves calls for efficient, benign and sustainable technologies for energy conversion and power generation. Fuel cells are among the most efficient and environmental friendly devices for energy conversion and power generation due to their zero-emission power source [109]. Fuel cells have been identified as one of the most promising and potent technologies which meet energy security, economic growth, and environmental sustainability requirements [110].

Fuel cells are environmental friendly devices for energy conversion, power generation, and one of the most promising candidates as zero-emission power sources [110]. Fuel cells are electrochemical devices which convert chemical energy obtained from a redox reaction directly into electrical energy [111]. These cells consist of an electrolyte material that is packed between two thin electrodes (porous anode and cathode). The input fuel passes over the anode and oxygen passes over the cathode where they are dissociated catalytically into ions and electrons. The electrons pass through an external electrical circuit to provide power while the ions move through the electrolyte towards the oppositely charged electrode [110,112].

In recent years, a great amount of experimental results have been accumulated dealing with chemisorption and electrochemical decomposition of various organic compounds on platinum group metals. The electrocatalytic oxidation of small organic molecules like methanol and formic acid at Pt electrodes has received considerable attention due to their promise as fuels in fuel cells. By far, the most attention has been given to the methanol system, either as pure fundamental studies or studies related to the direct methanol fuel cell. Several reviews are available, e.g. [113-122]. Formic acid is another potential fuel for fuel cells, and has received considerable attention over the years and has been reviewed several times, e.g. [123].

Methanol oxidation is suggested to proceed via several possible intermediates and pathways. Water is required for the overall conversion of methanol to carbon dioxide, which can be written as:

$$CH_3OH + H_2O \rightarrow CO_2 + 6H^+ + 6e^- \qquad (1)$$

In the early seventies Bagotzky et al. [124] proposed a general mechanistic scheme including all possible intermediates from methanol to CO_2. Up to eight intermediates were suggested, of which CO, formic acid and formaldehyde are the most interesting ones. In addition, Lopes et al. [125] found indications of a methoxy species in electrochemical systems that could further complicate the mechanistic scheme of methanol oxidation on platinum. Undoubtedly, the oxidation of methanol on platinum surfaces starts with dehydrogenation of the methanol molecule as shown by differential electrochemical mass spectrometry (DEMS) [126]. The first dehydrogenation step, equation (2), was shown to be the rate determining step on the Pt(111) and Pt(110) surfaces through measurements of the kinetic isotope effect and the Tafel slope of the reaction [127,128]. The rate determining step on the Pt(100) surface was shown to be the second dehydrogenation reaction, equation (3). The effect of surface structure on the electrocatalytic properties towards methanol oxidation has been demonstrated several times, e.g. [129-131]. For simplicity, we assume that one adsorbed molecule binds to only one surface platinum atom in the following simplified reaction scheme. According to Munk et al. [132], the complete stripping of all three methyl hydrogen atoms at lower potentials must occur on the flat terrace areas of the electrode surface, due to the fact that at least four adjacent adsorption sites are needed. Furthermore, successive dehydrogenation eventually leads to formation of adsorbed carbon monoxide

$$Pt-CH_3OH + Pt(site) \rightarrow Pt-CH_2OH + Pt-H \quad \textbf{(2)}$$

$$Pt-CH_2OH + Pt(site) \rightarrow Pt-CHOH + Pt-H \quad \textbf{(3)}$$

$$Pt-CHOH + Pt(site) \rightarrow Pt-COH + Pt-H \quad \textbf{(4)}$$

$$Pt-COH + Pt(site) \rightarrow Pt-CO + Pt-H \quad \textbf{(5)}$$

The dehydrogenation reactions lead to formation of adsorbed hydrogen atoms, which in turn will be followed by a one-electron transfer reaction to form a proton and an electron:

$$Pt-H \rightarrow Pt(site) + H^+ + e^- \quad \textbf{(6)}$$

The aim of the pioneering in-situ infrared spectroscopy studies in the early 1980s was to identify the product of dissociative adsorption of small organic molecules. It is now well known that the dissociative adsorption of many small organic molecules leads to large coverage of CO which can be linear, bridged or multiply bonded to the surface. A comprehensive review of the oxidation of small organic molecules as studied by in-situ infrared spectroscopy is given by Shi-Gang Sun [133]. Although many intermediates are detected by various methods, the exact structure of the adsorbed intermediates is unknown except for the adsorbed carbon monoxide molecule.

In order to review the formic acid oxidation over noble metals, it is instructive to compare the processes that take place in the methanol oxidation. Although formic acid, like methanol, is among the simplest organic compounds, the oxidation mechanism is not as simple as one might expect a priori. It took decades of work performed by several researchers to determine some of the simplest features of the mechanism for formic acid oxidation over metal electrodes [134]. Even today, some intermediates are not yet fully understood [135]. Fundamental work on the oxidation of formic acid over Pt and other noble metals like Ir, Rh, Pd and Au electrodes was performed in the 1970s by Capon and Parsons [136-139]. Before this pioneering work, the electrochemical oxidation mechanism was lacking several key steps. They proposed a dual path mechanism, shown in fig.10, which is the currently accepted scheme. After adsorption of the formic acid over the electrode, there are two

possible paths to product formation; direct oxidation to carbon dioxide that proceeds through a forementioned unknown intermediate or intermediates, and an indirect oxidation path that proceeds through carbon monoxide. It took some time to identify the carbon monoxide as an intermediate [140,141] in the indirectpath, previously believed to be a COH_{ads} species although the intermediate was branded a 'poisoning intermediate', a quality ascribed to carbon monoxide over Pt . This reaction mechanism was later confirmed by ^{18}O labeling [142] and in situ IR spectroscopy [143].

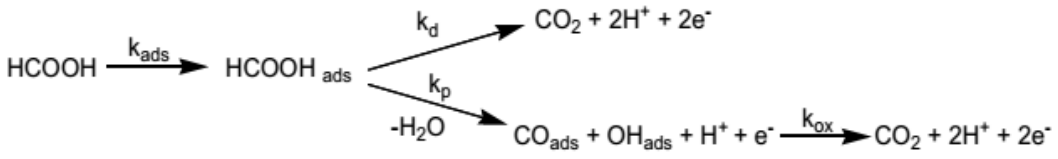

Fig.1.9. *Formic acid oxidation mechanism occuring at the surface of a metal electrode*

The tendency of both formic acid and methanol reactions to self-poisoning makes it clear that catalyst properties must be changed to avert the poisoning condition. In the present dissertion, palladium nanoparticles modified electrode was prepared electrochemically in order to improve the performance of a Direct Formic Acid Fuel Cell (DFAFC) and Direct Methanol Fuel Cell (DMFC).

1.6 Nuclear Fuel

One of the most important components of a nuclear reactor is its fuel. The fuel undergoes fission and the heat generated during this process is extracted to generate electricity. Uranium and plutonium are the actinides used as nuclear fuel in the reactors. The isotopes of these

heavy fissile elements e.g. ^{233}U, ^{235}U and ^{239}Pu undergo fission to generate energy. It is this material which faces the most severe environment inside the reactor. The fuel sees very high temperature (the centerline temperature of the fuel pellets goes upto 2000^{o}C), pressure and radiation field. Moreover, the fuel has to accommodate the radioactive fission products formed during the nuclear fission. With use, the central part of fuel pellets gets overheated and many fission products and interaction products, some of which are low density compounds, get accumulated into the fuel pellet. This leads to swelling of the fuel pellets. These conditions are remarkably dependent on the type of the fuel, fuel composition and trace impurities present in these fuels. In view of this, the nuclear fuel has to be well characterised with specific composition and trace impurity tolerance limits.

For fabricating high quality nuclear fuels, chemical and physical quality control of the starting, intermediate and final product of the fuel is essential. Chemical quality control ensures that the fuel material conforms to the chemical specifications laid down by the fuel designer. These specifications are very stringent and include the major, the minor and trace constituents which cause detrimental effect on fuel properties and performance under the reactor operating conditions. Therefore, trace and major element determinations in nuclear materials are of utmost importance. The process of chemical quality assurance for trace elements includes pre-concentration and separation of the impurities from the sample matrix, followed by their quantification. There are various ways by which these impurities get incorporated into the fuel. Starting from mining, till its fabrication, the fuel material goes through a series of wet chemical processes which include dissolution (in nitric acid), purification by solvent extraction and precipitation. During all these processes, the impurities form the various reagents used in the above processes get added to the nuclear fuel material.

Also during the nuclear fission, a number of fission products are produced which make the fuel matrix highly heterogeneous. A gamut of analytical methodologies is required for the chemical quality assurance of nuclear materials. There has been a remarkable advancement in the technology for the development of nuclear fuels and other materials in the last few years. To keep pace with such development, a similar development in the advancement of quality control related programs is desirable. A vast number of instrumental techniques are used for the chemical characterization of nuclear materials. Each technique has its own advantages and disadvantages. Therefore, for the best utilization of these techniques, proper selection depending on the need is essential. In order to develop a methodology for analytical characterization of materials, various steps have to be followed, which comprise of sampling of the material, preparation of suitable standards, calibration, sample preparation for measurement, data handling and processing along with the investigations of the associated problems and improvement of the analysis results. A comprehensive use of various analytical techniques is required for the chemical characterization of different materials in nuclear industry. These include determination of metallic and non-metallic impurities, total gas content as well as the nuclear fuel elements i.e. uranium and plutonium in alloy fuels and other reactor components. Electroanalytical chemistry of uranium and plutonium in various supporting electrolytes (acidic, basic, and non-aqueous) at different electrodes (Hg, Pt, Ag, Au, graphite and glassy carbon) is well documented in literature. A limited number of publications dealing with the applications of carbon nanotubes and conducting polymer modified electrodes for lanthanides and actinides electrochemistry are available. In this thesis, the investigations were carried out on the electrochemistry of Pu(IV)/Pu(III) and U(VI)/U(IV) couples employing electrodes modified with SWCNTs and polyaniline. The

study on electrochemical behaviour was then employed for simultaneous determination of U and Pu by voltammetry.

Neptunium (Np) is one of the actinides produced in nuclear reactors. It is located between U and Pu in the Periodic Table, suggesting that its chemical properties are qualitatively similar to those of U and Pu. Because of this chemical similarity as well as its considerable content in the spent nuclear fuels, the behavior of Np assumes importance in the fuel reprocessing process. Besides, the long half-life of ^{237}Np, 2.14×10^6 years and high solubility of Np under environmentally relevant conditions makes it problematic on the long-term repository of radioactive wastes. Hence in the present work electroanalytical performance of SWCNTs for Np(VI)/Np(V) couple was studied.

1.7 Thesis Outline

The broad aim of this work is the preparation, characterization and applications of electrodes modified with metal nanoparticles, conducting polymer and carbon nanotubes. These are applied for electrocatalytic reactions such as formic acid and methanol oxidation and also for studying the redox behavior of actinides along with their determination. The intention of these studies is to utilize the modified electrodes for determination of actinides in the nuclear fuel samples and to mitigate the effect of CO poisoning in direct formic acid fuel cells (DFAFC) and direct methanol fuel cells (DMFC).

In Chapter 1, the need of modification of electrode is discussed in detail. It includes the introduction to nanomaterials and their unique properties that make them ideal material for electrode modification. A brief description of fuel cells is also given. The synthesis and applications of conducting polymers as electrode modifier are discussed. The importance of

carbon nanotubes as electrode modifier and its applications are also included. This Chapter also gives an introduction to various materials used in nuclear reactors and the significance of analytical characterization of these materials.

Chapter 2 gives a brief introduction to electroanalytical chemistry, various electroanalytical techniques and the basic fundamental aspects of voltammetric and characterization techniques.

Chapter 3 comprises the synthesis of palladium nanoparticles (PdNPs) on platinum (Pt) electrode by employing a potentiostatic pulse method of electrodeposition. The mechanism of electrocrystallization of PdNPs on Pt was investigated in the system containing 1mM K_2PdCl_4 in 0.1M H_2SO_4. Experimental results showed that Pd electrodeposition follows the so-called Volmer–Weber growth mechanism.The synthesized Pd nanoparticles modified Pt electrode displayed significantly different voltammetric behavior compared to bare Pt electrode and also showed high catalytic activity towards the electrooxidation of formic acid and methanol.

Chapter 4 deals with the electrocatalysis at polyaniline modified Pt electrode. At polyaniline modified electrode, two systems were studied. Initially, influence of ionic speciation on electrocatalytic performance of polyaniline coated platinum electrode for Fe(III)/Fe(II) redox reaction was studied. Electrocatalysis of Fe(III)/Fe(II) reaction was studied by cyclic voltammetry (CV) and electrochemical impedance spectroscopy (EIS) for three different solution compositions viz. (i) $FeCl_3/FeCl_2$ in 1M HCl, (ii) $FeCl_3/FeCl_2$ in 0.5M H_2SO_4 and (iii) $Fe_2(SO_4)_3/FeSO_4$ in 0.5M H_2SO_4. Further, a mechanistic study was carried out on electrocatalysis of the Pu(IV)/Pu(III) redox reaction at a platinum electrode modified with polyaniline (PANI). In this, electrochemistry of Pu(IV)/Pu(III) couple in 1 M H_2SO_4 was

studied on bare and modified platinum electrode by cyclic voltammetry and electrochemical impedance spectroscopy. Electrocatalysis of Pu(IV)/Pu(III) redox reaction was observed on PANI-Pt. Pu(IV)/Pu(III) couple showed quasi-reversible electron transfer behavior on bare platinum electrode because of the PtO layer formation by Pu(IV) solution at the electrode-electrolyte interface. Electrocatalysis of Pu(IV)/Pu(III) couple on PANI-Pt was attributed to the cumulative effect of the Donnan interaction between PANI and Pu(IV) anionic complex, specific adsorption of Pu(IV) on the reactive centres, low charge transfer resistance across the electrode-electrolyte interface and a catalytic chemical reaction coupled with the electron transfer reaction.

Chapter 5 explains the electrocatalytic performance of SWCNT modified electrode. Three redox couples were studied at SWCNT modified electrode. Firstly, mechanistic study on the electrocatalysis of Pu(IV)/Pu(III) redox reaction at platinum electrode modified with single-walled Carbon nanotubes (SWCNTs) was carried out. Pu(IV)/Pu(III) couple showed quasi-reversible electron transfer behavior on bare platinum electrode because of the PtO layer formation by Pu(IV) solution at the electrode-electrolyte interface. In SWCNT-Pt, the direct interaction between Pu(IV) and platinum was blocked by SWCNTs and it diminished the oxide layer formation at the interface. The lower charge transfer resistance at SWCNT-Pt also promoted the rate of electron transfer reaction of Pu(IV)/Pu(III) couple. Electrochemical studies of U(VI)/U(IV) redox reaction in 1 M H_2SO_4 at single-walled carbon nanotubes (SWCNTs) modified gold (Au) electrode are also presented in this Chapter. In this context, electrochemistry of U(VI)/U(IV) couple in 1 M H_2SO_4 was studied on bare and modified gold (Au) electrodes by cyclic voltammetry (CV), differential pulse voltammetry (DPV) and electrochemical impedance spectroscopy (EIS). A detailed investigation was done to

determine the kinetic parameters at the modified electrode. It was found that the electrocatalysis of U(VI)/U(IV) couple on SWCNT-Au is driven by an increase in the rate constant of the electron transfer reaction compared to that with the bare gold electrode. After a detailed study on electrocatalytic mechanism of U(VI)/U(IV) couple and Pu(IV)/Pu(III) redox couple, studies were carried out to simultaneously determine Pu and U at SWCNT-Au electrode in the fuel samples. This Chapter also explains the electrochemical investigations on Np(VI)/Np(V) redox couple using single walled carbon nanotube modified glassy carbon electrode (SWCNT-GC).

1.8 References

1. R.F. Lane, A.T. Hubbard, Electrochemistry of chemisorbed molecules. 1. Reactants connected to electrodes through olefinic substituents.*J. Phys. Chem.,* **77** (1973) 1401.
2. L.R Faulkner, *Chem. Eng. News*, Chemical microstructures on electrodes, **62** (1984) 28.
3. R.W Murray, A.G Ewing, R.A Durst,Chemically modified electrodes milecular design for electroanalysis, *Anal. Chem*, **59** (1987) 379-A.
4. C. Burda, X. Chen, R. Narayanan andM. A. El-Sayed, Chemistry and properties of nanocrystals of different shapes., *Chem. Rev*., **105** (2005) 1025.
5. J. Jellinek. Nanoalloys: tuning properties and characteristics through size and composition, *Faraday Discuss*, **138** (2008)11.
6. F. Marken, A. Neudeck, A. M. Bond, *Electroanalytical Methods* (Ed.: F. Scholz), Springer-Verlag, Berlin Heidelberg, 2010, pp. 57-106.

7. T. J. Davies, R. G. Compton, The cyclic and linear sweep voltammetry of regular and random arrays of microdisc electrodes: Theory, *J. Electroanal. Chem.* **585** (2005) 63.
8. K. R. Ward, N. S. Lawrence, R. S. Hartshorne, R. G. Compton, The theory of cyclic voltammetry of electrochemically heterogeneous surfaces: comparison of different models for surface geometry and applications to highly ordered pyrolytic graphite, *Phys. Chem. Chem. Phys.* **14**(2012) 7264.
9. J. Heinze, Cyclic Voltammetry—"Electrochemical Spectroscopy". New Analytical Methods, *Angew. Chem. Int. Edit.* **23** (1984)831.
10. L. Setti, A. Fraleonimorgera, I. Mencarelli, A. Filippini, B. Ballarin, M. Dibiase, An HRP-based amperometric biosensor fabricated by thermal inkjet printing, *Sensor. Actuat. B-Chem.* **126 (**2007)252.
11. D. Grujicic, B. Pesic, Electrodeposition of copper: the nucleation mechanisms, *Electrochim. Acta* **47** (2002) 2901.
12. L. P. Bicelli, B. Bozzini, C. Mele, L. D'Urzo, A review of nanostructural aspects of metal deposition, *Int. J. Electrochem. Sci.* **3**(2008)356.
13. S. Maheswari, P. Sridhar, S. Pitchumani, Carbon-Supported Silver as Cathode Electrocatalyst for Alkaline Polymer Electrolyte Membrane Fuel Cells, *Electrocatalysis* **3(**2011) 13.
14. C. Song, J. Zhang, in *PEM Fuel Cell Electrocatalysts and Catalyst* Layers (Ed.: J. Zhang), Springer London, 2008, pp. 89-134.
15. A. B. Velichenko, D. V. Girenko, F. I. Danilov, Mechanism of lead dioxide electrodeposition, *J. Electroanal. Chem*. **405 (**1996) 127.

16. C.K. Chiang, C.R. Fincher, Y.W. Park, A.J. Heeger, H. Shirakawa, E.J. Louis, S.C. Gau and A.G. MacDiarmid, Electrical conductivity in doped polyacetylene, *Phy. Rev. Lett*., **39** (1977) 1098.
17. S. Roth and M. Filzmoser, Conducting polymers—thirteen years of Polyacetylene Doping, *Adv. Mater.,* **2** (1990) 356.
18. S. Roth and H. Bleier, Solitons in polyacetylene, *Adv. In Physics,* **36** (1987) 385.
19. H. Shirakawa, E.J. Louis, A.G. MacDiarmid, and A.J. Heeger, Synthesis of Electrically Conducting Organic Polymers: Halogen Derivatives of Polyacetylene, (CH)x, *J.C.S Chem Commun*., (1977) 578.
20. C.K. Chiang, Y.W. Park, A.J. Heeger, H. Shirakawa, E.J. Louis and A.G. MacDiarmid, Conducting polymers: Halogen doped polyacetylene, *J. Chem. Phys.*, **69** (1978) 5098.
21. A.F. Diaz and J.A. Logan, Electroactive polyaniline films, *J. Electroanal. Chem.,* **111** (1980) 111.
22. A.F. Diaz and J. I. Castillo, A polymer electrode with variable conductivity: Polypyrrole, *J. Chem. Comm.,* **21**(1980).397.
23. D.M. Ivory, G.G.Miller, J.M.Sowa, L.W.Shacklette, R.R.Chance and Baughman, Highly conducting charge-transfer complexes of poly(p-phenylene), *J. Chem. Phys.,* **71**(1979) 1506.
24. G. Tourillon and F. Garnier, New electrochemically generated organic conducting polymers, *J. Electroanal. Chem.,* **135** (1981) 173.
25. G.E. Wnek, J.C.W. Chien,F.E. Karazs and C.P.Lillja, Electrically conducting derivative of poly(p-phenylene vinylene), *Polymer,* **20** (1979) 1441.

26. G.G. Wallace, G.M.Spinks, L.A.P.Kane-Maguire, and P.R. Teasdale *Conductive Electroactive Polymers*, CRC Press, Taylor & Francis Group.
27. J. Stejskal, P. Kratochvil, and A. D. Jenkins, Polyaniline: Forms and Formation, *Collection of Czechoslovak Chemical Communications*, **60** (1995) 314.
28. T. Lindfors and A. Ivaska., pH sensitivity of polyaniline and its substituted derivatives, *J. Electroanal. Chem.*, **531** (2002). 65.
29. S. Asavapiriyanont, G.K. Chandler, G.A. Gunawardena and D. Pletcher, The electrodeposition of polypyrrole films from aqueous solutions, *J. Electroanal. Chem*., **177** (1984) 229.
30. R.A. Bull, Fu-Ren. F. Fan and A.J. Bard, Polymer films on electrodes - electrochemical behavior at polypyrrole-coated platinum and tantalum electrodes, *J. Electrochem. Soc.,* **129** (1982) 1009.
31. C.O. Too, S.A. Ashraf, H. Ge, K.J. Gilmore, S.G. Pyne and G.G. Wallace, Electropolymerization of 4-(3-pyrrolyl)-4-oxobutyric acid by in situ potentiodynamic pre-reduction/oxidation, *Polymer,* **34** (1993) 2684.
32. J.R. Reynolds, P.A. Poropatic and R.L. Toyooka, Electrochemical copolymerization of pyrrole with N-substituted pyrroles. Effect of composition on electrical conductivity, *Macromolecules*, **20** (1987) 958.
33. M. Salmon and G. Bidan, Chiral Polypyrroles from Optically Active Pyrrole Monomers, *J. Electrochem. Soc.,* **132**(1985) 1897.
34. T.F. Otero and C. Santamaria, Dependence of polypyrrole production on potential, *Synth. Met.,* **51** (1992) 313.

35. H. Eisazadeh, K.J. Gilmore, A.J. Hodgson, G. Spinks and G.G. Wallace, Electrochemical production of conducting polymer colloids, *Colloids and Surf.* **103** (1995) 281.
36. A.F. Diaz and J. Bargon, in *Handbook of Conducting Polymers*, Vol. 1, T.A. Skotheim (Ed.), Marcel Dekker, New York,1986, 82.
37. P. Hulser and F. Beck, Electrodeposition of polypyrrole layers on aluminium from aqueous electrolytes, *J. Applied Electrchem*. **20** (1990) 596.
38. F. Beck and P. Hulser, *J. Electranal. Chem*., **289** (1990) 159.
39. P. Hulser and F. Beck, Electrodeposition of Polypyrrole Powder on Aluminum from Aqueous Electrolytes, *J. Electrochem. Soc.,* **137** (1990) 2067.
40. K. Imanishi, M. Satoh, Y. Yasuda, R. Taushima and S. Aoki, Solvent effect on electrochemical polymerization of aromatic compounds, *J. Electranal. Chem*., 242 (1988) 203.
41. J. L. Sauvajol, D.Chenouni, J.P. Lere-Porte, C. Chorro, B. Bouicala and J. Petrissans, Resonant Raman spectra and photoluminescence in polythiophene, *Synth. Met.*, **38** (1990) 1.
42. F. Tadjar, S. Ymmel, M. Janda, P. Duchek, P. Holy and I. Stibor, Collect. Czech. Electrochemical oxidation of pyrrole derivatives in alcoholic medium, *Chem. Commun.,* **54**(1989) 1299.
43. J.M.Ko, H.W. Rhee, S.M. Park and C.Y. Kim, Morphology and Electrochemical Properties of Polypyrrole Films Prepared in Aqueous and Nonaqueous Solvents, *J.Electrochem. Soc.,* **137** (1990) 905.

44. F.T.A. Vork, B.C.A.M. Schuernans and E. Barenderecht, Influence of inserted anions on the properties of polypyrrole, *Electrochim Acta,* **35** (1990)567.

45. J. Roncali, F. Garnier and M. Lemaire, Poly mono-, bi- and trithiophene: Effect of oligomer chain length on the polymer properties, *Synth. Met.,* **15** (1986) 323.

46. J.Roncali1, R. Garreau, D. Delabouglise, F.Garnier, M.Lemaire, Recent developments in the synthesis and functionalization of conducting poly(thiophenes), *Makromolekulare Chemie. Macromolecular Symposia,* **20** (1988) 601.

47. M. Akisato, S. Tanaka and K. Kaeriyama, Electrochemical preparation of conducting poly(3-methylthiophene): comparison with polythiophene and poly(3-ethylthiophene), *Synth. Met.,* **14** (1986) 279.

48. A.J. Downard and D. Pletcher, The influence of water on the electrodeposition of polypyrrole in acetonitrile, *J. Electrochem. Chem*., **206** (1986) 147.

49. Kiyoharu Isobe, Tsutomu Fukunaga, Wataru Takashima, and Keiichi Kaneto, Selective electrodeposition of conducting polymers, *Synthetic Metals* **85** (1997) 1435.

50. M. Satoh, K. Kaneto, K. Yoshino, Dependences of electrical and mechanical properties of conducting polypyrrole films on conditions of electrochemical polymerization in an aqueous medium. *Synth. Met.,* **14** (1986) 289.

51. M. Ogasawara, K. Funahashi, T. Demura, T. Hagiwara and K. Iwata, Enhancement of electrical conductivity of polypyrrole by stretching, *Synth. Met.,* **14** (1986) 61.

52. S.C. Sharma, S. Krishnamoorthy, S.V. Naidu. C.I. Eom, S. Krichene and J.R. Reynolds, Positron Annihilation and Conductivity Correlations in Poly(pyrrole tosylate) and Poly(pyrrole fluoride), *Phy. Rev.* **B 41**(1992) 5258.

53. L.S Curtin, G.C. Komplin and W.J. Pietro., Diffuse anion exchange in polypyrrole films, *J. Phys. Chem.,* **92** (1988) 12.

54. L.F Warren and D.P Anderson, Polypyrrole Films from Aqueous Electrolytes: the Effect of Anions upon Order, *J. Electrochem. Soc.,* **134** (1987) 101.

55. D.S. Maddison and C.M. Jenden, Dopant Exchange in Conducting Polypyrrole Films, *Polyme. Int.,* **27** (1992) 231.

56. P. Fedorko, M. Trznadel, A. Pron, D. Djurado, J. Planès and J. Travers; New analytical approach to the insulator–metal transition in conductive polyaniline.*Synthetic Metals*, **160** (2010), 1668.

57. E. Genies, A. Boyle, M. Lapkowski and Tsintavis, Polyaniline: A historical survey *Synthetic Metals*, **36**, (1990), 139.

58. A. Pron and P. Rannou; Processible conjugated polymers: from organic semiconductors to organic metals and superconductors, *Progress in Polymer Science,* **27**, (2002), 135.

59. G. Wallace, G. Spinks, L. Kane-Maguire and P. Teasdale; *Conductive Electroactive Polymers*, CRC Press, Taylor & Francis Group, (2009).

60. J. Stejskal, I. Sapurina and M. Trchová; Polyaniline nanostructures and the role of aniline oligomers in their formation, *Progress in Polymer Science,* **35**(2010)1420.

61. K. Tanaka, S. Wang and T. Yamabe, Will bipolarons be formed in heavily oxidized polyaniline? *Synthetic Metals*, **36**, (1990)129.

62. S. Mu, J. Kan, J. Lu and L. Zhuang; Interconversion of polarons and bipolarons of polyaniline during the electrochemical polymerization of aniline *Journal of Electroanalytical Chemistry*, **446** (1998)107.

63. R. Patil R, Y. Harima. K. Yamashita K, Komaguchi, Y. Itagaki and M. Shiotani; Charge carriers in polyaniline film: a correlation between mobility and in-situ ESR Meausurements, *Journal of Electroanalytical Chemistry*, **518** (2002) 13.

64. J. Chiang and A. MacDiarmid, Polyaniline: Protonic acid doping of the emeraldine form to the metallic regime. *Synthetic Metals*, **13** (1986) 193.

65. G. Inzelt; Conducting *Polymers – A New Era in Electrochemistry*, Springer-Verlag.

66. P. Kahol, A. Dyakonov, and B. McCormick B, An electron-spin-resonance study of polymer interactions with moisture in polyaniline and its derivatives, *Synthetic Metals*, 89 (1997) 17.

67. H. Zhou, J. Wen, X. Ning, C. Fu, J. Chen and Y. Kuang, Electrosynthesis of polyaniline films on titanium by pulse potentiostatic method, *Synthetic Metals*, **157** (2007) 98.

68. M. Probst and R. Holze, Time- and temperature-dependent changes of the in situ conductivity of polyaniline and polyindoline, *Electrochimica Acta*, **40** (1995) 213.

69. G. Andrade, M. Aguirre and S. Biaggi, Influence of the first potential scan on the morphology and electrical properties ofpotentiodynamically grown polyaniline films. *Electrochimica Acta*, **44** (1998) 633.

70. G. Zotti, S. Cattarin and N. Comiss; Cyclic potential sweep electropolymerization of aniline: The role of anions in the polymerization mechanism, *J. Electroanal. Chem.and Interfacial Electrochemistry*, **239**(1988) 387.

71. S. Mu and J. Kan; The effect of salts on the electrochemical polymerization of aniline, *Electrochimica Acta*, **4** (1996) 1593.

72. S. Park and H. Joong, Recent Advances in Electrochemical Studies of π-Conjugated Polymers. *Builllten of the Korean Chemical Society*, **26** (2005) 697.

73. X.Wang, Fabrication of ultralong and electrically uniform single-walled carbon nanotubes on clean substrates, *Nano Letters* **9** (2009) 3137.

74. S. Iijima and T. Ichihashi, Single-shell carbon nanotubes of 1-nm diameter, *Nature,* **363** (1993) 603.

75. D.S. Bethune, Cobalt-catalysed growth of carbon nanotubes with single-atomic-layer walls, *Nature*,**363** (1993) 605.

76. M. Dresselhaus, G. Dresselhaus, and P. Eklund, *Science of Fullerenes and Carbon Nanotubes* Academic Press, San Diego (1996).

77. S. Iijima, Helical microtubules of graphitic carbon, *Nature*, **354** (1991) 56.

78. M. Bockrath et al., Single-Electron Transport in Ropes of Carbon Nanotubes, *Science*, **275** (1997) 1922.

79. S.J. Tans et al. Individual single-wall carbon nanotubes as quantum wires, Nature, 386 (1997) 474.

80. S. Frank et al., Carbon Nanotube Quantum Resistors, *Science*, **280** 1744 (1998)

81. J.W.G. Wildoer et al., Electronic structure of atomically resolved carbon nanotubes, *Nature*, **391** (1998) 59.

82. T.W. Odom et al., Atomic structure and electronic properties of single-walled carbon nanotubes, *Nature*, **391** (1998) 62.

83. Z. Yao et al., Carbon nanotube intramolecular junctions, *Nature* **402** (1999) 273.

84. M. Ouyang et al., Energy Gaps in "Metallic" Single-Walled Carbon Nanotubes, *Science*, **292** (2001) 702.

85. Seunghun Hong, S. Myung; Nanotube Electronics: A flexible approach to mobility, *Nature Nanotechnology* **2**(2007) 207.

86. P. Delaney et al., Broken symmetry and pseudogaps in ropes of carbon nanotubes, *Nature*, **391** (1998) 466.

87. P. Lambin et al., Electronic band structure of multilayered carbon tubules, *Comp. Mat. Sci*., **2** (1994) 350.

88. J. Haruyama et al. Superconductivity in Entirely End-Bonded Multiwalled Carbon Nanotubes, *Physical Review Letters* **96**(2006) 57001.

89. Eric et al.; Thermal Conductance of an Individual Single-Wall Carbon Nanotube above Room Temperature, *Nano Letters* **6** (2005) 96.

90. P. Kim, et al.; Thermal Transport Measurements of Individual Multiwalled Nanotubes, *Physical Review Letters* **87** (2001) 215502.

91. J.P. Liu, Elastic Properties of Carbon Nanotubes and Nanoropes, *Phys. Rev. Lett.,* **79** (1997) 1297.

92. A. Garg, J. Han, and S. B. Sinnott, Interactions of Carbon-Nanotubule Proximal Probe Tips with Diamond and Graphene, *Phys. Rev. Lett.,* **81** (1998) 2260.

93. T. Ebbesen et al., Electrical conductivity of individual carbon nanotubes, *Nature*, **382** (1996)54.

94. E.Wong, P Sheehan, and C. Lieber, Nanobeam Mechanics: Elasticity, Strength, and Toughness of Nanorods and Nanotubes, *Science,* **277** (1997) 1971.

95. J.P. Salvetat, Mechanical properties of carbon nanotubes, *Appl. Phys. A*, **69** (1999) 255.

96. J. Lu and J. Han, Carbon Nanotubes and Nanotube-based Nano Devices, *Int. J. High Speed Elec. Sys.,* **9** (1998) 101.

97. L. Yang and J. Han, Electronic Structure of Deformed Carbon Nanotubes, *Phys. Rev. Lett*., **85** (2000) 154.

98. G. Baumgartner et al., Hall effect and magnetoresistance of carbon nanotube films, *Phys. Rev.* B, **55** (1997) 6704.

99. J.P. Lu, Novel Magnetic Properties of Carbon Nanotubes, *Phys. Rev. Lett.,* **74** (1995)1123.

100. M. E. Itkis, D. E. Perea, R. Jung, S. Niyogi and R. C. Haddon, *J. Am. Chem. Soc*., **127** (2005) 3439.

101. X. Liu, L. Guo, D. Morris, A. B. Kane and R. H. Hurt,*Carbon*, 46(2008) 489.

102. M. Pumera,*Langmuir*, 23(2007) 6453

103. R. R. Moore, C. E. Banks and R. G. Compton, *Anal. Chem*., **76** (2004) 2677.

104. A. Ambrosi and M. Pumera, *Chem.–Eur. J.,* **16** (2010) 10946.

105. E. J. E. Stuart and M. Pumera, *Chem.–Asian J.,* **6** (2011) 1019.

106. K. R. Kneton and R. L. McCreery, Anal. Chem., 1992, 64, 2518.

107. Craig E. Banks, Trevor J. Davies, Gregory G. Wildgoose and Richard G. Compton, *Chem. Commun*., (2005) 829.

108. A. Berenjian, N.Chan, H. Jafarizadeh Malmiri, Volatile organic compounds removal methods: A review, *Am J Biochem Biotechno*; **l8** (2012) 220.

109. Xianguo L: *Principles of Fuel Cells.New York London*: Taylor and Francis group; 1962.

110. Ma J, Sahai Y: Chitosan biopolymer for fuel cell applications, *Carbohydrate Polymers;* 92(2013)955.

111. Ye. YS, J. Rick, B.J Hwang, Water Soluble Polymers as Proton Exchange Membranes for Fuel Cells, *Polymers*; **4**(2012)913.

112. N.A. Hampson, M.J. Willars, B.D. McNicol, The methanol-air fuel cell: A selective review of methanol oxidation mechanisms at platinum electrodes in acid electrolytes, *J. Power Sources*, **4**(1979) 191.

113. B.D. McNicol, Electrocatalytic problems associated with the development of direct methanol-air fuel cells, *J. Electroanal. Chem*., **118** (1981) 71.

114. R. Parsons, T.J. VanderNoot, The oxidation of small organic molecules: A survey of recent fuel cell related research, *J. Electroanal. Chem*., **257**(1988) 9.

115. T.D. Jarvi, E.M. Stuve, in: *Electrocatalysis*, J. Lipkowski, P.N. Ross (Eds.), Wiley-VCH, New York, 1998, 75.

116. S. Wasmus, A. Küver, Methanol oxidation and direct methanol fuel cells: a selective review, *J. Electroanal. Chem*., **461** (1999) 14.

117. J. Kua, W.A. Goddard, Oxidation of Methanol on 2nd and 3rd Row Group VIII Transition Metals (Pt, Ir, Os, Pd, Rh, and Ru): Application to Direct Methanol Fuel Cell, *J. Am. Chem. Soc.,* **121** (1999) 10928.

118. T. Iwasita, Electrocatalysis of methanol oxidation, *Electrochim. Acta*, **47**(2002) 3663.

119. N.M. Markovic, P.N. Ross Jr., Surface science studies of model fuel cell electrocatalysts, *Surf. Sci. Reports*,**45**(2002) 117

120. W. Vielstich, in: *Encyclopedia of Electrochemistry*, A.J. Bard, M. Stratmann (Eds.), **2**, Wiley-VCH Verlag GmbH & Co, Weinheim, 2003, 466.

121. C. Sánchez, E. Leiva, in: *Handbook of Fuel Cells - Fundamentals, Technology and Applications,* W. Vielstich, H.A. Gasteiger, A. Lamm (Eds.), John Wiley & Sons, Chichester, (2003), 93.

122. A. Capon, R. Parsons*,* The oxidation of formic acid at noble metal electrodes: I. Review of previous work*, J. Electroanal. Chem*.,**44**(1973) 1.

123. V. S. Bagotzky, YU. B. Vassiliev, O. A. Khazova, Generalized scheme of chemisorption, electrooxidation and electroreduction of simple organic compounds on platinum group metals, *J. Electroanal. Chem.,* **81**(1977) 229

124. M.I.S. Lopes, B. Beden, F. Hahn, J.M. Leger, C. Lamy, Generalized scheme of chemisorption, electrooxidation and electroreduction of simple organic compounds on platinum group metals, *J. Electroanal. Chem*., **282**(1990) 287.

125. W. Vielstich, X.H. Xia, Comments on "Electrochemistry of Methanol atLow Index Crystal Planes of Platinum: AnIntegrated Voltammetric andChronoamperometric Study"*J. Phys. Chem*., **99**(1995) 10421.

126. K. Franaszczuk, E. Herrero, P. Zelenay, A. Wieckowski, J. Wang, R.I. Masel, A Comparison of Electrochemical and Gas-Phase Decomposition of Methanol on Platinum Surfaces *J. Phys. Chem*., **96**(1992) 8509.

127. E. Herrero, K. Franaszczuk, A. Wieckowski, Electrochemistry of Methanol at Low Index Crystal Planes of Platinum: An Integrated Voltammetric and Chronoamperometric Study*J. Phys. Chem*., **98**(1994) 5074.

128. C. Lamy, J.M. Leger, J. Clavilier, R. Parsons, Structural effects in electrocatalysis: A comparative study of the oxidation of CO, HCOOH and CH3OH on single crystal Pt electrodes, *J. Electroanal. Chem*., **150**(1983) 71.

129. J. Shin, C. Korzeniewski, Infrared Spectroscopic Detection of CO Formed at Step and Terrace Sites on a Corrugated Electrode Surface Plane during Methanol Oxidation*J. Phys. Chem*., **99**(1995) 3419.

130. X.H. Xia, T. Iwasita, F. Ge, W. Vielstich, Structural effects and reactivity in methanol oxidation on polycrystalline and single crystal platinum, *Electrochim. Acta,* **41**(1996) 711.

131. J. Munk, P.A. Christensen, A. Hamnett and E. Skou, The electrochemical oxidation of methanol on platinum and platinum + ruthenium particulate electrodes studied by in-situ FTIR spectroscopy and electrochemical mass spectrometry, *J. Electroanal. Chem*.,**401**(1996) 215.

132. S.G. Sun, in: *Electrocatalysis*, J. Lipkowski, P.N. Ross (Eds.), WileyVCH, New York, 1998, 243.

133. R. Parsons, and T. Vandernoot, The oxidation of small organic molecules: A survey of recent fuel cell related research, *J. Electroanal. Chem.,* **257**(1988) 9.

134. N.M. Markovic and P. N. Ross, Surface science studies of model fuel cell electrocatalysts, *Surf. Sci. Rep*. **45**(2002) 121.

135. A.Capon, and R.Parsons, The oxidation of formic acid at noble metal electrodes Part III. Intermediates and mechanism on platinum electrodes, *J. Electroanal. Chem*., **45**(1973) 205.

136. A. Capon and R.Parsons, The oxidation of formic acid on noble metal electrodes: II. A comparison of the behaviour of pure electrodes, *J. Electroanal. Chem*., **44**(1973) 239.

137. A. Capon, and R. Parsons, The oxidation of formic acid at noble metal electrodes: I. Review of previous work, *J. Electroanal. Chem*., **44**(1973)1.

138. A. Capon, and R.Parsons, The oxidation of formic acid at noble metal electrodes: I. Review of previous work, *J. Electroanal. Chem*., **65**(1975.) 285.

139. B. Beden, C. Lamy, A. Bewick and K. Kunimatsu, The oxidation of formic acid at noble metal electrodes: I. Review of previous work, *J. Electroanal. Chem*., **121**(1981) 343.

140. N.R.d. Tacconi, J.M. Leger, B.Beden, and C. J. Lamy, Electrosorption and electrocatalytic oxidation of formic acid on platinum + rhodium alloys, *J. Electroanal. Chem*., **134** (1982) 117.

141. O. Wolter, J. Willsau, and J. Heitbaum, Reaction Pathways of the Anodic Oxidation of Formic Acid on Pt Evidenced by 18O Labeling—A DEMS Study, *J. Electrochem. Soc*. **132**(1985)1635.

142. B. Beden, A. Bewick, and C. Lamy, A study by electrochemically modulated infrared reflectance spectroscopy of the electrosorption of formic acid at a platinum electrode, *J. Electroanal. Chem*. **148** (1983)147.

143. K. Kunimatsu, and H. Kita, Infrared spectroscopic study of methanol and formic acid absorbates on a platinum electrode: Part II. Role of the linear CO(a) derived from methanol and formic acid in the electrocatalytic oxidation of CH3OH and HCOOH, *J. Electroanal. Chem.,* **218**(1987) 155.

CHAPTER 2

Electrochemical Methods and Characterization Techniques

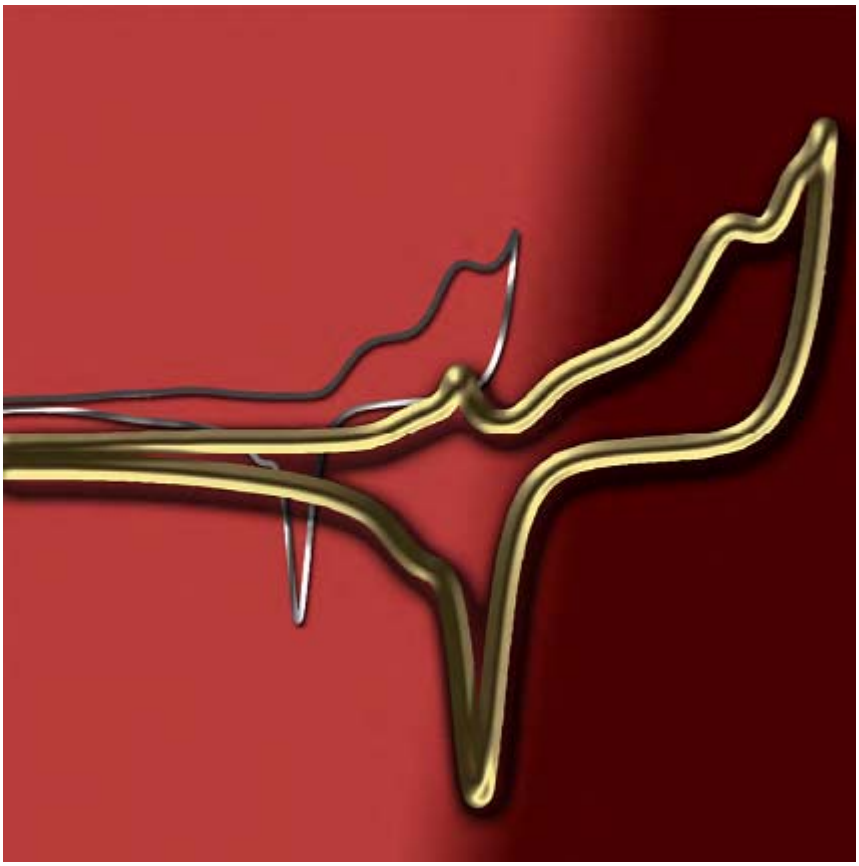

2.1 Polarization of Interfaces

2.1.1 Interfacial Region

Electron transfer is an event in a molecular scale where a negatively charged entity passes through between an electrode and species in solution. The reason for electron transfer to occur is the potential gradient present at the electrode surface, which results from difference in the potential values when two different materials or phases come in contact with each other. For example, if the potential difference between a local electrode and the adjacent solution is 1 V, measured over a gap of 1 nm, then the potential gradient shall be of the order of 10^9 V m^{-1} [1]. When studying the rate of electron transfer, a considerable thought on the potential gradient at the interfacial region is of vital importance.Whenever potential is applied to the electrode surface, a charging characteristics involving the electrostatic effect is observed. Ions and dipoles with opposite charges are most likely attracted to the electrode surface. This eventually results in the formation of "electrical double layer". Movement of ions to the electrode surface causes changes in the potential field and this factor is indispensable when considering the kinetics of electron transfer.

2.1.2 Electrical Double Layer

Suppose there is no electron transfer occurring at the interface of the elecrode and the solution. In other words, no chemical changes take place and so no Faradaic current passes. Such an electrode is called ideally polarized electrode as no electrode reactions occurs within a certain range of potential values [2]. Ideally polarized electrode behaves like a capacitor and only capacitive current flows upon change of potential. Lot of electrodes

poseses this kind of characteristics but only within an electrode potential range called the double-layer range.

As mentioned previously, if a potential is applied to an electrode immersed in a solution, the electrode surface will become charged. The amount of charge on the electrode surface is proportional to the electrode material, the electrolyte and potential applied. If the potential applied is negative, then the electron will flow into the surface eventually turning the surface to be negatively charged. On the contrary, if the applied potential is positive, electron will move out of the surface, gradually making it positively charged. Accompanying this phenomenon is the rational that for every electrode/electrolyte combination, there must be a potential at which the surface shall be neutrally charged. This potential is called zero charge, E_{pzc}. Surface charge on the electrode is in fact balanced by the movement of counter ions from the bulk solution. Extending the argument above, whenever the electrode potential is negative to E_{pzc}, its surface will become negative. Balancing this, the cations and dipoles such as water molecules begin to be attracted to the electrode surface. Similarly, if the potential applied is positive relative to the E_{pzc}, the electrode surface becomes positively charged thus inviting anions and dipoles to its surface. It may be noted that in this case, the orientation of the dipoles will be reversed. Either way, there shall be an organized layer consisting of cations or anions formed very close to the electrode surface resulting from the potential changes. Higher is the applied potential, the stronger is the electrostatic forces produced. As a matter of fact, competition for sites on the electrode surface does exist between the ions and water

dipoles in order to form a well organized double layer. An example of the formation of double layer is depicted in Figure 2.1 [1].

Thus when the potential of an electrode in an aqueous electrolyte is negative to E_{pzc} , its surface will be negatively charged and both cations and dipoles, particularly water molecules, will be attracted to the surface. Moreover, the more negative is the applied potential, the stronger are the electrostatic forces leading to the formation of an organized layer of cations adjacent to the electrode surface. Conversely, positive to E_{pzc}, the electrode surface will be positively charged and the anions and dipoles will be attracted with the orientation of the dipole reversed. In practice, there will be competition between the ions and water dipoles for sites on the surface. The electrostatic forces leading to a totally organized structure are opposed by the thermal motion of the ions. Figure 2.1 shows the generally accepted model for the interfacial region when $E<E_{pzc}$.

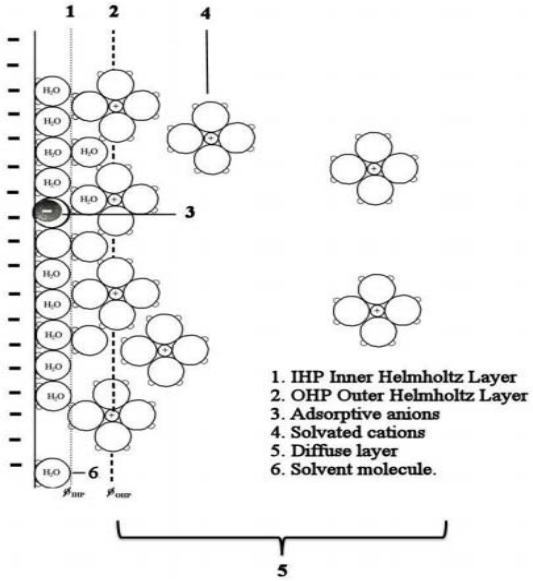

Fig.2.1 *Model of electrical double layer at the interfacial region at the electrode surface for potential negative to the potential of zero charge*

2.1.3 Charging Currents

Any change in the potential of an electrode is the driving force of change in the charge on the metal side of the electrode surface. Coupled to this, ions and dipoles reorganization will also occur in the double layer on the solution side. Changing the potential of the electrode means that there will be electrons flowing into or out of the electrode. In practice, these electrons will eventually pass out through the external circuit and virtually seen as current called "charging current"

Charging current is in addition to the Faradaic current and this comes from the reactive species in the cell. Its presence is always regarded as "noise" as it complicates the signals produced by the reaction desired in the particular experiment setup. It shall be emphasized that the effect of charging current is only a minor problem for short timescale experiments as reorganization of double layer according to the potential change occurs very fast and once the new structure has been formed, the charging current effect can be totally neglected [1].

For example, in cyclic voltammetric experiment, the charging current may be estimated from Equation 1. A typical capacitance value is 0.2 F m^{-2} . Therefore, at scan rates of 0.1 and 100 V s^{-1}, the observed capacitive current density j_{cap} will be 0.02 and 20 A m^{-2}, respectively.

$$J_{cap} = C \times \nu \qquad (1)$$

The current density is given by equation 1. Here C is the capacitance and ν is the potential scan rate. The capacitive current at high scan rate is of the same order of magnitude or higher compared to the Faradaic current for a diffusion controlled reaction.

2.2. Electrode Kinetics

An example of a reduction for a cation can be taken from Figure 2.1. In order for the electron transfer to occur at a potential negative to E_{pzc}, the cation must be as close as possible to the electrode. Let us say it has to sit on the plane of the closest approach. It is important to note that whether or not the electron transfer occurs at the interface, the structure and properties of the double layer remain the same. Also, it may be emphasized that the resulting structure as well as the behaviour of the double layer originates from the electrostatic effect and not the chemical effect. For these reasons, in a system where the electroactive species exist in a large excess of inert electrolyte, solely the ions will determine the characteristics of the double layer. In practice, the effect of double layer is always minimized by using inert electrolyte.

2.3. Adsorption at Electrode Surface

Adsorption is the binding of species from the solution phase to the electrode surface. The adsorbates may be atoms, ions, molecules, reactant, intermediate, or product of the electrode reaction regardless of whether they are organic or inorganic in their nature. Whatever they are, adsorbates do affect the reaction rate as well as the mechanism involved at the electrode. Adsorption of both organic and inorganic species involving either ions or even neutral molecules can occur at the electrode surface and in variety of environments. For instance, consider a covalent bond formed at the electrode surface for the following reactions, e.g.

$$H^+ + e^- + Pt \longleftrightarrow Pt\text{-}H \qquad (2)$$

$$CH_3OH + 2\,Pt \longleftrightarrow Pt\text{-}CH_2OH^+ + Pt\text{-}H \qquad (3)$$

In addition to covalent bonding-based technique, adsorption can also occur by means of electrostatic forces. This can be achieved if the electrode surface is electrostatically charged either positive or negative, which eventually attracts ions or dipoles with opposite charges. The accumulation of species with counter charge enables adsorption via electrostatic method. Feasibility to adsorb electroactive species of interest from solution onto the electrode surface at open circuit is a great advantage. One can always vary the surface charge by varying the electrical potential applied to the electrode surface. Generating a positively or negatively charged electrode surface is also a very simple process as it only requires the application of required potential to the electrode of interest.

2.4. Mass Transport

The supply of reactant and removal of product to / from the electrode surface are essential to a continuing chemical change. For electron transfer to occur, the reactants have to transport themselves towards the electrode surface, and once the reaction is complete, the product will automatically diffuse away from the electrode surface. Generally, there are three different modes of transportations i.e. diffusion, convection, and migration.

Diffusion. The difference of concentration between two points in a solution normally ends up with the movement of a more concentrated species to the area of lower concentration. This will last until the concentration between them becomes equal. This phenomenon which originates from the concentration gradient is called diffusion [1]. It plays an important role

when considering reaction on the electrode. Very often, the electron transfer process occurs in the vicinity of an electrode. For example, when a species O undergoes a reduction process at a considerable rate to become R at the electrode, the concentration of the former at the electrode surface will be lower than in the bulk solution. In other words, the concentration of the reduced species R at the electrode surface will be higher than that in the bulk solution. Fick's first law defines diffusion as diffusional flux which represents the number of moles diffusing per unit area (Equation 4). Fick derived his second law which applies to cases where the change of concentration within a specific area occurs (Equation 5) [3]. In these equations, j_{ox} is the flux, D is the diffusion coefficient, [Ox] is the concentration of the species, and x is the distance of the species from the electrode surface.

$$j_{ox} = -D_{ox} \frac{\partial [Ox]}{\partial x} \tag{4}$$

$$\frac{\partial [Ox]}{\partial t} = -D_{ox} \frac{\partial^2 [Ox]}{\partial x^2} \tag{5}$$

In most of the electrochemical measurements where the oxidation and reduction of active species occurs due to applied electrical potential, the Fick's second law is preferable as the former processes always result in changes of concentration at the electrode surface with the elapse of time.

Convection. The presence of thermal gradient or difference in density within a solution can lead to another form of mass transport namely convection. Convection may

occur in nature or is deliberately induced by means of applying external forces such as shaking or sparging the solution in the electrochemical cell where the electrode reaction occurs. In general, in an unstirred solution, convection is always caused by the chemical reaction in the vicinity of the electrode surface which probably generates slight changes in density or even the temperature. Meanwhile, unnatural convection is always considered as unfavourable as these changes eventually induce the movement within the cell solution. Very often, in electrochemical experiments, convection can be controlled by flowing the electrolyte solution over the electrode surface at a known rate or by the usage of rotating disc electrode [4].

Migration. Migration is a form of mass transport which originates due to the potential gradient induced by the movement of charged species such as ions in the electrochemical cells. As in all electrochemical experiments, the application of electrical voltages between electrodes allows the passing of current creating potential drop at the electrode /electrolyte solution surface. Migration, which occurs due to electrostatic forces, is an integral part of the electrode reaction since it balances any changes in the charge capacity. However, it is not compulsorily desired in all circumstances of electrochemical reactions. To overcome this problem, very often the addition or usage of supporting electrolyte solution to the electroactive solution is done to minimize the effect of migration. Even though the reactant or product in the electrode cell may be charged species, but they will be enclosed by the ions of the supporting electrolyte solution due to the presence of excess electrolyte solution. Therefore, these ions are the charged species which move and not the electroactive species themselves [1].

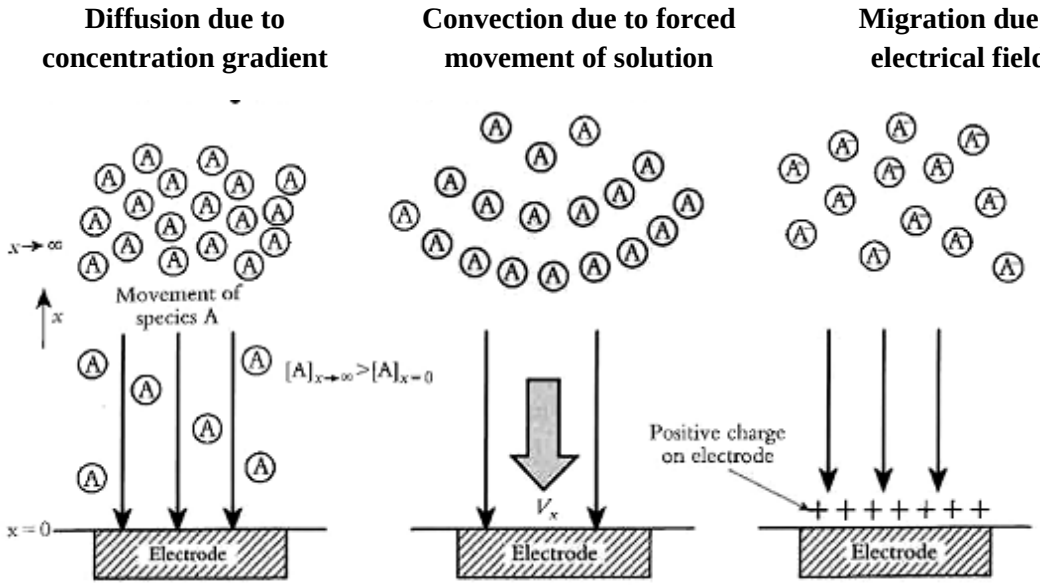

Fig.2.2. *Three different forms of mass transport to the electrode surface for electroative species in solution*

2.5. Voltammetric Techniques

2.5.1 Electrochemical Experimental Considerations

Electrochemistry is the study of electron transfer reactions between electrodes and reactant molecules. During the present work, techniques used for the study of these reactions included cyclic voltammetry (CV), differential pulse voltammetry (DPV), chronoamperometry (CA) and electrochemical impedance spectroscopy (EIS). There are many experimental set ups that can be used for these measurements but the most common used is the three electrode cell. This involves placing the working electrode, reference electrode and counter electrode in a cell containing solution of the redox system under investigation and an inert background electrolyte. The solution is purged with nitrogen or argon gas to remove oxygen and the experiment is controlled using a potentiostat and personal computer.

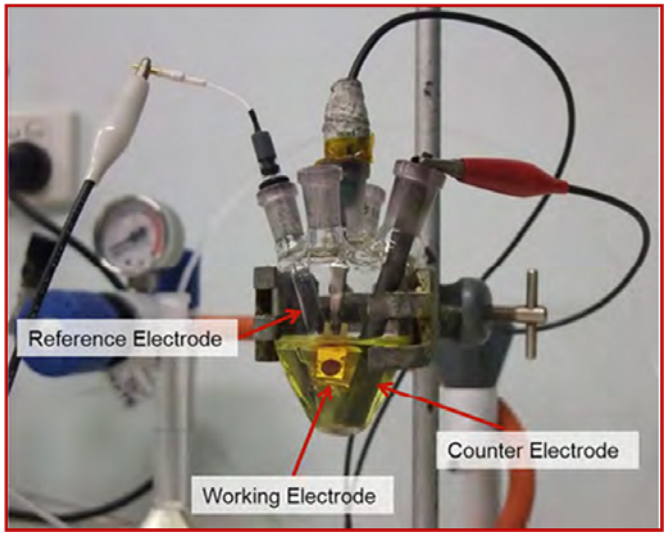

Fig2.3. *Standard electrochemical cell consisting of three electrodes i.e reference electrode, working electrode, and counter electrode.*

The most important part when conducting voltammetric measurements is the apparatus, called potentiostat. It acts as a potential provider to the electrochemical cell and records the resulting flowing current. The output of a voltammetric scan is called voltammogram, which shows the relationship between the applied potential and the current produced. Typically, a definite potential is applied between the reference electrode and the working electrode. Since electron transfer occurs at the working electrode, it is of vital importance to ensure that consistent measurements between the former electrodes is possible, thus the counter electrode is then introduced into the cell.

Most fundamental set ups in the electrochemical cell are designed with an inert gas inlet/outlet. This is required so as to minimize the interference of signals from oxygen during experiments. Nitrogen gas and argon gas are the two most well-known examples of inert gas. Nitrogen is preferred for its low cost, while argon is another option as it is heavier than air.

2.5.2. Cyclic Voltammetry (CV)

Of all the electrochemical methods available for studying the electrode processes, cyclic voltammetry (CV) is probably the most widely used. It offers rapid determination of redox potentials of the electroactive species of interest and convenient evaluation of the effect of the medium on the redox process. It is rarely used for quantitative determinations, but is widely used for the study of redox processes, for understanding reaction intermediates, and for obtaining stability of reaction products. CV consists of linearly scanning the potential of stationary working electrode at a particular scan rate in the forward direction, and then reversing over the same potentialrange in the opposite direction.

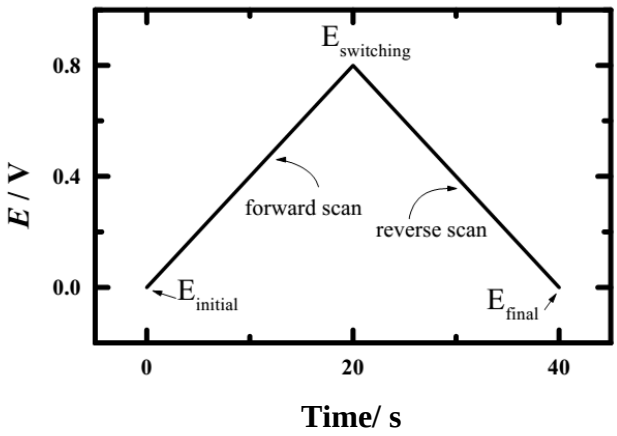

Fig. 2.4. *Variation of potential with time during a cyclic voltammetry experiment.*

For example, the initial scan could be in the negative direction to the switching potential. At that point, the scan would be reversed to run in the positive direction. Depending on the analysis, one full cycle, a partial cycle, or a series of cycles can be performed. The response obtained from a CV can be very simple as shown in Figure 2.5 for the reversible redox system:

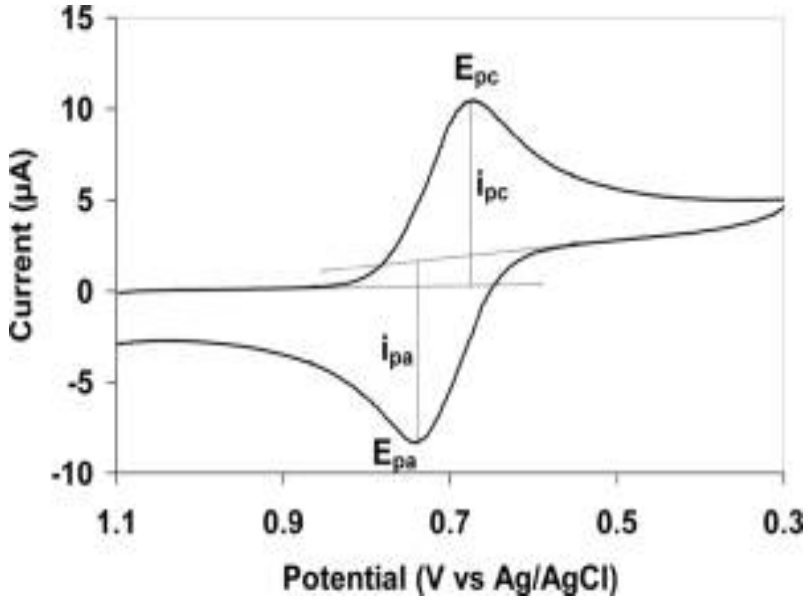

Fig.2.5. *Simple reversible cyclic voltammogram*

A stationary working electrode in an unstirred solution is employed, and the potential is varied at a definite rate as a linear function of time. Typical sweep rates are in the range of 0.5 - 100 V s^{-1}, and the current potential curves no longer have the S-shape known from techniques with infinitesimally small sweep rates, but exhibit peaks. If a rapid triangular sweep is applied, and an oscilloscope or a fast x-y recorder is used, a cyclic voltammogram is obtained. If, for example, the sweep towards lower potentials produces reduced molecules in the vicinity of the electrode, then they are re-oxidized during the reverse sweep to the same concentration which was initially present in the solution, provided that the rate at which the potential is taken back to its initial value is more rapid than the diffusion processes needed to establish equilibrium with the bulk of the solution. If the reduced species undergoes irreversible secondary reactions in a shorter

period than that of triangular sweep, then new waves may be found in the reverse sweep and the height of the wave corresponding to the forward reaction is reduced.

The peak current i_p in the voltammogram is given by Randles-Sevcik equation

$$i_p = \left(2.69 \times 10^5\right) n^{3/2} A D^{1/2} \upsilon^{1/2} C \qquad (6)$$

Here i_p is the peak current (in amperes), n is the number of electrons passed per molecule of the analyte oxidized or reduced, A is the electrode area (in cm^2), D is the diffusion coefficient of analyte ($cm^2 s^{-1}$), ν is the potential sweep rate ($V\ s^{-1}$), and C is the concentration of analyte in bulk solution ($mol\ cm^{-3}$). The midpoint potential of the two peaks in the voltammogram is given by

$$E_{mid} = \frac{E_{red} + E_{ox}}{2} \qquad (7)$$

The midpoint potential E_{mid} can be written as shown in equation 7. Here, E_{red} is the reduction potential, E_{ox} is the oxidation potential, and n is the number of electrons transferred per molecule. The maximum potential E_p in the current-potential curve in the linear scan voltammetric experiment for a reversible one-electron transfer is given by Equation 8.

$$E_p = E_{1/2} - \frac{28.5}{n} \quad \text{mV at 25°C} \qquad \textbf{(8)}$$

Finally, the separation between the two peaks of the voltammogram is given by

$$\Delta Ep = E_{ox} - E_{red} = 2.303RTnF = 59mV/n \text{ (at 25 ° C)} \qquad \textbf{(9)}$$

Hence, depending on what is already known about a given system, one can determine the concentration, the diffusion coefficient, the number of electrons per molecule of the analyte oxidized or reduced, and the redox potential for the analyte.

On the reverse scan, the position of the reoxidation peak is not identical with the potential of the forward scan and depends on the switching potential, if the reverse sweep starts at less than 100 mV/n cathodic of the reduction peak. If the switching potential however, is set further apart, the separation of the two peaks will be 59 mV/n and is independent of the scan rate of the potential scan. These two criteria along with the equal height of the steps in the forward and reverse reactions, are commonly taken as diagnostics for reversible, purely diffusion controlled charge transfer. Cyclic voltammetry has been used to obtain potentials which could also have been measured by slow techniques, and at the same time to demonstrate reversibility of the electron transfers.

If the scan rate in cyclic voltammetry is increased to values greater than 0.1 V s^{-1}, then the redox couples do not behave like ideal reversible systems because electron transfer rates are not infinitely large and the current is controlled by a combination of

diffusion and charge transfer kinetics. This is called the quasi-reversible case and cycling at varying scan rates can be used to measure electron transfer rates.

Reversible and Irreversible Reactions

The term reversible can be misleading and sometimes can be confusing in chemistry as it has different meanings depending on the context of the reaction. In general, reversibility can be divided into two categories; chemical and electrochemical. In order to explain the term 'reversible' clearly, the following simple reaction is considered.

$$\mathbf{O + ne^- \leftrightarrow R} \qquad \mathbf{(10)}$$

The reaction scheme shows that the reactant, in the reduced form, is being transformed into a product by means of having an n number of electron on the time scale of the voltammetric experiment. From the chemical point of view, this Ox/Red couple can be reproduced chemically as represented by the double-sided arrow. Therefore the oxidation reaction can then be expressed as

$$\boldsymbol{R \leftrightarrow O + ne^-} \qquad (11)$$

Meanwhile, the heterogeneous process taking place between a working electrode and an electroactive species at the vicinity of the electrode surface results in electron transfer. In electrochemical experiments, electron transfer can be affected by the potential applied and the concentration of the electroactive species at the electrode. Therefore, the rate constants play a very important role in determining the electrochemical reversibility of a reaction. Using the same chemically reversible reaction scheme given above, electrochemical

reversibility can be explained in the following way. Suppose that the rate constants for reduction and oxidation are k_{red} and k_{ox} respectively.

$$O + ne^- \rightarrow R \qquad \textbf{(12)}$$

When the applied potential is equal to E^0 of the redox couple at equilibrium, the standard electrochemical rate constant can be represented as k^o and will have the units of cm s^{-1}, derived from the concentration of the electroactive species shown in mol $cm^{-3}$and electron transfer to the electrode surface with surface area in cm^2. Here rate constant for electron transfer in both the forward and backward directions of the above reaction scheme can be represented as

$$k_{red} = k^0 \exp\left(\frac{-\alpha_{red} nFE}{RT}\right) \qquad \textbf{(13)}$$

$$k_{ox} = k_{red} \exp\left(\frac{\alpha_{ox} nFE}{RT}\right) \qquad \textbf{(14)}$$

Here the rate constants for both the reduction and oxidation processes driven by the potential difference or overpotential, $\eta = E - E^0$, from the applied electrical potential, E, can be shown by

$$k_{red} = k^0 \exp\left(\frac{-\alpha_{red} nF(E - E_0)}{RT}\right) \quad \textbf{(15)}$$

$$k_{ox} = k^0 \exp\left(\frac{-\alpha_{OX} nF(E - E_0)}{RT}\right) \quad \textbf{(16)}$$

k^o is the rate constant at the electrode surface at equilibrium, α_{red} is the cathodic transfer coefficient, α_{ox} is the anodic transfer coefficient, and R is the gas constant [8.314 (VC) / (mol K)]. α is defined as the fraction of the interfacial potential at the electrode-solution interface that helps in lowering the activation energy barrier for electron transfer process.

Electrochemical reversibility of reaction can be determined by cyclic voltammetric experiments. This method has proven to be extremely helpful when voltammetric responses are being measured within a wide range of scan rates as it is a common practice to record voltammograms over a wide potential window so as to determine the reversibility of a reaction. In practice, there are three parameters which can be used.

(a) Peak to peak separation (ΔE_p)

In a reversible voltammogram, the magnitude of the peak to peak separation, ΔEp, shall be approximately 59 mV at room temperature (298 K) for one electron process regardless of scan rate values. On the contrary, in the case of quasi- and irreversible conditions, the ΔE_p will depend on the potential sweep rate.

(b) Peak current (I_p)

In both the reversible and the irreversible conditions, the peak current generated is proportional to the square root of the scan rate values. However, for quasireversible, scan rate does not hold any effect. At room temperature (at 298 K), simple one electron reduction of O to R can be given as

Reversible,

$$I_p = 0.446FA[O]_{bulk}\sqrt{\frac{FD\upsilon}{RT}} \quad \textbf{(17)}$$

$$= 2.69\times10^5 AD^{1/2}[O]_{bulk}\sqrt{\upsilon} \quad \textbf{(18)}$$

Irreversible,

$$I_p = 0.49\sqrt{\alpha}FA[O]_{bulk}\sqrt{\frac{FD\upsilon}{RT}} \quad \textbf{(19)}$$

$$= 2.99\times10^5 \alpha D^{1/2}[O]_{bulk}A\sqrt{\upsilon} \quad \textbf{(20)}$$

For room temperature experiments, following assumptions apply: electrode surface area, A = 1 cm^2, concentration of species O, [O] = 10^{-3} M, charge transfer coefficient, $\alpha = \beta = 0.5$ cm s^{-1}, diffusion coefficient for species O and R, $D^0 = D^R = 10^{-5} cm^2 s^{-1}$.

c) Waveshape of the forward peak.

The difference between the peak current potential, E_p, and half peak current potential, $E_{1/2}$, comes in handy when distinguishing a reversible voltammetric signal from an irreversible one as discussed below. All the values for the parameters used in the equations correspond to those at room temperature (at 298 K).

Under reversible condition,

$$\boldsymbol{E}_{\boldsymbol{p}} - \boldsymbol{E}_{1/2} = 2.218\frac{\boldsymbol{RT}}{\boldsymbol{F}} \qquad \textbf{(21)}$$

Whereas, under irreversible reduction

$$\boldsymbol{E}_{\boldsymbol{p}} - \boldsymbol{E}_{1/2} = 1.857\frac{\boldsymbol{RT}}{\boldsymbol{F}} \qquad \textbf{(22)}$$

or

$$\boldsymbol{E}_{\boldsymbol{p}} - \boldsymbol{E}_{1/2} = \frac{44.7}{\alpha}\,\mathrm{mV} \qquad \textbf{(23)}$$

and under irreversible oxidation

$$\left|E_p - E_{1/2}\right| = 1.857\frac{RT}{(1-\alpha)F} \qquad \textbf{(24)}$$

During the present work, cyclic voltammetry experiments were performed using CH Instruments potentiostat (CHI 760D) with the three electrodes set up. All potentials are quoted against the Ag/AgCl reference electrode unless otherwise stated.

2.5.3. Differential Pulse Voltammetry (DPV)

The characteristics of cyclic voltammetric method discussed above has revealed that they are useful analytical tools in electrochemical measurements as the current flowing, resulting from the electroactive species in the solution, is proportional to the concentration. Relationship between current and concentration gives quantitative information on the system studied and this can be clearly seen if diffusion controls the current magnitude. Although sensitivity-wise, CV is a superior method, it lacks the ability to distinguish between Faradaic and capacitive currents. In differential pulse voltammetry, (DPV), fixed voltage pulses are superimposed on a linear potential ramp and are applied to the working electrode at a period of selected time just before the potential pulse drops. The current is measured twice, first at a point just before the pulse is being imposed, and then again just before the pulse begins to drop. The interesting point in DPV is that when a potential pulse is applied to an electrode, the capacitive current flows proportionally, but decays exponentially with time. The magnitude of the Faradaic current, on the other hand, decreases as an exponential function versus $(t)^{1/2}$. Figure 2.6 shows a typical diagram on how potential pulses are applied on a linear ramp. The first current measured, $i(t_1)$ is subtracted from the second one, $i(t_2)$, and the difference [$\Delta t = i(t_2) - i(t_1)$] is plotted against the applied potential. The resulting voltammogram shows current peaks which are in direct proportion to the concentration of the electroactive species of interest.

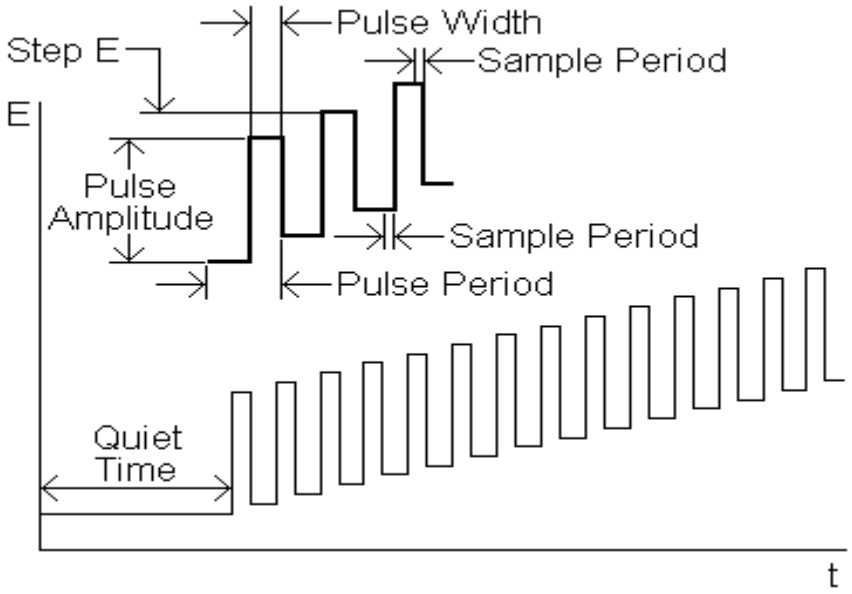

Fig.2.6. *Excitation signal for differential pulse voltammetry.*

In DPV, the charging current contribution is quite small, about more than an order of magnitude less than that in normal-pulse voltammetry, and is, therefore, negligible. Conversely, the Faradaic current decays according to the square root of time, producing an excellent signal to noise ratio. Due to these enhanced characteristics, DPV enables the detection at nano-molar level (1 μg L^{-1}) thus proving useful in electrochemical sensing applications. All DPV experiments were performed in this work were recorded on a CH Instruments potentiostat (CHI 760D) using the standard three-electrode setup.

2.5.4. Chronoamperometry (CA)

Chronoamperometry involves applying a fixed potential to a working electrode for a defined period of time. This technique is often used in electrocatalytic applications, where the potential is fixed at a value which will maximise the production of the desired species over an extended period of time while maintaining the activity of the electrode surface. Chronoamperometry is also used in electroanalysis, where it can be used to monitor the

presence of a known species by recording the current passed as a function of time. The Faradaic component of this current for a planar electrode at time t is described by the Cottrell equation: [5]

$$i = \frac{nFAD^{1/2}C_0}{\pi^{1/2}t^{1/2}} \quad \textbf{(25)}$$

Chronoamperometry is also used extensively in the electrochemical formation of a variety of materials. This material synthesis aspect is generally performed once the electrochemical behaviour of the working electrode/plating solution interface has been determined through the use of other electrochemical techniques such as cyclic voltammetry. These supporting techniques allow the parameters to be determined for the chronoamperometry. These include the initial potential and the appropriate potential range required for electrodeposition to occur. The deposition time can then be varied in consideration of the initial electrode surface as well as the desired size, shape and coverage of the electrodeposit. Chronoamperometry is a powerful tool, not only for the generation of nanostructured surfaces but it can also shed light on the growth of nanostructures formed through other protocols. This is especially true for the chemical synthesis of nanoparticles, where one of the rate determining steps for the reduction of the metallic salts is the chemical composition of the solution, and in particular, the choice of the chemical reductant. While many investigations have been performed for the chemical growth of such nanostructures, chronoamperometry is a facile method to understand the reduction behaviour of metallic salts as a function of the applied potential. This applied potential is of vital importance to the growth of the nanostructures as it can

influence the shape, size, crystallographic orientation and nucleation behaviour of the nanostructures [6]. Additionally, as the electrochemical reaction can be terminated by controlling the deposition time, intermediate structures can easily be isolated and studied, providing a means of investigating the growth of the nanostructured materials. Chronoamperometry has been used in this work for the synthesis of palladium nanoparticles, as well as for the investigation of the nanoparticles towards electrocatalytic applications. These experiments were performed using a CH Instruments potentiostat (CHI 760D) with the three-electrode configuration.

2.5.5. Electrochemical Impedance Spectroscopy (EIS)

Electrochemical impedance spectroscopy is used to investigate the electrical and electrochemical behaviour of an electrode/electrolyte interface. Impedance is similar in concept to the more familiar notion of resistance. However, impedance is not restricted by several definitions placed on an ideal resistor, such as that the response is independent of the frequency, the current and voltage through the resistor are in phase, and it follows Ohm's law for all currents and voltages [7]. In the complex setting of an AC signal applied to an electrode/electrolyte interface, impedance provides a more adequate measure of the opposition to the flow of current.

Electrochemical impedance experiments are performed by the application of an AC signal of fixed amplitude and a set potential to the working electrode, and the frequency of the ac signal is varied typically between 10^{-2} Hz to 10^{6} Hz. The impedance (Z) or dynamic resistance to the sinusoidal current flow is calculated as the ratio of the applied potential to

the current passed at time t (Equation 26), which is analogous to the measurement of resistance in linear systems. This relationship is then calculated using the right side of Equation 26 [7], which is expressed as a function of the maximum voltage (V^0), the maximum current (I^0), the angular frequency of the signal ($\omega=2\pi f$, where f is the frequency of the ac signal), the phase difference (θ) between the voltage and current and the time (t).

$$Z = \frac{V(t)}{I(t)} = \frac{V_0 \sin(\omega t)}{I_0 \sin(\omega t + \theta)} \quad \textbf{(26)}$$

The impedance may also be written in the Cartesian form given in Equation 27 [7], where the impedance at a given angular frequency is the sum of a real impedance value (Z_r) and an imaginary impedance value (Z_i) multiplied by j.

$$Z(\omega) = Z_r(\omega) + jZ_i(\omega) \quad \textbf{(27)}$$

This equation is the basis of the Nyquist plot, in which $-Z_i$ is plotted against Z_r (also referred to as -Z" and Z', respectively). These plots may contain a number of different elements including hemispherical or depressed hemispherical regions as well as linear sections. While the analysis of these plots is not a trivial matter, a great deal of information can be gained about the system. Typically, these impedance spectra are analysed by matching the different features present with the electrical behaviour of an equivalent circuit, often composed of elements such as resistors, capacitors and inductors which may be connected in series or in parallel. This combination of elements describes a number of basic processes, including ohmic resistance, capacitance, constant phase elements (CPEs) and Warburg impedance [8].

EIS has been used in this work to investigate whether the modification of electrode showed altered impedance behaviour compared to that of bare electrodes. EIS spectra were recorded using the Autolab PGSTAT-30 with FRA (Eco-Chimie) software using a standard three-electrode setup.

2.6. Material Characterisation Techniques

While the electrochemical formation and behaviour of electrodeposited films is of critical importance in the creation of materials for electrocatalytic applications, it is equally as important to understand the physical structure of the material. This stems from the well-reported connection between the electrochemical behaviour and factors such as the size, shape, porosity, crystallography and chemical composition of the electrodeposited material. A number of different material characterisation techniques were employed in this work, including scanning electron microscopy (SEM), energy dispersive X-ray spectroscopy (EDX), X-ray photoelectron spectroscopy (XPS), UV Visible spectroscopy and are briefly described below.

2.6.1 Scanning Electron Microscopy (SEM)

One of the most common methods for characterising the morphology of electrodeposited materials is scanning electron microscopy (SEM). While based on similar principles to the conventional optical microscopy, SEM offers a number of advantages for the analysis of electrodeposited surfaces. One of these is the high resolving power which can be achieved by SEM. In this technique, the sample is probed using a beam of electrons rather than visible light, where the former has a considerably smaller wavelength of 0.4 Å for an electron with an energy of 1000 eV [9]. Imaging is achieved by directing a beam of electrons from an

electron gun source down an evacuated chamber through the use of magnetic lenses which collimate and focus the beam to a fine point [10]. When this electron beam is incident upon the sample, a number of reactions are possible. These include the release of secondary electrons, where the excitation of a surface electron causes its emission from the surface, or the release of X-rays, light or heat. The incident electrons, known as primary electrons, may also be detected, either through their reflection from the surface as backscattered electrons or after their transmission through the surface [11]. The emission of secondary electrons is a surface sensitive phenomenon and is used in the case of SEM to provide a three-dimensional image of the surface by scanning (or rastering) the electron beam across the surface and correlating the intensity of the detected secondary electrons with the position of the beam on the surface. Imaging in this method can be used to resolve surface features smaller than 10 nm (down to 1 nm). SEM has been used in this work to characterise the morphology of the deposits in order to understand how the deposition parameters affect the coverage, shape and size of the deposits.

2.6.2. X-ray Photoelectron Spectroscopy (XPS)

Another form of elemental analysis is X-ray photoelectron spectroscopy (XPS). The general principle of this technique is that a beam of incident X-rays excites electrons from atoms in the surface, which can lead to the emission of the electrons from the surface [12]. The detection of emitted electrons has a few important consequences for XPS, such as the need to operate under high vacuum [13-14] so that the mean free path of the emitted electrons is increased. High vacuum is also required to minimize any losses in the energy of the emitted electrons. Since the energy of the X-ray beam (hv) is known, the kinetic energy of the

emitted electrons (E_K) can be measured and a correction for the work function of the solid (E_W) can be made and thus the characteristic binding energies (E_B) of the elements present on the surface can be determined[14] as given by Equation 28 [15]. Any loss in the kinetic energies due to collision with gases in the chamber will lead to alterations in the recorded binding energies and intensities, and so a high vacuum is required to obtain reliable results.

$$E_K = h\nu - E_B - E_W \qquad \textbf{(28)}$$

The analysis of a sample by XPS is a particularly surface sensitive technique, with electrons emitted from approximately the top 10 nm of the surface [13, 16]. Although the incident X-rays may penetrate further into the sample, the emitted electrons from these regions do not possess enough energy to overcome the inelastic collisions which take place as they travel to the surface of the material and are, therefore, not used to provide any information on the surface composition [12]. Another advantage of XPS as an analytical tool compared to EDX is that it offers greater amount of information than just the elemental composition of the surface. For example, the electronic configuration of the electron orbitals can be observed at defined binding energies as separate peaks, such as the 5/2 and 3/2 orbitals of the Palladium 3d shell. The binding energies of the outermost electron shells are often of interest in XPS as they are more susceptible to changes with respect to the chemical environment. For example, in the case of a native oxide on a Palladium film, the binding energy of the Pd $3d_{5/2}$ and $3d_{3/2}$ orbitals will shift to higher binding energies, as the more electronegative oxygen atoms withdraw the electron densities of these palladium orbitals and the emission of electrons from

these partially positive palladium atoms becomes increasingly difficult. These properties allow the detection of surface oxides, alloying (where the altered electronic configuration shifts the binding energy of the constituent atoms) and the oxidation states of elements, demonstrating the power of XPS for the chemical analysis of a wide variety of surfaces [15]. During the present work, XPS was used to confirm the presence of palladium nanoparticles over platinum substrate and to investigate whether the metal has been oxidised onto the surface. The measurements were carried out by Mac-2 analyzer using the Mg Kα line (1253.6 eV) as the incident radiation.

2.6.3. Ultraviolet and Visible (UV-VIS) Spectroscopy

UV-VIS spectroscopy involves the measurement of the absorption of near-ultraviolet and visible light as a function of wavelength by a sample. The visible region of the spectrum comprises of photon energies of 36 to 72 kcal/mole, and the near ultraviolet region extends this energy range to 143 kcal/mole. These energies are sufficient enough to promote outer electrons to higher energy levels. UV-VIS spectroscopy is usually applied to molecules and inorganic ions or complexes in solution. The uv-vis spectra have broad features that are of limited use for sample identification but are very useful for quantitative measurements. The concentration of an analyte in solution can be determined by measuring the absorbance at a particular wavelength and applying the Beer-Lambert Law:

$$A = \varepsilon\, c\, l$$

(Where A= absorbance, c = sample concentration in moles/liter & l = length of light path through the sample in cm.) UV-VIS spectroscopy was used in the present work to determine

the predominant species present in three different electrolytic compositions viz. (i) $FeCl_3/FeCl_2$ in 1 M HCl, (ii) $FeCl_3/FeCl_2$ in 0.5 M H_2SO_4, and (iii) $Fe_2(SO_4)_3/FeSO_4$ in 0.5 M H_2SO_4.

2.6.4. Energy-Dispersive-X-Ray-Fluorescence (ED-XRF)

Energy-Dispersive-X-ray-Fluorescence is a convinient analytical tool for elemental analysis. The atoms in the sample material, which could be any solid, powder or liquid, are excited by X-Rays emitted from a X-ray tube. All element specific X-ray fluorescence signals emitted by the atoms after the photoelectric ionisation are measured simultaneously in a fixed mounted semi-conductor detector. An energy dispersive X-ray fluorescence (EDXRF) spectrometer makes use of the fact that the pulse height of the detector signal is proportional to the X-ray photon energy. Usually a multichannel analyzer is used for display and providing the data. Here each channel counts the number of photons with a certain energy. The radiation intensity of each element signal, which is proportional to the concentration of the element in the sample, is recalculated internally from a stored set of calibration curves and can be shown directly in concentration units. EDXRF can detect elements in the Periodic Table between atomic numbers 11 (Na) and 92 (U). Samples can be analyzed non-destructively. Elements in concentrations from as low as a few parts per million to 100% may be analyzed. EDXRF was used in the present work to determine presence of trace metallic impurities in the Single walled Carbon Nanotubes (SWCNTs). The spectra were recorded by Jordan Valley EX-3600-TEC spectrometer having Rh target and Ge secondary target operated at 40 kV and 500 mA.

2.7. References

1. D. Pletcher, *A First Course in Electrode Processes*, Electrochemical Consultancy, 1991.
2. R. P. Buck, Diffuse layer charge relaxation at the ideally polarized electrode *J. Electroanal. Chem.* **23** (1969) 219.
3. A. Fick, On liquid diffusion. *Journal of Membrane Science* **100** (1995) 33.
4. A. M. Bond, *Broadening Electrochemical Horizons*, Oxford University Press, Oxford, 2002.
5. D. Grujicic, B. Pesic, Electrodeposition of copper: the nucleation mechanisms. *Electrochim. Acta* **47** (2002) 2901.
6. L. P. Bicelli, B. Bozzini, C. Mele, L. D'Urzo, Int. A Review of Nanostructural Aspects of Metal Electrodeposition, *J. Electrochem. Sci.* **3** (2008) 356.
7. E. Azzarello, E. Masi, S. Mancuso, in *Plant Electrophysiology* (Ed.: A. G. Volkov), Springer Berlin Heidelberg, 2012, pp. 205.
8. X.-Z. Yuan, C. Song, H. Wang, J. Zhang, in *Electrochemical Impedance Spectroscopy in PEM Fuel Cells*, Springer London, 2010, pp. 139.
9. M. M. Woolfson, in *The Fundamentals of Imaging from Particles to Galaxies*, Imperial College Press, London, 2012, pp. 41.
10. FEI, *An Introduction to Electron Microscopy*, 2010.
11. S. Liao, B. Li, Y. Li, in *PEM Fuel Cell Electrocatalysts and Catalyst Layers Fundamentals and Applications*, Springer London, London, 2008, pp. 487.
12. D. Pleul, F. Simon, in *Polymer Surfaces and Interfaces*(Ed.: M. Stamm), Springer Berlin Heidelberg, 2008, pp. 71.

13. D. Sebilleau, in *Magnetism: A Synchrotron Radiation Approach*, Vol. 697(Eds.: E. Beaurepaire, H. Bulou, F. Scheurer, J.-P. Kappler), 2006, pp. 15.
14. H.-L. Lee, N. T. Flynn, in Handbook of Applied Solid State Spectroscopy (Ed.: D. R. Vij), Springer, Springer US, 2006, pp. 485.
15. H. R. Verma, in *Atomic and Nuclear Analytical Methods*, Springer Berlin Heidelberg, 2007, pp. 213.
16. N. H. Turner, in *Encyclopedia of Analytical Chemistry*, John Wiley & Sons, 2006, pp. 1.

CHAPTER 3

Synthesis of Palladium Nanoparticles using Potentiostatic Pulse Electrodeposition

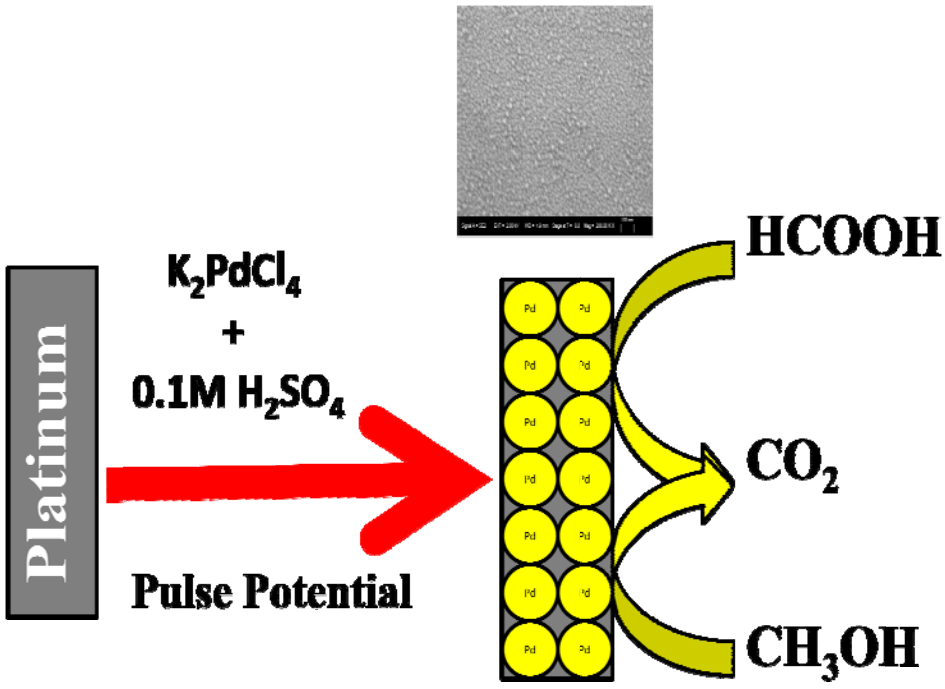

3.1 Introduction

In recent years, the fabrication of nanostructured materials and the exploration of their properties have attracted much attention from scientists in various fields [1–3]. Continuing interest in nanosized noble metal particles has been driven by their promising physical and chemical properties, which are quite different from those of the bulk materials [4–6]. Intensive studies have been devoted to their use as catalysts and sensors, as well in a new generation of optical, electronic and magnetic devices [7–11]. These applications are closely related to their size- or shape-dependent properties such as size quantization, optical and electronic properties, surface effects, chemical reactivity, and self-assembly ability. Among these studies, some have been directed towards the synthesis of palladium (Pd) nanoclusters [12–15], because of the important role played by Pd in catalysis [16], hydrogen storage [17], and chemical sensors [18].

Pd is an important transition metal with high catalytic activity [19,20], although it is not used as widely as Pt [21]. Recently, much attention has been focused on the preparation of Pd nanoparticles [22] because of large surface area-to-volume ratio, lower price than that of Pt, and especially the unique function in absorption of hydrogen [23,24]. Pd nanoparticles have been prepared by a variety of techniques including chemical liquid deposition [25], refluxing alcohol reduction, hydrogen reduction and electrochemical deposition, where in general, the nanoparticles are formed by reduction of metal ions presence of stabilizers [26-30]. Moreover, most of the nanoparticles must be pre-synthesized through reduction of a metal

salt by reducing agents in solution [31,32]. Often the catalyst particles are stabilized in a suitable solid matrix or by surface modification using polymers or ligands [33-35]. However, poor stability of the Pd particles under these conditions has been reported. In addition, this type of stabilization results in the loss of catalytic activity to a great extent [36]. During the present studies, a direct method for the deposition of Pd nanoparticles on a platinum electrode was developed. A considerable effort has been made in recent years to use tiny fuel cells as replacements for batteries in portable electronics. The advantages of using miniature fuel cells over conventional batteries are their much higher stored energy density and ability to be immediately recharged by replacing the fuel cartridge [37]. The electrochemical oxidation of small organic molecules such as CH_3OH and HCOOH has been the field of intensive research for the development of direct fuel cell [38-42].

Formic acid electro-oxidation is a two-electron electrochemical reaction on Pt electrode and is known to occur via a so-called dual pathway mechanism [43-46]. The direct oxidation of formic acid to CO_2 proceeds via a reactive intermediate (mainly HCOOad) formation (Pathway I). On the other hand, the indirect pathway involves the formation of adsorbed CO intermediate (CO_{ad}). The formed CO_{ad} is a strong poisoning species and is finally oxidized to CO_2 at higher potential (Pathway II).

Pathway I: $$HCOOH \rightarrow HCOO_{ad} \rightarrow CO_2 + H^+ + e- \quad (1)$$

Pathway II: $$HCOOH \rightarrow CO_{ad} + H_2O \rightarrow CO_2 + 2H^+ + 2e- \quad (2)$$

For direct formic acid fuel cells, Pathway I is a desirable reaction route to enhance the overall cell efficiency and avoid poisoning of the catalyst. However, oxidation of formic acid on pure Pt electrode surface predominantly takes place through Pathway II which significantly reduces Pt electrocatalytic activity. Therefore, much attention has been focused on the surface modification to mitigate the poisoning of Pt [47–49].

Electro-oxidation of methanol on Pt electrode surface is combined with several steps of dehydrogenation to form CO which is oxidized to CO_2. Poisoning of the electrode surface by CO molecules formed during the methanol oxidation is one of the limitations in the development of direct methanol fuel cells (DMFCs) for commercial applications. Modification of Pt with other metals or metal oxides is considered as one of the best ways to solve this problem.

The present study demonstrates the enhanced electrocatalytic oxidation of formic acid and methanol using palladium nanoparticles (PdNPs) modified Pt electrode. The electrode modification was carried out by potentiostatic electrodeposition of Pd metal on Pt electrode. Mechanism of electrocrystallization of Pd nanoparticles was investigated by cyclic voltammetry and chronoamperometry. Highly monodispersed and homogeneous PdNPs were deposited on the Pt electrode from the electrolyte. Field emission scanning electron microscopy (FESEM) and X-ray photoelectron spectroscopy (XPS) were used to characterize the Pd nanoparticles. The new findings are of fundamental importance to understand

electrochemical formation mechanism of PdNPs allowing a relatively narrow size distribution.

3.2. Experimental

3.2.1. Chemicals and materials

All the chemicals like potassium tetrachloropalladate (K_2PdCl_4), sulphuric acid (H_2SO_4), methanol (CH_3OH), formic acid (HCOOH) and potassium hydroxide (KOH) were of G. R. (Guaranteed Reagent) grade. All the solutions were prepared in Millipore Milli-Q water (~18 MΩ cm).

3.2.2. Electrochemical measurements

Cyclic voltammetry and chronoamperometry were performed using CHI 760D electrochemical workstation with a three electrode voltammetric cell having platinum disk working electrode (area, A = 0.031 cm^2), platinum wire counter electrode and Ag/AgCl reference electrode. All potentials are quoted with respect to Ag/AgCl reference electrode. All experiments were carried out at room temperature (25 ± 1^0C). The solutions were deoxygenated using high purity nitrogen prior to electrochemical experiments. Each measurement was repeated thrice and the average numerical value of each parameter is quoted for discussion (relative error < ± 0.1%).

3.2.3. Characterization of the modified electrode

The morphology of PdNPs was recorded by Auriga make FE-SEM. XPS measurements were carried out by Mac-2 analyzer using Mg Kα line (1253.6 eV) as the incident radiation. The binding energies were calibrated considering the Au $4f_{7/2}$ peak at 83.95 eV. Shift of the binding energy due to surface charging effect was calibrated by assuming binding energy peak of Au $4f_{7/2}$ to be always 83.95 eV .

3.3. Results and discussion

3.3.1. Electrochemical deposition of PdNPs on Pt

3.3.1a. Cyclic voltammetry of 1 mM K_2PdCl_4 in 0.1 M H_2SO_4 at Pt electrode

The cyclic voltammogram of 1 mM K_2PdCl_4 in 0.1 M H_2SO_4 at Pt electrode is shown in Fig. 3.1. During the potential scan in cathodic direction, a surge of cathodic current starts from 0.345 V for the reduction of $[PdCl_4]^{2-}$/Pd as described in equation 3.

$$[PdCl_4]^{2-} + 2e^- \Rightarrow Pd + 4Cl^- \qquad (3)$$

The cathodic peak was observed at 0.287 V. In the reverse scan direction, two crossovers were observed at 0.329 V and 0.402 V between the forward and reverse scans. At more positive potential, the anodic current increased due to the oxidation of the deposited Pd. A broad and short anodic peak was observed with a peak potential at 0.604 V. It indicates that the anodic dissolution of Pd deposits is quite sluggish due to the low chloride concentration in the electrolyte solution and/or the formation of chemisorbed oxygen or a

passive oxide film on the Pd surface. An insignificant amount of Pd still remained on the Pt surface though the anodic scan was completed at 1.1 V. During the potential scan in cathodic direction in the second cycle, both the cathodic onset and peak potentials shifted to 0.503 V and 0.378 V, respectively. However, the anodic peak potential remained the same during the potential scan in anodic direction in the second cycle. Therefore, the characteristic nucleation loop during the first scan cycle and the shift of the cathodic peak to lesser cathodic potential during the second scan cycle suggests that the deposition of Pd(II) on Pd is both kinetically and thermodynamically favourable when compared to the deposition of Pd(II) on Pt. Therefore, Pt does not provide any favourable interaction on Pd deposition i.e. Pd adatoms-adatoms interaction is stronger than the interaction of Pd adatoms with the Pt surface. Thus, Pd deposits on Pt by forming nuclei followed by the three dimensional growth according to the Volmer-Weber growth mechanism.

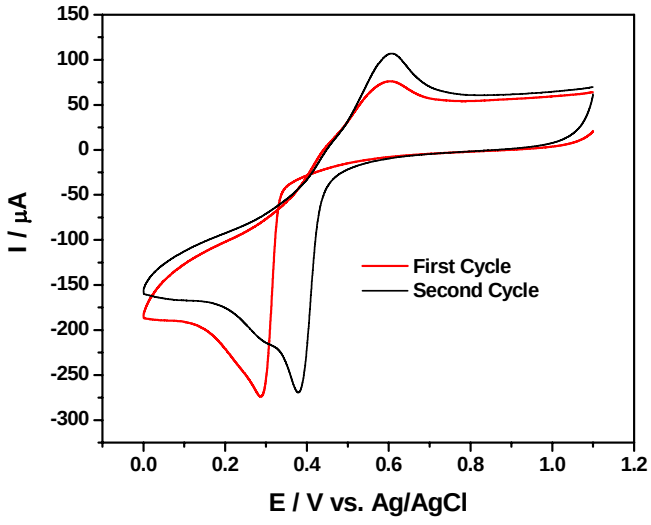

Fig.3.1. *Cyclic voltammogram of 1 mM K_2PdCl_4 in 0.1 M H_2SO_4 at Pt electrode for consecutive first and second cycles*

3.3.1.b Nucleation and growth of PdNPs on Pt electrode

The nucleation and growth phenomena in the initial stages of Pd deposition were investigated by potentiostatic transient measurements. Fig. 3.2 shows current transients obtained at different electrode potentials in the range 0.15V ≤E ≤0.38V. The transients exhibit an initial current decay during 0.001–0.025 s, which cannot be related to the double-layer charging. Such steep falling currents in the initial parts of transients have often been observed in various electrodeposition systems and were related to different processes such as adsorption [50, 51], multistep charge transfer reactions [52] and redox-processes influencing the state of the substrate surface [53].

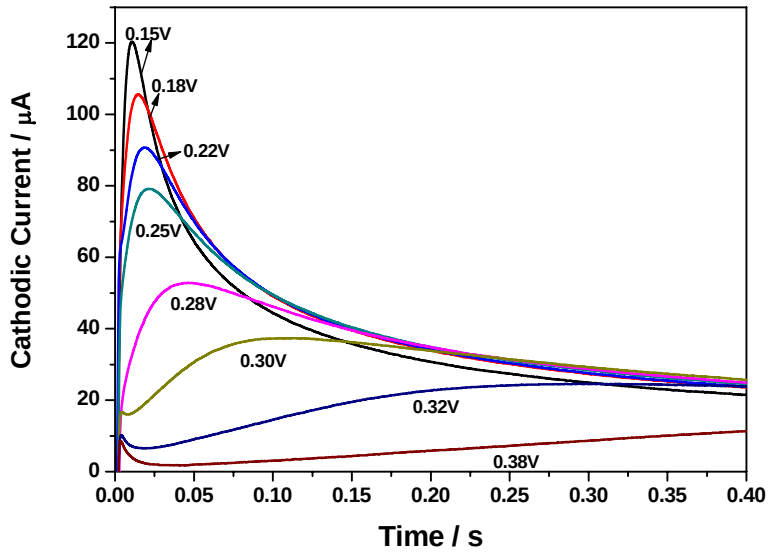

Fig. 3.2. *Current transients for electrocrystallization of palladium at different electrode potentials in the system containing 1 mM K_2PdCl_4 in 0.1 M H_2SO_4 at Pt electrode*

After the initial current decay, the transients in Fig. 3.2 show the characteristic current increase due to nucleation and growth of Pd nanoparticles. The current maxima observed at high cathodic potentials result from the overlap of growing particles and/or their diffusion zones [54-58].

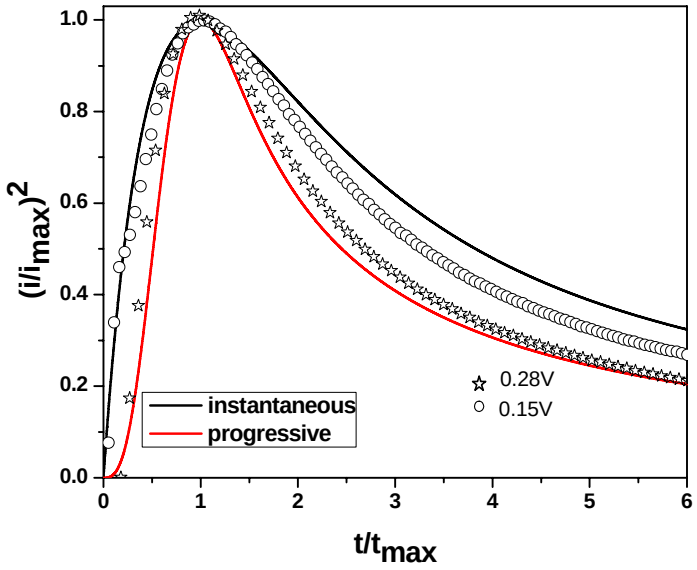

Fig.3.3. *Non-dimensional $(i/i_{max})^2$ vs.(t/t_{max}) plots of current transients for electrocrystallization of palladium at E = 0.28 V and E = 0.15 V compared to the theoretical curves corresponding to the models for progressive nucleation (solid line) and instantaneous nucleation (dashed line).*

According to the model including diffusion-controlled growth of hemispherical particles proposed by Scharifker and Hills [58], the deposition transients for progressive and instantaneous nucleation can be described by the equations:

$$\left(\frac{i}{i_{max}}\right)^2_{progressive} = 1.2254\left(\frac{t_{max}}{t}\right)\left\{1 - exp\left[-2.3367\left(\frac{t}{t_{max}}\right)^2\right]\right\}^2 \quad \text{..... (4)}$$

$$\left(\frac{i}{i_{max}}\right)^2_{instantaneous} = 1.9542\left(\frac{t_{max}}{t}\right)\left\{1 - exp\left[-1.2564\left(\frac{t}{t_{max}}\right)\right]\right\}^2 \quad \text{..... (5)}$$

Experimental current transients for 0.28V and 0.15V are represented in Fig. 3.3 in a non-dimensional $(i/i_{max})^2$ vs. t/t_{max} plot and are compared with the theoretical curves given by Eqs. (4) and (5).

It is clearly seen, that the experimental current transient at 0.28V corresponds to the model involving progressive nucleation. The transient at 0.15V fits relatively well with the theoretical curve for instantaneous nucleation. Hence, for further studies, PdNPs/Pt were prepared by potentiostatic deposition at 0.15 V and the time of deposition was varied.

3.3.2. Characterization of Pd modified Pt electrode

3.3.2.a Field emission scanning electron microscopy (FESEM)

Figures 3.4A, 3.4B and 3.4C show typical FESEM images of Pd nanoparticles electrochemically synthesized at applied potential of 0.15V for 2 seconds, 5 seconds and 10 seconds, respectively. The PdNPs are well-dispersed spherical particles. Their mean diameters and particle diameter distributions were determined by measuring the sizes of at least 200 particles. Mean diameter of the particles prepared at 2 seconds deposition time was 15 nm. When the deposition time was increased to 5 seconds and 10 seconds, the mean diameter increased to 30 nm and 40 nm respectively. These results clearly show that the particle size can be controlled by varying the time of deposition.

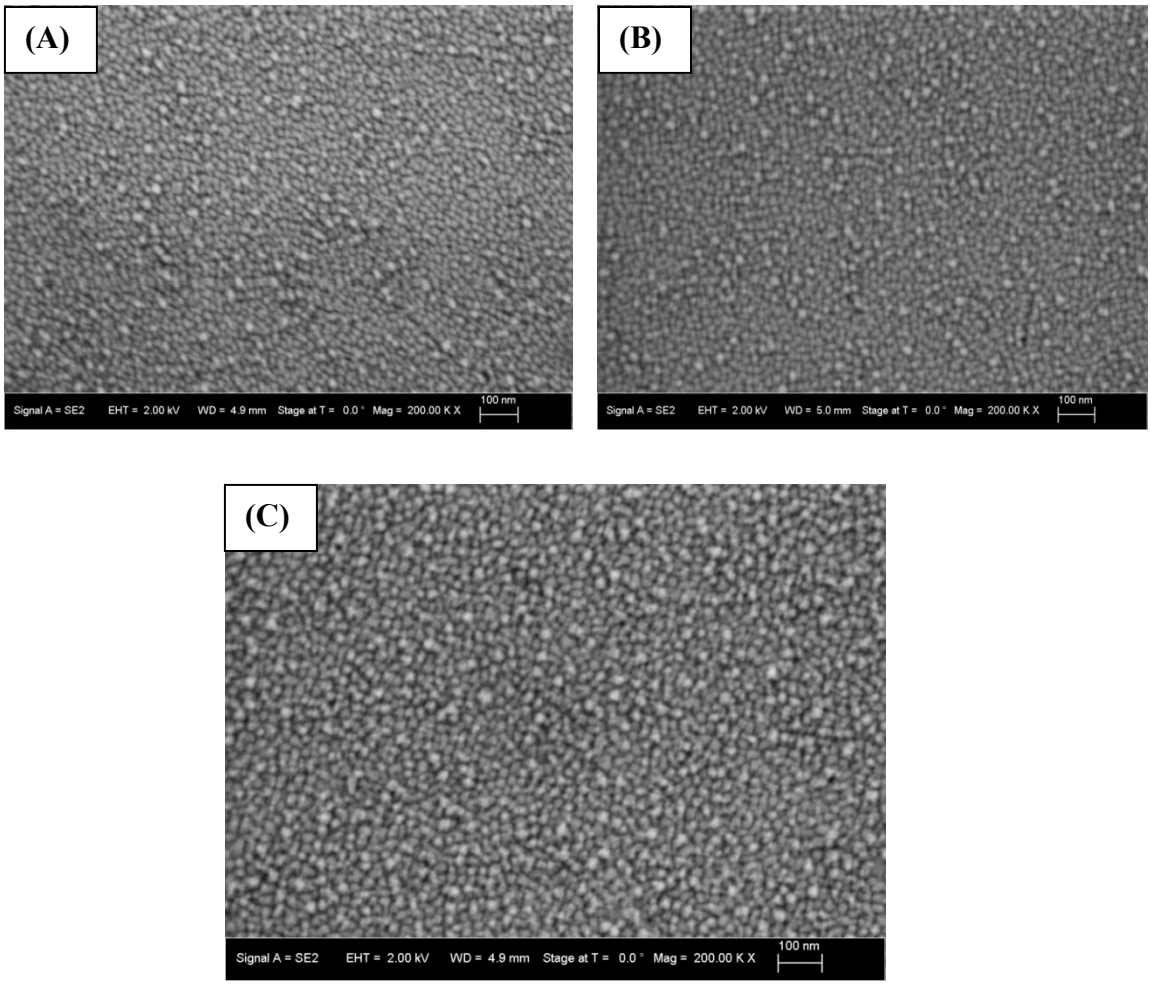

Fig. 3.4*. FESEM images of Pd nanoparticles electrochemically synthesized at applied potential of 0.15 V for (A) 2 seconds and (B) 5 seconds (C) 10 seconds.*

3.3.2b X-ray photoelectron spectroscopy (XPS)

The XPS measurements were carried out for PdNPs deposited on Pt electrode. The initial survey of the binding energy spectrum is shown in Fig. 3.5A and it shows the presence of Pt (4f,4d peaks), Au (4f,3d,5s peaks), Pd-species (3d,3p peaks) and O species (1s peak). The narrow scan spectra in the Au 4f, O 1s and Pd 3d regions for the PdNPs are presented in Fig. 3.5B–D, respectively. The peaks of O 1s and Pd $3d_{5/2}$ were observed at 531.7 eV (Fig. 5C)

and 335.7 eV (Fig. 3.5D), respectively. The Pd $3d_{5/2}$ peak observed at 335.7 eV was attributed to metallic palladium [Pd(0)] and this was in agreement with the results available in literature [59]. The $3d_{3/2}$ peak occurring at higher BE values (BE = 341.5 eV), was due to Pd atoms with lower charge densities. A small shift from the literature value was observed for the chemisorbed oxygen over palladium metal (PdO).

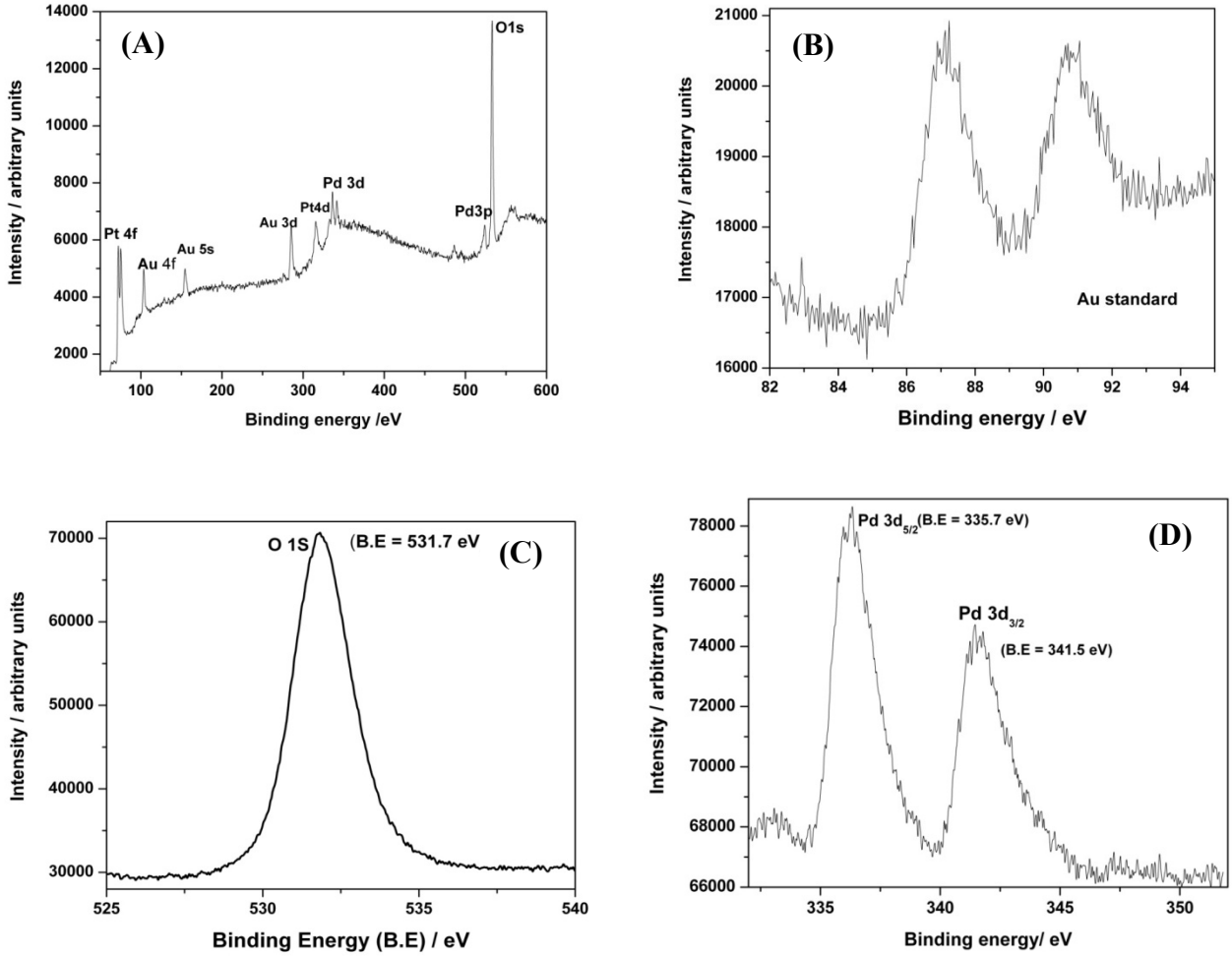

Fig. 3.5. The *XPS spectra of PdNPs. (A) Survey scan, (B) Au 4f region, (C) O 1s region and (D) Pd $3d_{5/2}$ region.*

The above mentioned characterizations of PdNPs suggest that the PdNPs synthesized by the potentiostatic deposition were in metallic form with the presence of chemisorbed oxygen on its surface.

3.3.2 c Effective catalytic surface area (ECSA)

The electroactive surface area of Pd was measured from the palladium oxide stripping analysis [61-64]. The charge value under the striping peak was determined to be 83.49 μC and with the conversion factor of 424 μC cm^{-2} for Pd oxide stripping current (Fig. 3.6), the effective catalytic surface area (ECSA) for the PdNPs/Pt was found to be 0.197 cm^2. This is a large real surface area for the platinum disk electrode with an initial geometric area of 0.031 cm^2. This large surface area arises due to the presence of Pd nanoparticles. The enhanced availability of effective active centers at the modified electrode makes it an ideal electrocatalytic material.

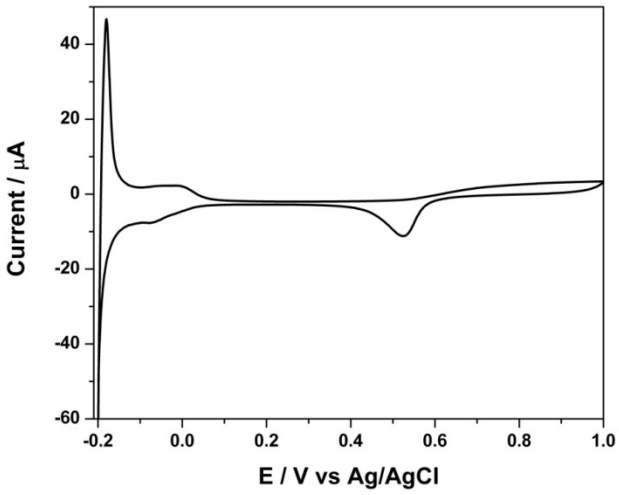

Fig.3.6. *Cyclic voltammogram of Pd nanoparticles in 0.5 M H_2SO_4 at a scan rate of* 0.01 Vs^{-1}

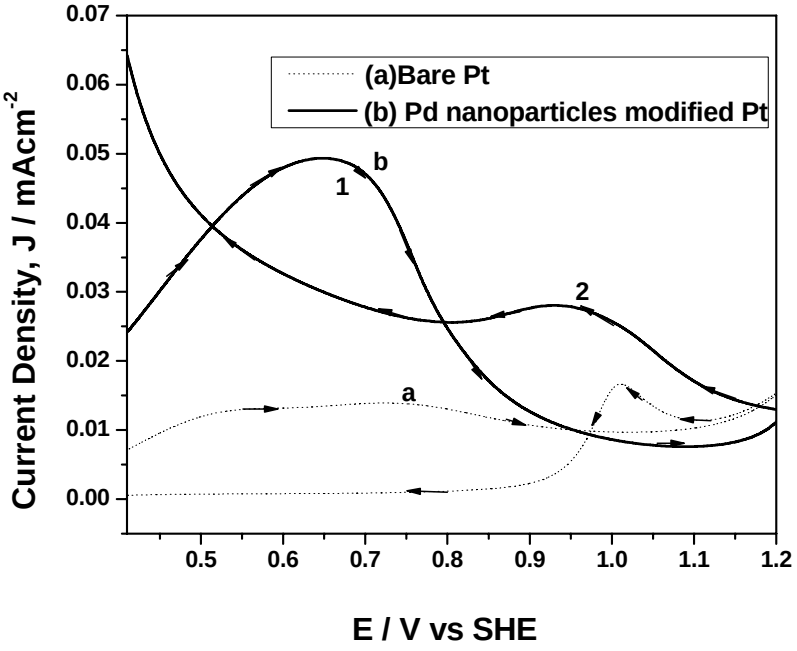

Fig. 3.7*. Cyclic voltammograms (CVs) obtained at bare Pt electrode (curve a) and PdNPs modified Pt electrodes (curve b) in 0.5 M H_2SO_4containing 0.5 M formic acid.*

3.4 Electrochemical oxidation of HCOOH at bare and PdNPs/Pt electrode

Fig. 3.7 shows CVs obtained at bare Pt electrode (a) and Pd nanoparticles (b) modified Pt electrode in 0.5 M H_2SO_4 containing 0.5 M formic acid. Two oxidation peaks were observed at 0.40 V and 0.80 V at the bare Pt electrode during the forward potential scan from 0.2 V to 1 V (curve a). The first broad anodic peak at 0.4 V is assigned to the direct oxidation of formic acid to CO_2 (Pathway I) and the second anodic peak at 0.80 V is related to the oxidation of the CO_{ad} generated during the self-dissociation of formic acid (Pathway II). Effective surface area for the electrooxidation of formic acid is reduced by the presence of

the adsorbed CO intermediates. On the contrary, it is obvious from curve b that modification of Pt electrode by PdNPs greatly improves the catalytic activity of Pt electrode for formic acid oxidation, i.e., the first oxidation peak current (1) is much larger than the second one (2) during the forward scan. It is attributed to the fact that the dehydration of formic acid to form CO requires at least two neighboring Pt sites at the surface (the so-called ensemble effect) [65]. Therefore, the presence of PdNPs on the Pt surface may block the adjacent Pt atoms favouring direct oxidation of formic acid. Secondly, the adsorption energies of the formic acid on Pt and Pd are almost the same. However, the calculated effective barrier for formic acid dehydrogenation is the lowest on Pd surface (0.76 eV) and the highest on Pt surface (1.56 eV) [66]. It is also obvious that the Pd nanoparticles modified Pt electrode shows a remarkably enhanced electrocatalysis for formic acid oxidation. These results suggest that oxidation of formic acid at Pd nanoparticle-modified Pt electrode proceeds mainly through the direct pathway (Pathway I).

3.5 Electrochemical oxidation of CH_3OH at bare and PdNPs/Pt electrode

Fig. 3.8 shows the CVs obtained at bare Pt electrode (a) and Pd nanoparticles (b) modified Pt electrode in 0.5 M KOH containing 0.5 M methanol. Electrooxidation of methanol on the Pt electrode initiates at -0.55 V and reaches the maximum current at around -0.18 V in the positive-going potential scan. Enhancement in the activity for methanol oxidation on PdNPs/Pt electrode may be attributed to the increase of the ECSA.

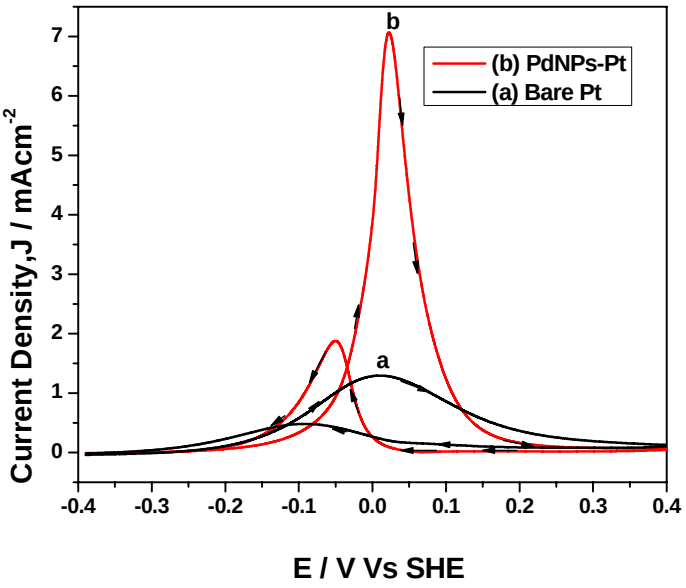

Fig. 3.8. *Cyclic voltammograms (CVs) obtained at bare Pt electrode (curve a) and PdNPs modified Pt electrode (curve b) in 0.5 M KOH containing 0.5 M methanol*

It is interesting to note that CVs for Pd nanoparticles show a very high and large oxidation peak centered at a more negative potential (-0.23 V) in the anodic scan followed by a high and broad secondary oxidation peak in the cathodic scan in contrast to those at the bare Pt electrode. Obviously, PdNPs significantly enhance catalytic activity of bare Pt electrode. The possible reason is that due to reduced CO-poisoning, more active sites on the PdNPs/Pt electrode surface are exposed to reactant molecules. In addition, the ordered architecture of PdNPs can provide a unidirectional electronic channel and reduce the grain boundaries. As is known, the ratio of the forward oxidation current peak (I_f) to the reverse current peak (I_b), I_f/I_b, is an index of the catalyst tolerance to the poisoning species [67]. A high ratio indicates more effective removal of the poisoning species on the catalyst surface. The I_f/I_b ratio of

PdNPs/Pt electrode in alkaline electrolyte was 1.4 times than that of the bare Pt electrode showing better catalyst tolerance to poisoning.

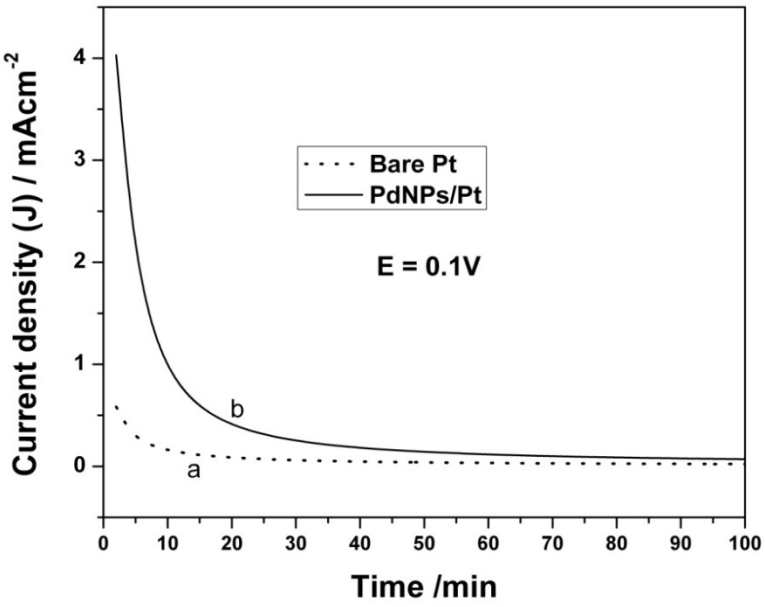

Fig.3.9. *Chronoamperometric curves of bare Pt (curve a) and PdNPs/Pt (curve b) for methanol oxidation, polarized at a constant potential of 0.1 V.*

Catalytic stability of PdNPs/Pt electrode was examined by chronoamperometry. Fig.3.9 shows the chronoamperometry curves recorded at 0.1 V in a solution containing 0.5 M CH_3OH in 0.5 M KOH. Amperometric current densities at the PdNPs/Pt are much higher than those at the bare Pt electrode. Also, a slow current decay was seen over 50 min in case of PdNPs/Pt (Fig. 3.9,curve b), indicating its high catalytic stability and high tolerance to CO like intermediates. Though the current decay was slower for the bare Pt electrode (Fig. 3.9, curve a), the current density was much lower compared to that of PdNPs/Pt electrode.

3.6 Conclusion

The results of this study show that electrocrystallization of palladium in the system containing 1mM K_2PdCl_4 in 0.1M H_2SO_4 at Pt electrode follows the Volmer–Weber growth mode. In the potential range $0.28V \leq E \leq 0.38V$, the electrocrystallization kinetics corresponded to the theoretical model for progressive nucleation. The results indicated that at more negative electrode potentials ($E \leq 0.28V$), the process of electrocrystallization occurs under conditions of instantaneous nucleation. Pd nanoparticles at Pt electrode were prepared by potentiostatic deposition method. The resulting electrode exhibited electrocatalytic activity towards the oxidation of formic acid and methanol, showing a marked improvement compared to bare Pt electrode. This is most likely due to the surface morphologies of the PdNPs which exhibited enhanced accessibility of the surface and produced abundant active sites for the electrocatalytic reactions.

3.7. References

1. Qifeng Zhang, Evan Uchaker, Stephanie L. Candelaria and Guozhong Cao, Nanomaterials for energy conversion and storage *Chem. Soc. Rev*., **42** (2013) 3127.
2. Blake J. Plowman, Suresh K. Bhargava and Anthony P. O'Mullane, Electrochemical fabrication of metallic nanostructured electrodes for electroanalytical applications *Analyst*, **136** (2011) 5107.

3. A. C. Templeton, F. P. Zamborini, W. P. Wuelfing and R. W. Murray, Controlled and reversible formation of nanoparticle aggregates and films using Cu^{2+}-carboxylate chemistry *Langmuir*, **16** (2000) 6682.
4. S. He, J. Yao, P. Jiang, D. Shi, H. Zhang, S. Xie, S. Pang and H. Gao, Formation of silver nanoparticles and self-assembled two-dimensional ordered superlattice *Langmuir*, **17** (2001) 1571.
5. N. Kometani, M. Tsubonishi, T. Fujita, K. Asami and Y. Yonezawa, Preparation and optical absorption spectra of dye-coated Au, Ag, and Au/Ag colloidal nanoparticles in aqueous solutions and in alternate assemblies *Langmuir*, **17** (2001) 578.
6. L. Han, D. R. Deniel, M. M. Maye and C. J. Zhong, Core-shell nanostructured nanoparticle films as chemically sensitive interfaces *Anal. Chem*., **73** (2001) 4441.
7. S. Link and M. A. El-Sayed, Shape and size dependence of radiative, non-radiative and photothermal properties of gold nanocrystals *Int. Rev. Phys. Chem*., **19** (2000) 409.
8. J. J. Storhoff and C. A. Mirkin, Programmed materials synthesis with DNA *Chem. Rev*., **99** (1999) 1849.
9. A. N. Shipway, E. Katz and I. Willner, Nanoparticle arrays on surfaces for electronic, optical, and sensor applications *Chem. Phys. Chem*., **1** (2000) 18.
10. S. Chen and R. W. Murray, Electrochemical quantized capacitance charging of surface ensembles of gold nanoparticles *J. Phys. Chem. B*, **103** (1999) 9996.

11. W. X. Zheng, M. M. Maye, F. L. Leibowitz and C. J. Zhong, Imparting biomimetic ion-gating recognition properties to electrodes with a hydrogen-bonding structured core - Shell nanoparticle network *Anal. Chem.,* **72** (2000) 2190.
12. E. Negishi, C. Cope´ret, S. Ma, S. Y. Lion and F. Liu, Cyclic carbopalladation. A versatile synthetic methodology for the construction of cyclic organic compounds *Chem. Rev.,* **96** (1996) 365.
13. A. de Meijere and F. E. Meyer, Fine feathers make fine birds: The heck reaction in modern garb *Angew. Chem. Int. Ed. Engl.*, **33** (1994) 2379.
14. J. P. Wolfe, R. A. Singer, B. H. Yang and S. L. Buchwald, Highly active palladium catalysts for Suzuki coupling reactions *J. Am. Chem. Soc*., **121** (1999) 9550.
15. A. Suzuki, Recent advances in the cross-coupling reactions of organoboron derivatives with organic electrophiles, 1995–1998 *J. Organomet. Chem*., **576** (1999) 147.
16. O.Niwa, D. Kato, R. Kurita, T.You, Y.Iwasaki, S.Hirono, Electrocatalytic detection of hydrogen peroxide using palladium- nanoparticle dispersed carbon film electrodes *Sens. Mater.,* **19** (2007) 225.
17. A.Rose, S.Maniguet, R.J. Mathew, C. Slater, J.Yao, A.E.Russell, Hydride phase formation in carbon supported palladium nanoparticle electrodes investigated using in situ EXAFS and XRD *Phys. Chem. Chem. Phys*., **5** (2003) 3220.
18. X.H.Zhu, X.Q.Lin, Novel nitrite sensing using a palladium-polyphenosafranine nano-composite *Anal. Sci.*, **23** (2007) 981.

19. M. Baldauf, D.M. Kolb , A hydrogen adsorption and absorption study with ultrathin Pd overlayers on Au(111) and Au(100) *Electrochim. Acta* , **38** (1993) 2145.

20. N.Hoshi, K. Kida, M. Nakamura, M. Nakada, K. Osada, Structural effects of electrochemical oxidation of formic acid on single crystal electrodes of palladium *J. Phys. Chem. B*, **110** (2006) 12480.

21. M. Baldauf, D.M. Kolb, Formic acid oxidation on ultrathin Pd films on Au(hkl) and Pt(hkl) electrodes *J. Phys. Chem*. **100** (1996) 11375.

22. J.H. Ding, D.L.Gin, Catalytic Pd nanoparticles synthesized using a lyotropic liquid crystal polymer template *Chem. Mater*. **12**, (2000), 22.

23. A.Czerwinski, I.Kiersztyn, M.Grden, J. Czapla, The study of hydrogen sorption in palladium limited volume electrodes (Pd-LVE): I. Acidic solutions *J. Electroanal. Chem*. **471** (1999) 190.

24. M.Grden, A. Piascik, Z. Koczorowski, Z, A.Czerwinski, *J. Electroanal. Chem.* **532** (2002) 35.

25. H. Ding and D. L. Gin, Catalytic Pd Nanoparticles Synthesized using a Lyotropic Liquid Crystal Polymer Template *Chem. Mater*., **12** (2000) 22.

26. He Li, S. Zhang, S.Yan, Ye Lin, Yanbiao Ren, Pd/C Catalysts synthesized by microwave assisted polyol method for methanol electro-oxidation *Int. J. Electrochem. Sci.*, **8** (2013) 2996.

27. H. N. Vasan and C. N. R. Rao, Nanoscale Ag-Pd and Cu-Pd alloys *J. Mater. Chem*., **5** (1995) 1755.

28. J. Prabhuram, R. Manoharan and H. N. Vasan, Effects of incorporation of Cu and Ag in Pd on electrochemical oxidation of methanol in alkaline solution *J. Appl. Electrochem*., **28** (1998) 935.

29. E. Sulman, V. Matveeva, A. Usanov, Y. Kosivtsov, G. Demidenko, L. Bronstein, D. Chernyshov and P. Valetsky, Hydrogenation of acetylene alcohols with novel Pd colloidal catalysts prepared in block copolymers micelles *J. Mol. Catal. A*, **146** (1999) 265.

30. G. Schmid, M. Harms, J. O. Malm, J. O. Bovin, R. J. Wan, H. W. Zandbergen and W. T. Fu, Ligand-stabilized giant palladium clusters: promising candidates in heterogeneous catalysis *J. Am. Chem. Soc*., **115** (1993) 2046.

31. J. F. Sa´nchez-Ramirez and U. Pal, Optical absorption of colloidal dispersion of bimetallic nanoparticles Au/Pd *Superficies y Vacio*, **13** (2001) 114.

32. M. Zhao and R. M. Crooks, Homogeneous hydrogenation catalysis with monodisperse, dendrimer- encapsulated Pd and Pt nanoparticles *Angew. Chem., Int. Ed.,* **38** (1999) 364.

33. E. Sulman, Y. Bodrova, V. Matveeva, N. Semagina, L. Cerveny, V. Kurtc, L. Bronstein, O. Platonova and P. Valetsky, Hydrogenation of dehydrolinalool with novel catalyst derived from Pd colloids stabilized in micelle cores of polystyrene-poly-4-vinylpyridine block copolymers *Appl.Catal. A*, **176** (1999) 75.

34. V. Chechik, M. Zhao and R. M. Crooks, Self-assembled inverted micelles prepared from a dendrimer template: Phase transfer of encapsulated guests *J. Am. Chem. Soc*., **121** (1999) 4910.

35. M. Zhao and R. M. Crooks, Dendrimer-encapsulated pt nanoparticles: Synthesis, characterization, and applications to catalysis *Adv. Mater*., **11** (1999) 217.

36. A. B. R. Mayer and J. E. Mark, Transition metal nanoparticles protected by amphiphilic block copolymers as tailored catalyst systems *Colloid Polym. Sci.,* **275** (1997) 333.

37. N. R. Jana, Z. L. Wang and T. Pal, Redox catalytic properties of palladium nanoparticles: surfactant and electron donor-acceptor effects *Langmuir*, **16** (2000) 2457.

38. B.J. Feder, New York Times, New York, 2003.

39. C. Lamy, A. Lima, V. Lerhun, F. Delime, C. Coutanceau, J.M. Leger, Recent advances in the development of direct alcohol fuel cells (DAFC) *J. Power Sources* , **105** (2002) 283.

40. J. Nordlund, G. Lindberbh, A Model for the Porous Direct Methanol Fuel Cells Anode *J. Electrochem. Soc.* **149** (2002) 1107.

41. T. Iwasita, Recent advances in the development of direct alcohol fuel cells (DAFC) *Electrochim. Acta,* **48** (2002)289.

42. R. Parson, Y. Vatsumura, *J. Electroanal. Chem*., **257** (1988) 9.

43. H. Nonaka, Y. Matsumura, Recent advances in the development of direct alcohol fuel cells (DAFC) *J. Electroanal. Chem*., **520** (2002) 101.

44. S. Park, Y. Xie, M.J. Weaver, Electrocatalytic pathways on carbon-supported platinum nanoparticles: Comparison of particle-size-dependent rates of methanol, formic acid, and formaldehyde electrooxidation *Langmuir,* **18** (2002) 5792.

45. B. Habibi, N. Delnavaz, Electrocatalytic oxidation of formic acid and formaldehyde on platinum nanoparticles decorated carbon-ceramic substrate *Int. J. Hydrogen Energy*, **35 (**2010) **8831**.

46. S.C. Chang, L.W.H. Leung, M.J. Weaver, Metal crystallinity effects in electrocatalysis as probed by real-time FTIR spectroscopy: Electrooxidation of formic acid, methanol, and ethanol on ordered low-index platinum surfaces *J. Phys. Chem*., **94** (1990) 6013.

47. W. Chen, J. Kim, S. Sun, S. Chen, Electro-oxidation of formic acid catalyzed by FePt nanoparticles *Phys. Chem. Chem. Phys*., **8** (2006) 2779.

48. E. Herrero, J.M. Feliu, A. Aldaz, Poison formation reaction from formic acid on Pt(100) electrodes modified by irreversibly adsorbed bismuth and antimony *J. Electroanal. Chem*., **368** (1994) 101.

49. M.S. El-Deab, L.A. Kibler, D.M. Kolb, Enhanced electro-oxidation of formic acid at manganese oxide single crystalline nanorod-modified Pt electrodes *Electrochem. Commun*., **11** (2009) 776.

50. M. Neurock, M. Janik, A. Wieckowski, A first principles comparison of the mechanism and site requirements for the electrocatalytic oxidation of methanol and formic acid over Pt *Faraday Discuss*., **140 (**2008) 363.

51. A. Radisic, P.M. Vereecken, J.B. Hannon, P.C. Searson, F.M. Ross, Quantifying electrochemical nucleation and growth of nanoscale clusters using real-time kinetic data *Nano Lett*., **6 (**2006) 238.

52. A. Radisic, F.M. Ross, P.C. Searson, In situ study of the growth kinetics of individual island electrodeposition of copper *J. Phys. Chem. B* **110** (2006) 7862.

53. A. Milchev, Th. Zapryanova, Nucleation and growth of copper under combined charge transfer and diffusion limitations: Part I *Electrochim. Acta* **51** (2006) 2926.

54. A. Kelaidopoulou, G. Kokkinidis, A. Milchev, Nucleation and growth of metal catalysts. Part I. Electrodeposition of platinum on tungsten *J. Electroanal. Chem* **444** (1998) 195.

55. G. Staikov, A. Milchev, in: G. Staikov (Ed.), *Electrocrystallization in Nanotechnology,* Wiley-VCH,Weinheim, 2007 (Chapter 1).

56. E. Budevski, G. Staikov, W.J. Lorenz, *Electrochemical phase formation and growth-An introduction to the initial stages of metal deposition*, VCH, Weinheim, 1996.

57. A. Milchev, *Electrocrystallization: Fundamentals of nucleation and growth, Kluwer Academic Publishers*, Boston/Dordrecht/London, 2002.

58. M. Paunovic, M. Schlesinger, *Fundamentals of Electrochemical Deposition*, Wiley-Interscience, New York, 1998.

59. B. Scharifker, G. Hills, Theoretical and experimental studies of multiple nucleation *Electrochim. Acta* **28** (1983) 879.

60. NIST X-Ray Photoelectron Spectroscopy Database NIST Standard Reference Database 20, Version 3.4. June 06, 2000 http:// srdata.nist.gov/xps/.

61. Rand D A J, Woods R. The nature of adsorbed oxygen on rhodium, palladium and gold electrodes *J. Electroanal. Chem*, **31** (1971) 29.

62. S. S. Mahapatra , J. Datta, Characterization of Pt-Pd/C Electrocatalyst for Methanol Oxidation in Alkaline Medium *Int. J. Electrochem*. 2011, Article ID:563495 (2011).

63. Z. X. Liang, T. S. Zhao, J. B. Xu and L. D. Zhu, Mechanism study of the ethanol oxidation reaction on palladium in alkaline media *Electrochim. Acta* **54** (2009) 2203.

64. M. Grden and A. Czerwinski, EQCM studies on Pd-Ni alloy oxidation in basic solution *J. Solid State Electrochem*. **12** (2008) 375.

65. S. Park, Y. Xie, and M. J. Weaver, Electrocatalytic pathways on carbon-supported platinum nanoparticles: Comparison of particle-size-dependent rates of methanol, formic acid, and formaldehyde electrooxidation *Langmuir* **18** (2002) 5792.

66. Q. Luo, G. Feng, M. Beller and H. Jiao. Formic acid dehydrogenation on Ni(111) and comparison with Pd(111) and Pt(111) *J. Phys. Chem. C* **116** (2012) 4149.

67. Y.Y. Mu, H.P. Liang, J. Hu , J.S.Hu, L. Jiang and L.J. Wan, Controllable Pt nanoparticle deposition on carbon nanotubes as an anode catalyst for direct methanol fuel cells *J. Phys. Chem. B* **109** (2005) 22212.

CHAPTER 4

Electrocatalysis at Polyaniline Modified Pt Electrode

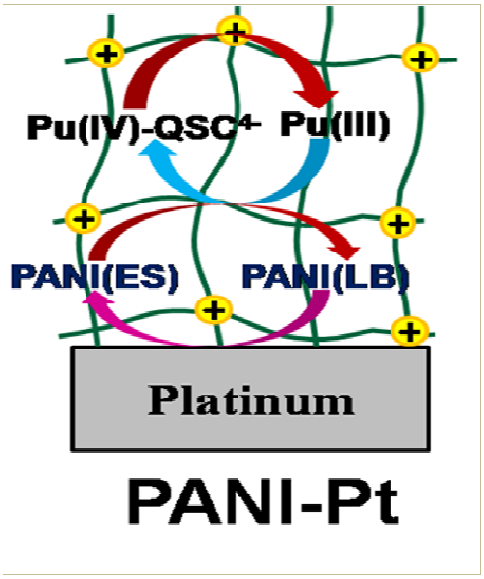

4.1 Introduction

Polyaniline (PANI) coated metal electrode has many applications in electroanalytical chemistry due to its electrocatalytic property of accelerating the rate of heterogeneous electron transfer. Thus, it has been utilized as a sensor material for biomolecules [1-4], small organic molecules [5], inorganic gases [6], noble metal ions like Ag(I) [7] and transition metal ions like Fe(III)/Fe(II) [8]. PANI can exist in three different oxidation states viz. fully reduced leucoemeraldine base (LB), half-oxidized emeraldine base (EB) and fully oxidized pernigraniline base (PB). LB, EB and PB all act as insulators. EB transforms into the conducting emeraldine salt (ES) through acid doping in the strong mineral acid medium. In ES form, the transport of charge carriers within PANI backbone enhances. As a result, the solute species diffuse into porous network of PANI film and participate in the redox reaction at the polymer-solution interface [9,10]. Thus electrocatalytic efficiency of PANI for a particular redox couple like Fe(III)/Fe(II) in mineral acid medium can be enhanced by improving either all or any of the three factors viz. (i) transport of charge carriers within PANI backbone, (ii) diffusion of solution species towards and within the PANI network and (iii) transfer of charge at polymer-solution interface. The electrocatalysis of Fe(III)/Fe(II) redox reaction in sulphuric acid medium at PANI modified platinum electrode was reported by Mandic et al [9], where inhibiting behavior of PANI for Fe(III)/Fe(II) redox reaction was observed. In this context, it is worthy to note that the predominant ionic species of the redox couple is guided by the type of solvent or electrolyte composition. Thus, behavior of PANI film for the same redox reaction viz. Fe(III)/Fe(II) can be improved by the judicial choice of electrolyte composition. It was, therefore, considered interesting to study the influence of

ionic speciation in different electrolytic compositions on the performance of electrocatalysis of PANI/Pt for Fe(III)/Fe(II) redox reaction. In this Chapter, studies performed for electrocatalytic activity of PANI coated platinum electrode for Fe(III)/Fe(II) redox reaction under three different electrolytic compositions viz. (i) $FeCl_3/FeCl_2$ in 1 M HCl, (ii) $FeCl_3/FeCl_2$ in 0.5 M H_2SO_4 and (iii) $Fe_2(SO_4)_3/FeSO_4$ in 0.5 M H_2SO_4 is presented. Donnan interactions of PANI film for these three compositions were investigated in comparison with $[Fe(CN)_6]^{3-}$/ $H_2[Fe(CN)_6]^{2-}$ which are known species of $K_3[Fe(CN)_6]/K_4[Fe(CN)_6]$ in 0.5 M H_2SO_4 [11]. Based on the electrocatalytic behavior of PANI on Fe(III)/Fe(II) redox reaction and the effect of ionic speciation in the electrocatalysis mechanism, experiments were performed to study the electroanalytical performance of PANI for Pu(IV)/Pu(III) couple . There were two motivating aspects, firstly the redox potentials of Fe(III)/Fe(II) and Pu(IV)/Pu(III) couples are similar in 1 M H_2SO_4 and secondly, the existence of Pu(IV) as an anionic complex in 1 M H_2SO_4. This chapter includes the investigations carried out on the chemistry of Pu(IV)/Pu(III) redox reaction on PANI modified platinum electrode. Detailed investigations were carried out to understand the electrocatalytic mechanism of Pu(IV)/Pu(III) couple at the modified electrode.

4.2 Influence of ionic speciation on electrocatalytic performance of polyaniline coated platinum electrode : Fe(III)/Fe(II) redox reaction

4.2.1 Experimental

All chemicals were of Analytical Reagent (A. R.) grade or better and were used as received. All the solutions were prepared in Millipore Milli-Q water. Experiments were carried out at 25 ± 1^0C. All solutions were deoxygenated using high purity nitrogen prior to electrochemical experiments. Electrochemical polymerization and cyclic voltammetry were performed using CHI 440A electrochemical workstation with a three electrode voltammetric cell having platinum disk working electrode (Pt coated quartz crystal microbalance (Pt-QCM) of 0.224 cm^2 area, platinum wire counter electrode and Ag/AgCl reference electrode. All the potentials are quoted with respect to Ag/AgCl reference electrode). Each measurement was repeated thrice and the average numerical value of each parameter is given for discussion (relative error < ± 0.1%). Electrochemical Impedance Spectroscopy (EIS) was performed using Autolab PGSTAT-30 with FRA (Eco-Chimie) software. Impedance was recorded at formal potentials of the respective redox couples (observed from the corresponding CVs on PANI/Pt electrode) with single sine excitation signal of 0.005 V for the frequency range 10^6 Hz to 10^{-2} Hz. Impedance spectra were fitted to electrical equivalent circuits (EEC) and the fits had $\chi^2 \leq 10^{-2}$. Errors of all calculated parameters were within 5% of the reported values. For impedance measurements, platinum disk electrode of area 0.032 cm2 was used as a working electrode. The morphology of PANI film was determined by TESCAN-VEGA-MV 2300T/40 SEM. Absorption spectra were recorded by Evolution-300

UV–Vis spectrophotometer. EDXRF spectra were recorded by Jordan Valley EX-3600-TEC spectrometer having Rh target and Ge secondary target operated at 40 kV and 500 μA.

4.2.2 Results and discussion

Fig. 4.1 shows the 1st (curve-1), 6th (PANI-6, curve-2) and 12th (PANI-12, curve-3) CV cycles recorded between -0.2 V and 1.3 V at 0.1 V s^{-1} during the polyaniline deposition from 0.1 M aniline + 0.5 M H_2SO_4. In 1st cycle, the anodic peak 'a' at 1.13 V appears due to oxidation of aniline producing a large number of aniline cation radicals. The cathodic peaks at 0.66 V and 0.43 V represent reduction of the short chain oligomers produced from aniline cation radicals near the electrode surface.

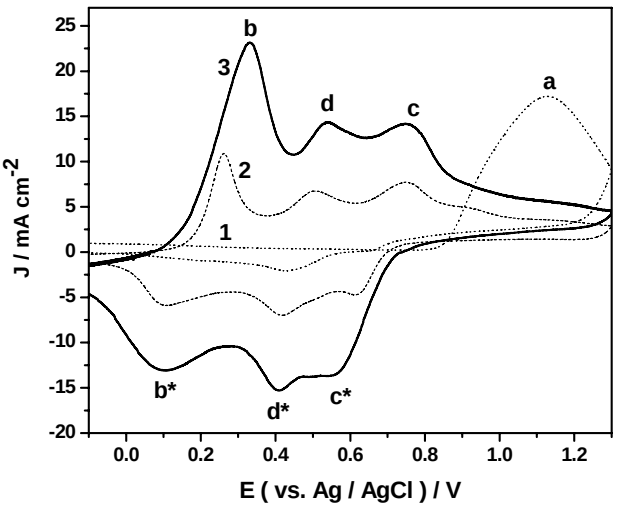

Fig. 4.1. *Cyclic voltammograms during the electropolymerization of aniline on Pt in 0.1 M aniline + 0.5 M H_2SO_4 solution at a scan rate of 0.1 V s^{-1} for (1) 1st (...), (2) 6th (---) and (3) 12th (__) cycles.*

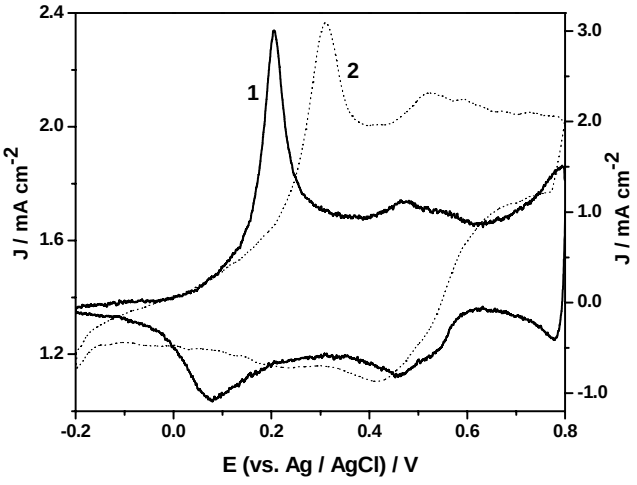

Fig. 4.2. *Cyclic voltammograms of PANI-6 in (1) 0.5 M H_2SO_4 (__) and (2) 1 M HCl (...) at scan rate of 0.01 V s^{-1}.*

The anodic peak 'a' disappeared from the second potential cycle onwards due to autocatalytic growth of PANI. PANI-6 and PANI-12 show three distinct pairs of redox peaks b/b*, c/c* and d/d*. The peaks b/b* and c/c* are attributed to redox transitions between LB/EB and EB/PB forms of PANI, respectively. However, for peaks d/d*, some studies suggest these arising from the presence of polymer containing phenazine rings [12], with others proposing these from oxidation and reduction of degradation products (viz. benzoquinone/hydroquinone) trapped inside the polymer matrix [13]. During growth of PANI, current of each redox peak increases with number of cycles and separation between the pair of peaks (i.e. b/b* , c/c* or d/d*) increases due to thickening of PANI film. Fig. 4.2 shows CVs of PANI-6 in 0.5 M H_2SO_4 (curve-1) and in 1 M HCl (curve-2) which were undistorted for minimum ten consecutive potential cycles between -0.2 V and 0.8 V at 0.1 V s^{-1}. The peaks at 0.2 V (curve-1) and 0.3 V (curve-2) represent the redox transitions between LB/EB in the respective acid solutions.

PANI-6 (Fig. 4.3(A)) exhibits porous film morphology with pore size of a few hundred nm to several μm, whereas PANI-12 (Fig. 4.3(B)) shows crude and spongy polymer network. Cross-sectional view of the back-scattered image (Fig. 4.3(C)) reveals that average thickness of PANI-12 is ~7 μm, whereas its secondary image (inset of Fig.4.3(C)) shows a homogeneous distribution of porous network throughout the entire film. The consumption of charge (ΔQ) for redox switching from LB to EB state was calculated as 31 mC cm^{-2} and 16 mC cm^{-2} for PANI-12 and PANI-6, respectively. Thus the thickness of PANI-6 can be estimated as 3.5 μm assuming the growth of PANI to be linear.

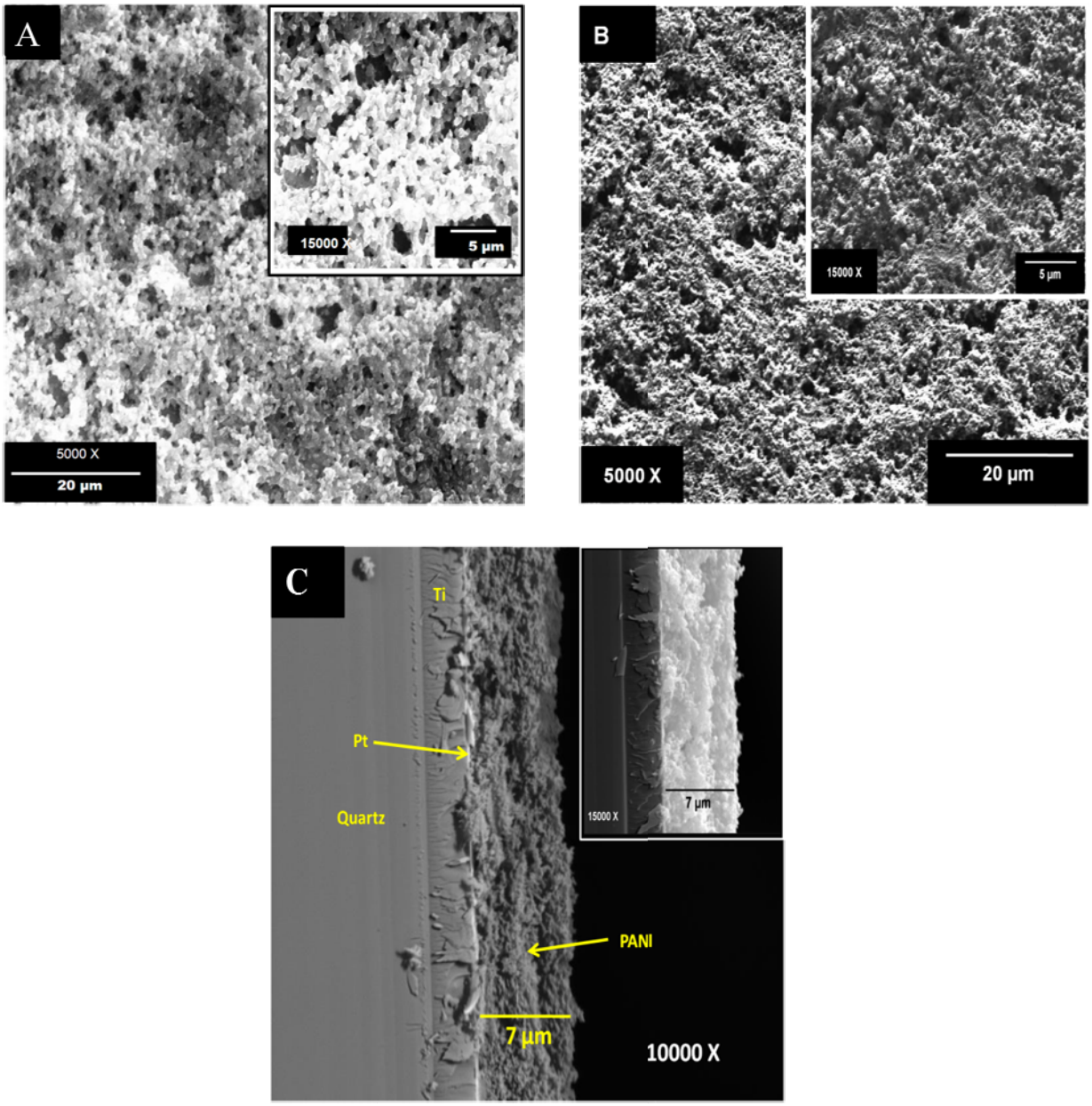

Fig. 4.3. *SEM images of (A) PANI-6 and (B) PANI-12; where each inset shows the higher magnification image of the same. (C) The back-scattered electron images for the cross-section of PANI-12. Inset: Secondary electron image of the same. The electrode used is the Pt coated quartz crystal microbalance (Pt-EQCM).*

There is a probability that more than one species can exist simultaneously in the aqueous solution with the absorbance maxima (Fig. 4.4) corresponding to the predominant species. Absorbance maxima at 420 nm and 304 nm (curve-1) correspond to NC→Fe electronic

transition in $[Fe(CN)_6]^{3-}$ [11,14]. The maxima at 336 nm (curve-2) and at 304 nm (curves-3 and 4) correspond, respectively, to Cl→Fe electronic transition in $[FeCl_4]^-$ tetrahedra [15-17] and to the weak H_2O→Fe electronic transition in $[Fe(H_2O)_6]^{3+}$ octahedra [16-18].

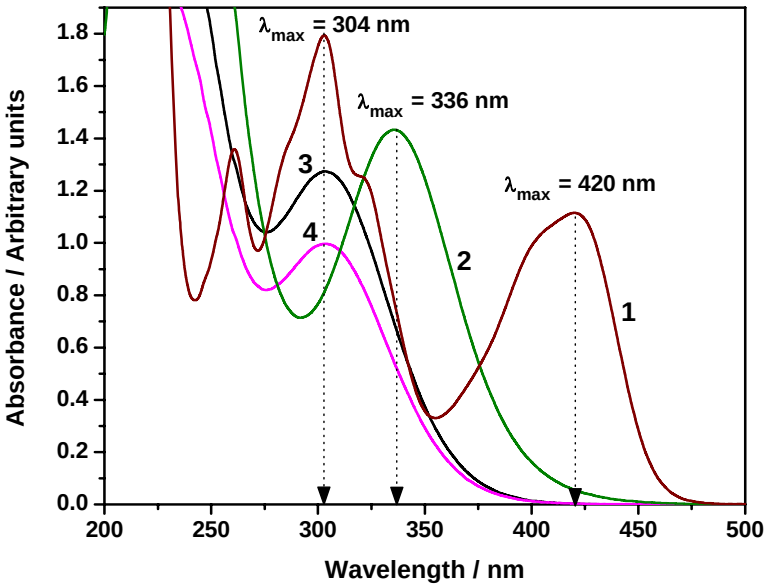

Fig.4. 4. *UV-Vis absorbance spectra of 50 mM (1) $K_3[Fe(CN)_6]$ in 0.5 M H_2SO_4 (__), (2) $FeCl_3$ in 1 M HCl (__), (3) $FeCl_3$ in 0.5 M H_2SO_4 (__) and (4) $Fe_2(SO_4)_3$ in 0.5 M H_2SO_4 (__).*

CVs of 50 mM $K_3[Fe(CN)_6]$ in 0.5 M H_2SO_4 on Pt, PANI-6 and PANI-12 between -0.2 V and 0.8 V at 0.01 Vs^{-1} are presented in Fig. 4.5(A). Cathodic as well as anodic peak currents increased for PANI coated platinum electrode compared to bare platinum electrode as shown in the inset of Fig. 4.5(A); moreover they increased exponentially as the thickness of PANI increased. A dramatic enhancement of the reversibility of Fe(III)/Fe(II) reaction at PANI/Pt was observed compared to bare Pt. Potential difference (ΔE_p) between cathodic and anodic

peaks decreased from 88 mV for bare Pt to 54 mV for PANI-12. On further increasing thickness of PANI film, ΔE_p got saturated, yet the peak currents still increased. However, the reversible nature of CV was destroyed and the peak currents were suppressed from the third potential cycle onwards (Fig. 4.5(B)). Subsequently, PANI/Pt electrode was removed from 50 mM $K_3[Fe(CN)_6]$ in 0.5 M H_2SO_4 solution after completion of the 3rd cycle at 0.01 Vs^{-1} and washed several times with 0.5 M H_2SO_4 (now onwards it would be abbreviated as 'Post-CV-PANI-12/Pt'). Finally, the 'Post-CV-PANI-12/Pt' was characterized by EDXRF and EIS (at E_{dc} = 0.150 V which corresponds to the E_0' of LB/EB transition). EDXRF spectrum showed intense Fe K_α-line at 6.39 keV (Fig. 4.5(C)) for the 'Post-CV-PANI-12/Pt'. The impedance spectra of freshly prepared PANI-12/Pt and the 'Post-CV-PANI-12/Pt' are shown in (Fig. 4.5(D)) and the corresponding EEC fitted to the spectra are shown in Fig. 4.5(E). The PANI-12/Pt and 'Post-CV-PANI-12/Pt' in blank acid solution was found to be the best fitted with EEC shown in Fig. 4.5(E1) and 4.5(E2), respectively. Impedance spectra revealed that charge transfer resistance (R_{ct1}) of PANI/Pt increased from 45 Ω to 118 Ω for 'Post-CV-PANI-12/Pt'. From both the EDXRF and impedance spectroscopy studies, it can be concluded that Prussian blue, a redox polymer ($E_0' \sim$ 0.2 V), gradually grew inside PANI matrix during CV experiments with 50 mM $K_3[Fe(CN)_6]$ in 0.5 M H_2SO_4 and it hindered the transport of charge carriers through the PANI backbone leading to deviation from reversibility during CV experiment in $K_3[Fe(CN)_6]$ solution [19].

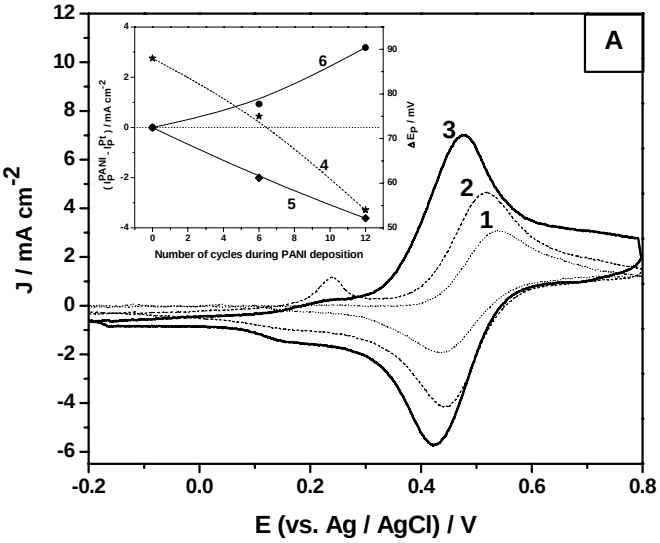

Fig.4. 5. (A) *Cyclic voltammograms of 50 mM $K_3[Fe(CN)_6]$ in 0.5 M H_2SO_4 on (1) Pt (...), (2) PANI-6 (---) and (3) PANI-12 (__) at scan rate of 0.01 V s^{-1}. Inset: The variation of (4) separation between cathodic and anodic peak potentials (ΔE_p) and the difference of (5) cathodic and (6) anodic currents between the PANI film electrode and bare Platinum (i.e. I_p^{PANI} - I_p^{Pt}) versus the PANI film thickness in terms of the number of potential cycles during PANI deposition.*

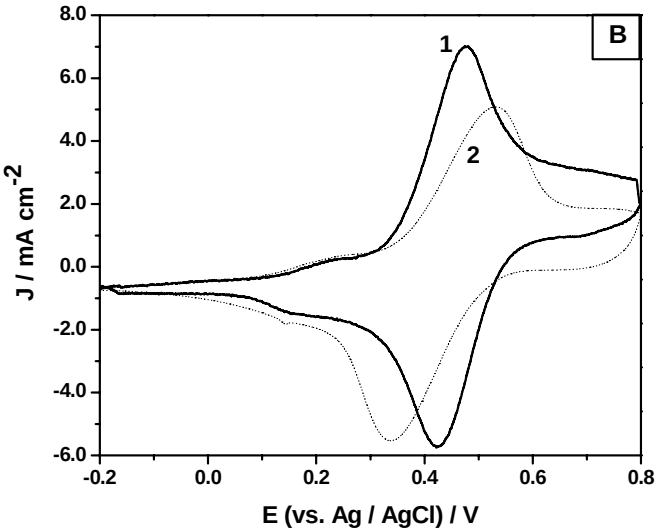

(B) *The cyclic voltammograms of PANI-12/Pt in 50 mM $K_3[Fe(CN)_6]$ + 0.5 M H_2SO_4 at scan rate 0.01 V s^{-1} during (1) 1st and (2) 3rd cycles.*

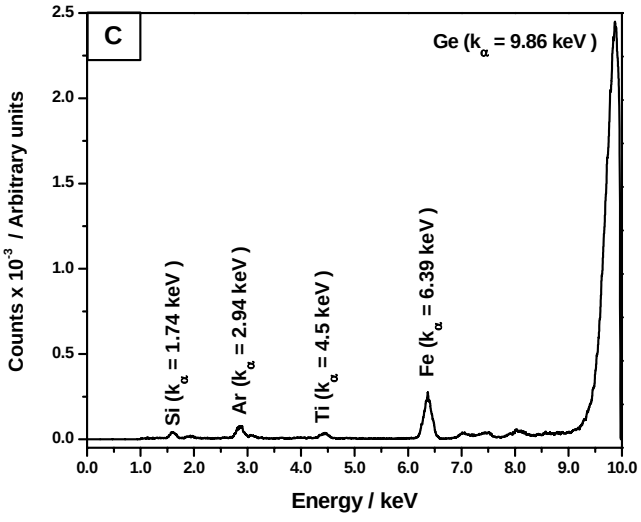

(C) *EDXRF spectrum of 'Post-CV-PANI-12/Pt'.*

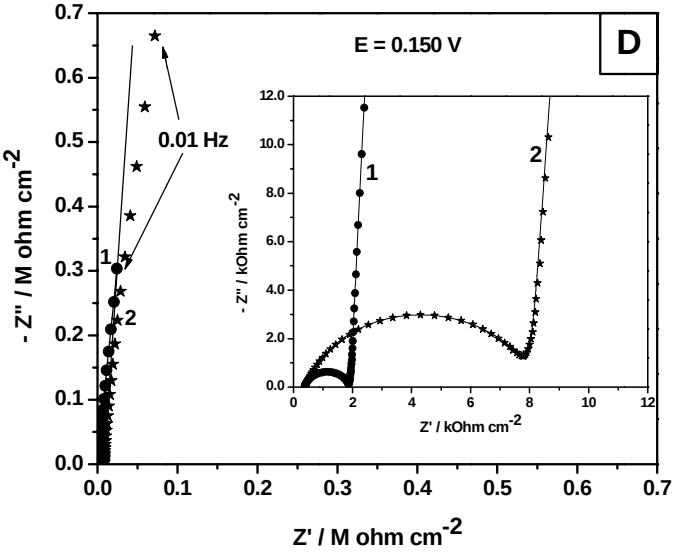

(D) *The Nyquist plot for (1) PANI-12/Pt (solid circular dots) and (2) 'Post-CV-PANI-12'. Solid lines represent the calculated impedance obtained by fitting of the experimental data to electrical equivalent circuit (EEC) as shown in Fig. 4.5(E).*

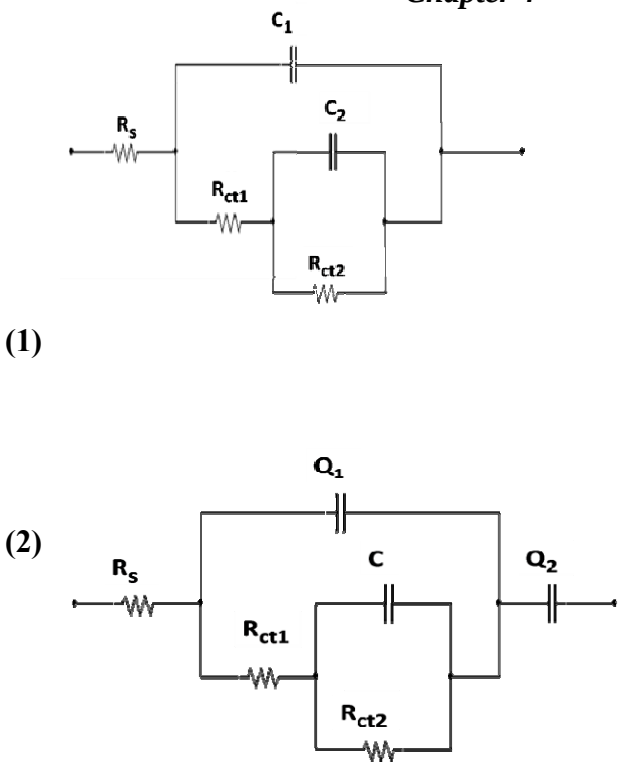

(E) *The best fitted EEC for (1) PANI-12/Pt and (2) 'Post-CV-PANI-12/Pt'.*

Fig.4.6 shows CVs of 50 mM (A) $FeCl_3$ in 1 M HCl, (B) $FeCl_3$ in 0.5 M H_2SO_4 and (C) $Fe_2(SO_4)_3$ in 0.5 M H_2SO_4 on Pt and PANI-12/Pt in the -0.2 V to 0.8 V potential range at 0.01 Vs^{-1}. Potential differences (ΔE_p) between the cathodic and anodic peaks for bare Pt (ΔE_p^{Pt}) and PANI-12/Pt (ΔE_p^{PANI}) and ratio of peak currents (I_p^{PANI}/ I_p^{Pt}) are given in Table 4.1. From Fig. 4.6 and ΔE_p^{Pt} values reported in Table4.1, it is clear that Fe(III)/Fe(II) redox reaction at bare platinum electrode shows more electrochemical reversibility for $FeCl_3$ in 1 M HCl solution, whereas quasi-reversible electron transfer kinetics becomes more prominent as HCl is replaced by H_2SO_4 and finally maximum for $Fe_2(SO_4)_3$ in 0.5 M H_2SO_4 solution. The charge transfer resistance as shown in Table4.2 also followed the same trend as it increased from 177 Ω for $FeCl_3$ in 1 M HCl solution to nearly 821 Ω for $Fe_2(SO_4)_3$ in 0.5 M H_2SO_4 solution. These observations may be attributed to higher Marcus reorganization energy of

Fe(III)/Fe(II) redox reaction for octahedral hydrated complex than for tetrahedral chloro complex. However, the voltammetric peak currents at PANI-12/Pt increased almost twice of that at bare Pt for all the three solution compositions.

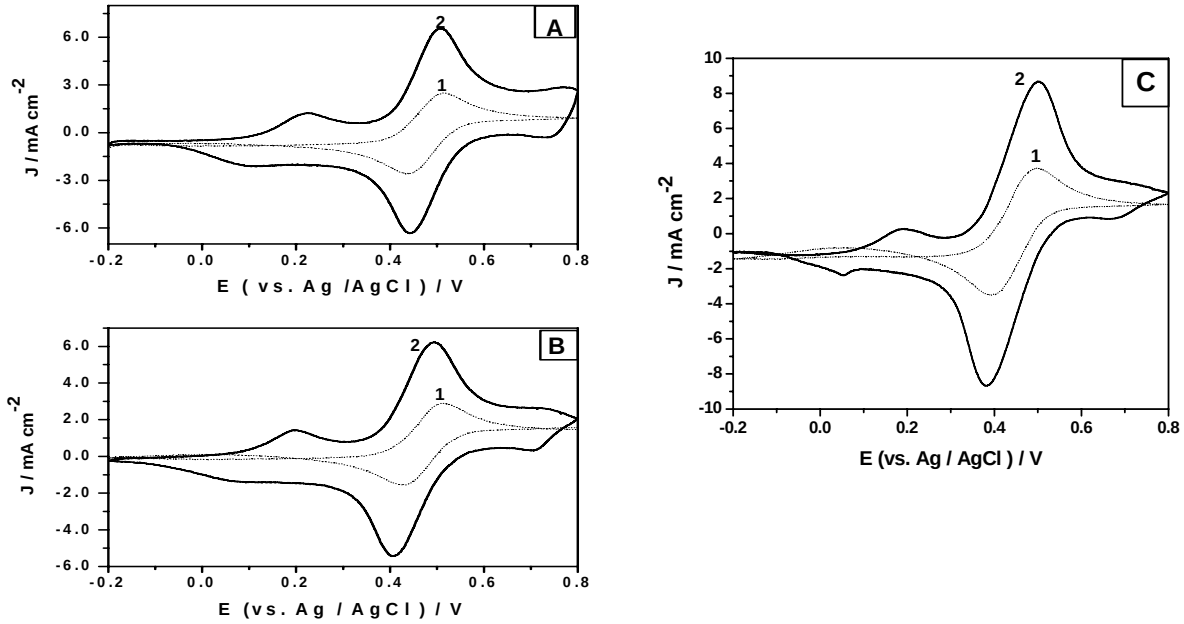

Fig. 4.6. *Cyclic voltammograms of 50 mM* ***(A)*** *$FeCl_3$ in 1 M HCl,* ***(B)*** *$FeCl_3$ in 0.5 M H_2SO_4 and* ***(C)*** *$Fe_2(SO_4)_3$ in 0.5 M H_2SO_4 on (1) bare Pt (...) and (2) PANI-12/Pt (__) at scan rate of 0.01 V s^{-1}.*

Fig. 4.7 shows the Nyquist plots of PANI-12/Pt in 50 mM (curve-1) (A) $FeCl_3$/ $FeCl_2$ in 1 M HCl, (B) $FeCl_3$/ $FeCl_2$ in 0.5 M H_2SO_4 and (C) $Fe_2(SO_4)_3$/ $FeSO_4$ in 0.5 M H_2SO_4 and the same for the blank solution (curve-2). The charge transfer resistance (R_{ct}, Ω), infinite diffusion parameter (W, Ω^{-1} $s^{1/2}$) and finite diffusion resistance (R_d, Ω) of the analyte ions inside the polyaniline matrix were determined by fitting the impedance data both in presence and in absence of analyte with EEC shown in Fig. 4.7(D) and Fig. 4.5(E1).

Table 4.1 *Peak parameters of the cyclic voltammograms for three different solution compositions.*

Solution Composition	I_P^{PANI} / I_P^{Pt}	ΔE_p^{Pt} / mV	ΔE_p^{PANI} / mV
50 mM $FeCl_3$ + 1 M HCl	1.9	79	62
50 mM $FeCl_3$ + 0.5 M H_2SO_4	1.9	83	91
50 mM $Fe_2(SO_4)_3$ + 0.5 M H_2SO_4	1.8	103	120

Table 4.2 *The best fitted and derived parameters of the impedance spectra for three different solution compositions.*

Solution Composition	Charge transfer parameters			Infinite Diffusion Parameter ($W/ m\Omega^{-1} s^{1/2}$)	Finite Diffusion Resistance (R_d/ Ω)
	Bare Pt (R_{ct}/ Ω)	PANI-12/Pt			
		Without analyte (R_{ct2}/ Ω)	With analyte (R_{ct2}/ Ω)		
50 mM $FeCl_3$ + 1M HCl	177.1	141.5	0.65	8.5	6.6
50 mM $FeCl_3$ + 0.5 M H_2SO_4	449.2	134.7	1.1	4.6	28.7
50 mM $Fe_2(SO_4)_3$ + 0.5 M H_2SO_4	821.7	122.7	1.3	4.1	31.5

Finite diffusion impedance (Z_d) of the analyte inside PANI-12/Pt could be modeled as the RC transmission line in the electrical analogue of a tangent hyperbolic function.

$$Z_d = \frac{1}{Y_0\sqrt{(j\omega)}} \coth(B\sqrt{j\omega}) \qquad (1)$$

where, B ($s^{1/2}$) and Y_0 ($\Omega^{-1} s^{1/2}$) are the parameters varied with the diffusion matrix. After optimizing these values, R_d was calculated as: $R_d = B/Y_0$ [20].

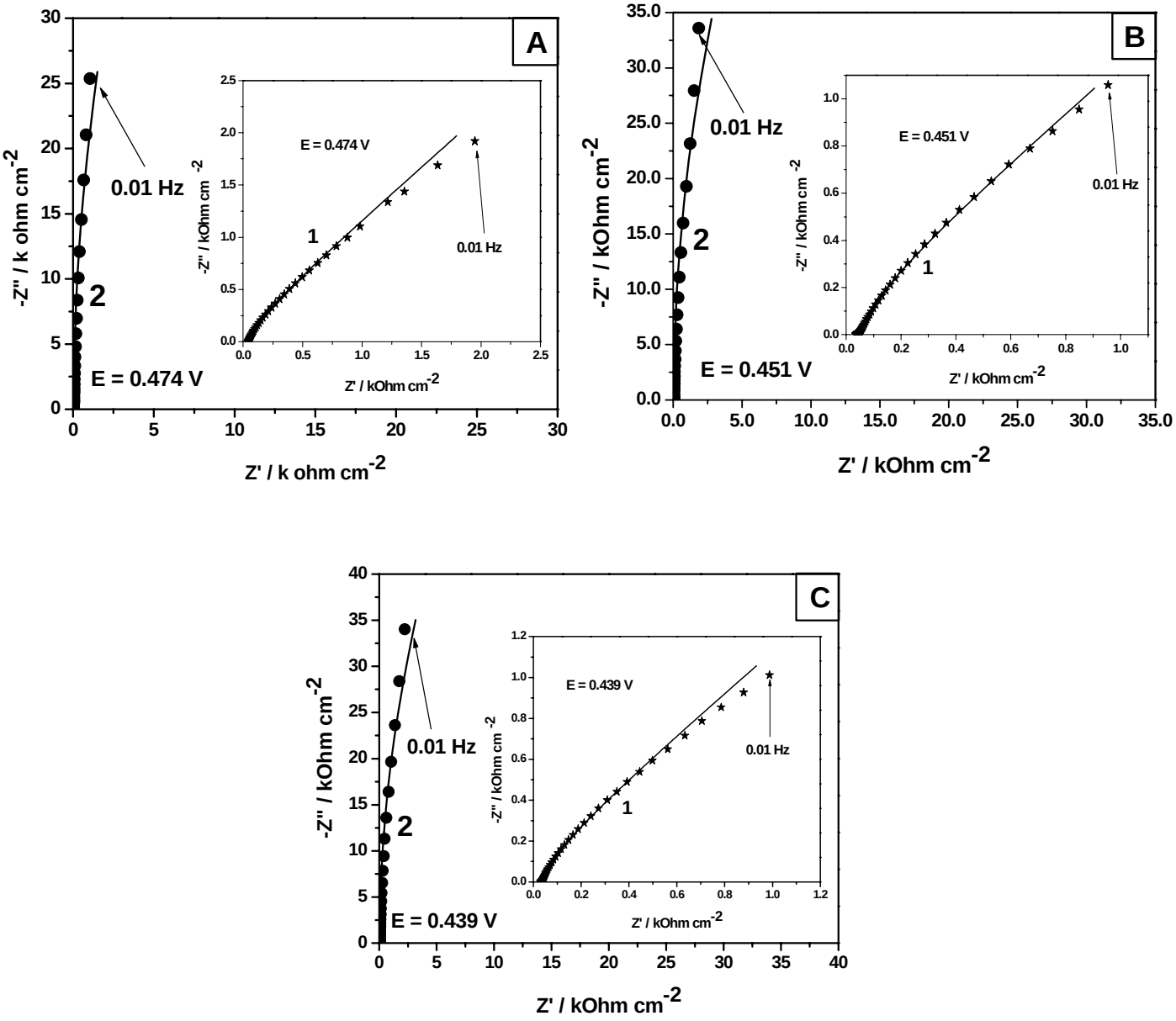

Fig. 4.7. *Nyquist plots for PANI-12/Pt electrode in (1) 50 mM* ***(A)*** *$FeCl_3$/ $FeCl_2$ in 1 M HCl,* ***(B)*** *$FeCl_3$/ $FeCl_2$ in 0.5 M H_2SO_4 and* ***(C)*** *$Fe_2(SO_4)_3$/ $FeSO_4$ in 0.5 M H_2SO_4 and (2) the same for the blank solution. The solid circular dots and* ******* *marks represent the impedance in absence and in presence of the redox analyte, respectively. E_{dc} of PANI-12/Pt electrode was fixed at 0.474 V (for A), 0.451 V (for B) and 0.439 V (for C), which are formal potentials of respective redox couples (observed from the corresponding CV of Fe(III)/Fe(II) redox reaction on PANI-12/Pt electrode). Solid lines represent calculated impedance obtained by fitting of experimental data to electrochemical equivalent circuits (EEC) as shown in Fig. 7(D).*

In 0.5 M H_2SO_4 and 1 M HCl, Nyquist plots (Figs. 4.7(A-C)) of PANI-12/Pt exhibited almost vertical capacitive lines extending down to the lowest frequency (0.01 Hz). A slight deviation from 90º line (just like a beginning of a semicircle) was observed at the lower frequency range and it may be attributed to the non-homogeneity of the film and the low mobility of proton inside the polymer matrix. In presence of redox species, the Nyquist plots inclined on the real component of the impedance axes because of the occurrence of charge transfer at the polymer-solution interface. Table 4.2 shows that the charge transfer resistance at the polymer-solution interface reduced dramatically compared to that at metal-solution interface and this may contribute to enhancement of the electrical current response during Fe(III)/Fe(II) redox reaction at PANI-12/Pt surface. It is interesting to note that the infinine diffusion parameter (W), which has a dimension of conductance, decreased from solution composition (A) to (C) and it suggests that the diffusion of the redox species from infinite solution towards PANI-12/Pt electrode becomes restricted as solution composition is changed from (A) to (C).

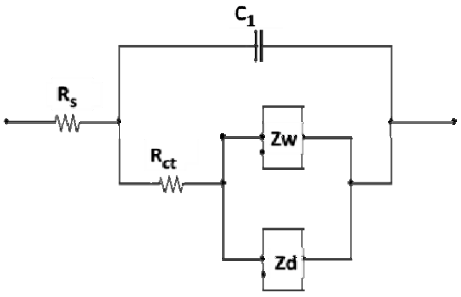

where, Zd ≡

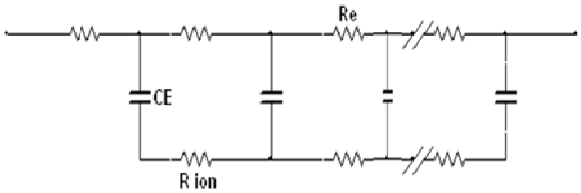

(D) *The best fitted EEC for PANI-12/Pt in presence of Fe(III)/Fe(II) redox analyte. The best fitted EEC for PANI-12/Pt in absence of Fe(III)/Fe(II) redox analyte is same as shown in Fig. 4.5(E1).*

Moreover, the finite diffusion resistance, which is characteristic of the diffusion behavior inside PANI matrix decreased simultaneously as the solution composition was changed from (A) to (C).

These results provide a good insight about the interaction of reacting species with PANI coated platinum electrode for the Fe(III)/Fe(II) reaction. For all the three solution compositions, redox peak currents during CV almost doubled for PANI-12/Pt with respect to those at bare Pt electrode and moreover, peak currents increased with increasing the film thickness. As Fe(III)/Fe(II) reaction happens at the polymer/solution interface and the corresponding charge transfer resistance is very low, thus porous PANI network provides larger area of interaction for the charge transfer process and finally amplifies the current response almost to the same extent for all the solution compositions. But variations in ΔE_p, R_d and W originate from different source. In high acidic solution ($[H^+]$~1 M), PANI exists as ES form with 50% protonation [21] and it introduces a Donnan potential ($\Delta\varphi_D$) at the polymer/solution interface throughout PANI matrix. In this case (where no additional 1:1 salt was used), the Donnan potential is expressed by the equation (2);

$$\Delta\varphi_D \cong \pm \frac{RT}{F} \ln\frac{C_F}{C_S} \qquad (2)$$

where (+) and (-) signs appear for coulombic repulsion originating from same polarity and for coulombic attraction originating from different polarity, respectively. Donnan potential is related to half wave potential of voltammogram by the equation (3);

$$E_{\frac{1}{2}} = E_0' \pm \Delta\varphi_D \qquad (3)$$

where, C_F and C_S are the concentrations of fixed charge sites in the polymer and of charged species in solution; E_0' is the formal potential of redox species; R, T and F are the universal gas constant, temperature in absolute scale and Faraday's constant, respectively. In Equation 3, the (+) and (-) signs denote the anodic and cathodic scan directions, respectively [9,22].

$[Fe(H_2O)_6]^{3+}/[Fe(H_2O)_6]^{2+}$ species were found to exist predominantly for $Fe_2(SO_4)_3$/ $FeSO_4$ solution in 0.5 M H_2SO_4. Thus a positive Donnan potential exists at the polymer solution interface and it shifts $E_{1/2}$ value to higher positive and negative potentials for the anodic and cathodic scan directions, respectively, during the CV experiment. Cyclic voltammogram of the Fe(III)/Fe(II) redox reaction, therefore, is stretched along the potential axis as compared to that on bare platinum electrode. This can be expressed as an inhibition effect of polyaniline modified electrode to the electrochemical reversibility of the Fe(III)/Fe(II) redox reaction. From the high finite and infinite diffusion resistance values, it can be understood that strong repulsion between polymer matrix and positively charged diffusing redox species not only hinders diffusion inside the polymer matrix but also hinders diffusion of the same towards the modified electrode. On the other hand, $[FeCl_4]^-/[FeCl_4]^{2-}$ species were found to exist predominantly for $FeCl_3/FeCl_2$ solution in 1 M HCl. Thus a negative Donnan potential exists at the polymer solution interface and it shifts the $E_{1/2}$ value to lesser positive and negative potentials for the anodic and cathodic scan directions, respectively, during CV experiment. Thus cyclic voltammogram of Fe(III)/Fe(II) redox reaction is compressed along the potential axis as compared to that on bare platinum electrode. This can be expressed as a facilitation effect of polyaniline modified electrode to the electrochemical reversibility of the Fe(III)/Fe(II) redox reaction. From very low finite and infinite diffusion resistance values, it

can be understood that strong attraction between the polymer matrix and negatively charged diffusing redox species not only accelerates the diffusion inside the polymer matrix but also accelerates the diffusion of the same towards the modified electrode.

An interesting phenomenon was observed on replacement of 1 M HCl by 0.5 M H_2SO_4 in the electrolytic composition. The electrocatalytic behavior of the system was just reversed when the solution composition of $FeCl_3$/ $FeCl_2$ in 1 M HCl was changed to $FeCl_3$/ $FeCl_2$ in 0.5 M H_2SO_4. Instead of facilitation in the Fe(III)/Fe(II) redox reaction, an inhibition effect was observed at polyaniline modified electrode. At the same time, the finite and infinite diffusion resistance values became almost comparable to those observed for $Fe_2(SO_4)_3$/ $FeSO_4$ solution in 0.5 M H_2SO_4 (Table 4.2). From Fig. 4.4 (curve 2-4), it is clear that the predominant species existing in the solution changed from $[FeCl_4]^-$/$[FeCl_4]^{2-}$ to $[Fe(H_2O)_6]^{3+}$/$[Fe(H_2O)_6]^{2+}$ as the solution composition was changed from $FeCl_3$/ $FeCl_2$ in 1 M HCl to $FeCl_3$/ $FeCl_2$ in 0.5 M H_2SO_4. Thus polyaniline modified platinum electrode showed rather inhibiting effect during the electrocatalysis. At this point, it can be assumed that either the ionic speciation of the diffusing redox species or the acid itself may cause reversal in the electrocatalytic behavior. In order to investigate this, the same set of experiments were done with $K_3[Fe(CN)_6]$/$K_4[Fe(CN)_6]$ solution in 0.5 M H_2SO_4, where $[Fe(CN)_6]^{3-}$/ $H_2[Fe(CN)_6]^{2-}$ is believed to be predominant redox species having the formal redox potential ($E_o^{'}$) at ~ 0.49 V vs. Ag/AgCl reference electrode [11]. Polyaniline modified platinum electrode not only facilitated Fe(III)/Fe(II) redox reaction for $K_3[Fe(CN)_6]$/$K_4[Fe(CN)_6]$ solution in 0.5 M H_2SO_4, but also the finite and infinite diffusion resistance values (7.9 $m\Omega^{-1}$ $s^{1/2}$ and 3.11 Ω, respectively) became almost comparable to those observed for the $FeCl_3$/ $FeCl_2$ in 1 M HCl

(Table 4.2). Thus it indicates that ionic speciation of the diffusing redox species has a great influence on electrocatalytic behavior of polyaniline modified platinum electrode in mineral acid medium and the predominant redox ionic species existing in the solution is governed by the electrolytic composition.

4.3 A Mechanistic study on the electrocatalysis of Pu(IV)/Pu(III) redox reaction at platinum electrode modified with single-walled carbon nanotubes (SWCNTs) and polyaniline (PANI)

4.3.1 Experimental

All the chemicals viz. aniline, nafion (sulfonated tetrafluoroethylene based fluoropolymer-copolymer) and sulphuric acid (H_2SO_4) were of G. R. (Guaranteed Reagent) grade and were used as received. All the solutions were prepared in Millipore Milli-Q water (~ 18 MΩ cm).

Working reference potassium plutonium sulphate dihydrate [$K_4Pu(SO_4)_4.\ 2H_2O$] was prepared in our laboratory as described elsewhere [23]. In brief, the crystals of $K_4Pu(SO_4)_4.\ 2H_2O$ were first prepared by slow evaporation of 1M H_2SO_4 containing K_2SO_4 and $Pu(SO_4)_2$ in 2:1 molar ratio. Then the crystals were washed several times with absolute alcohol and dried in a current of air. The anhydrous $K_4Pu(SO_4)_4$ was prepared by heating the hydrated crystals at 340°C for about three hours until constant weight. Known amount of the anhydrous $K_4Pu(SO_4)_4$ was quantitatively dissolved in 15 mL of 3M HNO_3 and the dissolved solution was fumed with 1M H_2SO_4 for converting to sulfate form. Residue was again treated with 1M H_2SO_4 and was evaporated to dryness. This particular step was repeated several times to ensure complete removal of nitrate. Finally, 25 mMPu(IV) in 1M H_2SO_4 was prepared by quantitatively diluting the residue with 1M H_2SO_4.

Electrochemical polymerization of aniline, cyclic voltammetry and differential pulse voltammetry were performed using CHI 440A electrochemical workstation with a three electrode voltammetric cell having platinum disk working electrode (area, A = 0.031 cm^2), platinum wire counter electrode and Ag/AgCl reference electrode. All the potentials are quoted with respect to Ag/AgCl (3 M KCl) reference electrode. All the experiments were carried out at room temperature (25 ± 1^0C). All solutions were deoxygenated using high purity nitrogen prior to electrochemical experiments. Each measurement was repeated thrice and the average numerical value of each parameter is quoted for discussion (relative error < ± 0.1%).

Electrochemical impedance spectroscopy (EIS) was performed using Autolab PGSTAT20 with FRA2 (Eco-Chimie) software. Impedance was recorded at open circuit potentials with single sine excitation signal of 0.005 V for the frequency range 10^6 Hz–10^{-2} Hz. Impedance spectra were fitted to electrical equivalent circuits (EEC) and the fits had $\chi^2 \leq 10^{-2}$. Errors of all the calculated parameters were within 5% of the reported values.

The morphology of PANI-Pt was recorded by Seron Incorporation AIS 2100 scanning electron microscope.

PANI film was electrodeposited potentiodynamically on platinum electrode from 0.1 M aniline solution in 0.5 M H_2SO_4 at a scan rate of 100 mV/s by repeating the potential scan for 12 cycles between -0.2 V and 1.3 V. However, the characteristic redox peaks of the Pu(IV)/Pu(III) couple were completely masked by the background signal of modified electrode. This was attributed to strong interference of the electroactive degradation products

viz. quinones and hydroquinones of PANI film in the voltammogram. Signature of Pu(IV)/Pu(III) redox reaction could not be recovered in spite of restricting the potential scan to three cycles. Therefore, a two step growth strategy was followed for depositing PANI film on platinum electrode from 0.1 M aniline solution in 0.5 M H_2SO_4. In the first step, the potential of platinum electrode was scanned between -0.2 V and 1.3 V at a scanning rate of 100 mVs^{-1}(Fig. 4.8).

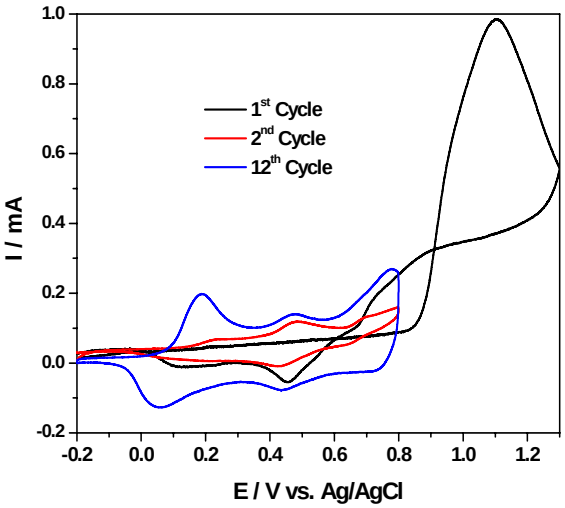

Fig. 4.8. *Cyclic voltammograms during the electropolymerization of aniline on Pt in 0.1 M aniline + 0.5 M H_2SO_4 solution at a scan rate of 0.1 V s^{-1} for 1st, 2nd and 12th cycles.*

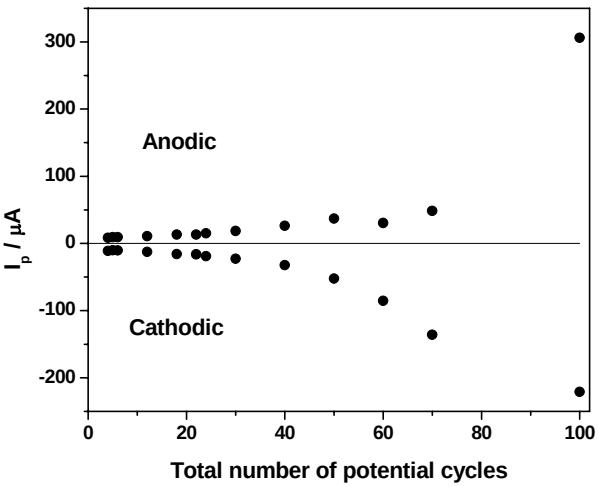

Fig. 4.9. *Cathodic and anodic peak currents of 25 mM Pu(IV)/Pu(III) couple in 1 M H_2SO_4 on PANI-Pt at a scan rate of 20 mV/s as a function of total number of potential cycles during the polymerization of aniline on Pt.*

This step was found to be sufficient to oxidize aniline monomers and to produce some oligomers which could grow autocatalytically during the second step where the switching potential was restricted up to 0.8 V for multiple cycles (Fig. 4.8). This strategy reduced the fragmentation of PANI and hence redox peaks of Pu(IV)/Pu(III) couple appeared prominently on PANI-Pt. The number of potential cycles in the second step was also optimized for PANI-Pt by monitoring redox peaks of 25 mM Pu(IV)/Pu(III) couple in 1M

H_2SO_4. The cathodic and anodic peak currents increased exponentially with increasing the number of potential cycles up to 100 (Fig. 4.9) and simultaneously peak-to-peak potential separation (ΔE_p) reduced drastically. However, fragmentation of the PANI matrix also increased when the number of the potential cycles was increased. This introduced two additional peaks of the electroactive fragments (most probably quinone and hydroquinone) in the vicinity of the redox peaks of Pu(IV)/Pu(III) couple (Fig. 4.10) [24]. The best results were obtained with eleven potential cycles in the second step of PANI deposition. Therefore, for all subsequent studies, PANI-Pt was prepared from 0.1 M aniline solution in 0.5 M H_2SO_4 by scanning the potential of platinum electrode between -0.2 V to 1.3 V and -0.2 V to 0.8 V for the first cycle and consecutive eleven cycles, respectively, at a scan rate of 100 mV/s.

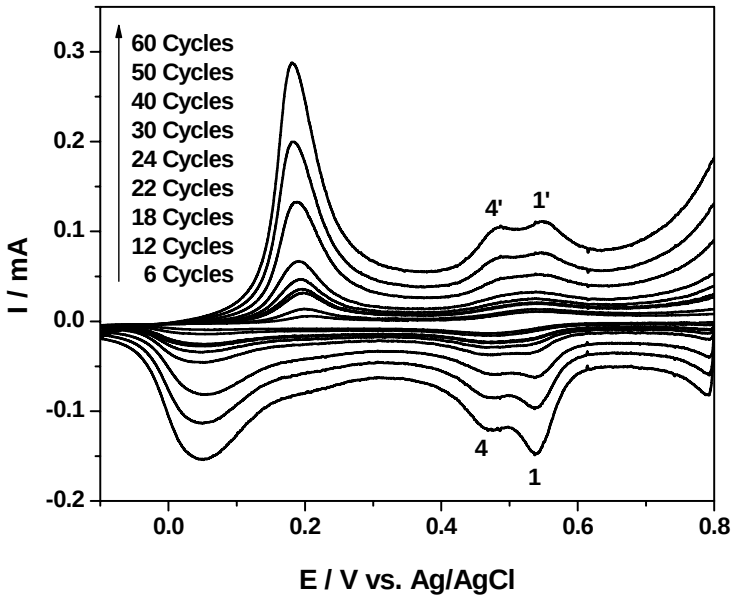

Fig. 4.10. *Cyclic voltammograms of 25 mM Pu(IV) in 1 M H_2SO_4 on PANI-Pt at a scan rate of 20 mV/s with respect to total number of potential cycles during polymerization of aniline on Pt.*

4.3.2.Results and discussion

4.3.2a. Electrochemistry of Pu(IV)/Pu(III) in 1 M H_2SO_4 on platinum disk electrode

Fig. 4.11 shows cyclic voltammogram of 25 mM Pu(IV) in 1M H_2SO_4 on platinum electrode at a scan rate of 20 mV/s. The cathodic peak (1) at 0.321 V and the anodic peak (1') at 0.587 V correspond to reduction of Pu(IV) to Pu(III) and vice-versa, respectively. The peak-to-peak potential separation (ΔE_p) of 266 mVwas attributed to the quasi-reversible electron transfer reaction of Pu(IV)/Pu(III) couple in 1 M H_2SO_4 on platinum electrode.The cyclic voltammograms of the same redox reaction were studied by varying the scan rate (ν) in the range of 10-500 mV/s.

The redox species can interact with the electrode surface by either pure diffusion or pure adsorption or a mixed adsorption-diffusion controlled process. The dominating process can be diagnosed by observing the slope of the straight line of log│Ip│ versus log (ν) plot. Theoretically, slopes of 0.5 and 1 should be observed for pure diffusional and adsorbed species, respectively. However, a slope lying between 0.5 and 1 represents the mixed adsorption-diffusion controlled process, where the value indicates the level of contribution from the two components [25,26]. In practical cases, the slope values lying between 0.20-0.60 and 0.75-1.10 are considered as pure diffusion and pure adsorption controlled processes, respectively. The slope lying between 0.60-0.75 is considered as a mixed adsorption-diffusion controlled process [27,28].The plots of log│Ip│versus log (ν) for both the cathodic and the anodic peaks yielded straight lines of slopes 0.33 (R^2 = 0.994) and 0.35 (R^2 = 0.987),

respectively. This clearly suggests that the electrochemical reaction of Pu(IV)/Pu(III) couple onto platinum electrode in 1 M H_2SO_4 solution is governed by the diffusion process.

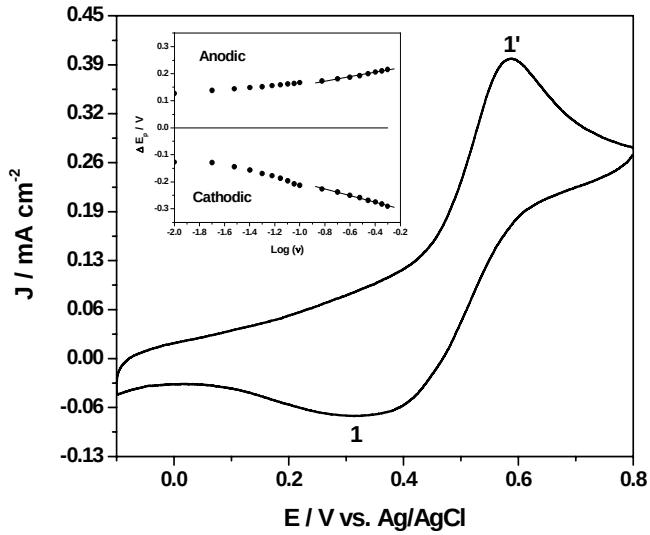

Fig.4.11. *Cyclic voltammogram of 25 mM Pu(IV) in 1 M H_2SO_4 on platinum electrode at a scan rate of 20 mV/s. Inset shows variation of the cathodic and anodic peak potentials (ΔE_p) with respect to E_0' as a function of scan rate.*

It was also noted that the cathodic (E_p^c) and anodic (E_p^a) peak potentials shifted towards more negative and positive directions, respectively, with increasing scan rate (Inset of Fig.4.11). ΔE_p also increased with increase in scan rate and showed linear dependence at higher scan rates (150-500 mV/s). Linear part of the plot was found to obey the Laviron equation [29]:

$$E_p^c = E_0' - \frac{2.303RT}{\alpha nF}\log(\frac{\alpha nF}{k_s RT}) - \frac{2.303RT}{\alpha nF}\log(\nu) \quad (4)$$

$$E_p^a = E_0' + \frac{2.303RT}{(1-\alpha)nF}\log(\frac{(1-\alpha)nF}{k_s RT}) + \frac{2.303RT}{(1-\alpha)nF}\log(\nu) \quad (5)$$

where, $E_0^{'} = (E_p^a + E_p^c)/2$ at very slow scan rate (5 mV/s), α is the cathodic electron transfer coefficient, n is the number of electrons transferred, R is the molar gas costant (8.314 J $mol^{-1}K^{-1}$), F is the Faraday constant (96495 C mol^{-1}), T is the temperature (298 K) and k_s(cm s^{-1}) is the apparent heterogeneous rate constant of electron transfer. Therefore, the slopes of the cathodic and anodic linear segments are -2.303RT/(αnF) and 2.303RT/{(1-α)nF}, respectively. The values of α and n calculated from the two slopes were 0.39 and 1.18. The apparent heterogeneous rate constant (k_s) of Pu(IV)/Pu(III) reduction was calculated as 1.06×10^{-1}cm s^{-1}. This suggests that the redox reaction of Pu(IV)/Pu(III) couple in 1 M H_2SO_4 solution is a quasi-reversible one-electron transfer process[30].The diffusion coefficient of 25 mM Pu(IV) in 1M H_2SO_4 solution was calculated as 3.4×10^{-8} cm^2s^{-1} by using the following equation[31] :

$$I_p^a = 2.99 \times 10^5 n^{3/2} \alpha^{1/2} D^{1/2} A C_{Pu(IV)} v^{1/2} \quad (6)$$

In 1 M H_2SO_4, Pu(IV) predominantly exists as quadrasulphate complex (QSC) ions $[Pu(SO_4)_4(H_2O)_4]^{4,}$ [32]. Therefore, diffusion coefficient of heavier QSC ions (about 700 amu) is pretty small. The overall observations suggest that the diffusing QSC ions are reduced at platinum electrode in 1M H_2SO_4 through quasi-reversible (α = 0.39) single electron transfer process. At this point, it is important to note that Pu(IV)/Pu(III) couple is expected to exhibit reversible electron transfer process because it does not involve any plutonium–oxygen bond formation or cleavage reaction. However, the results are contrary to the expectations. A close look into the electrode-electrolyte interface will reveals a direct contact between the QSC ions in 1M H_2SO_4 and polycrystalline platinum electrode. The

strong physisorption of water molecules occurred on platinum in the potential range 0.27-0.85 V vs. NHE due to the electrostatic interaction between partial by positively charged platinum surface and partially negatively charged oxygen atom of the water molecules [33]. In higher potential range (0.85 V < E <1.15 V vs. NHE), half monolayer of chemisorbed oxygen builds up on the platinum surface. Platinum(II) oxide (PtO) is formed due to the mutual charge transfer between platinum to chemisorbed oxygen at potential greater than 1.15 V vs. NHE. Bi-sulphate ions (HSO_4^-) are mostly desorbed at the onset of the surface oxide formation and, therefore, do not influence the oxide growth on the platinum surface [34]. On other hand, the formal potential of Pu(IV)/Pu(III) couple in 1 M H_2SO_4 is ~0.76 V vs. NHE. Therefore, Pu(IV) and Pt form a galvanic cell [Pt,PtO/Pu(IV),Pu(III)] where Pu(IV) is reduced to Pu(III) at the cost of oxidizing the surface platinum atoms to PtO at the interface of QSC ions and polycrystalline platinum.This oxide layer affects the thermodynamics of the electrochemical reaction, changes the electronic properties of the platinum surface, imposes a barrier to charge transfer reaction across the surface oxide film and blocks the active sites on the metal surface. Therefore, the electrochemical reaction of Pu(IV)/Pu(III) couple on platinum electrode in 1 M sulphuric acid solution exhibits a quasi-reversible electron transfer process.

4.3.2b. Electrochemistry of Pu(IV)/Pu(III) in 1 M H_2SO_4 on PANI-Pt

Fig. 4.12(A) and 4.12(B) show the SEM images of top and cross-sectional views of PANI-Pt, respectively. About 450 nm thick porous PANI fibers were observed on the platinum surface. The entire platinum surface was covered by PANI.

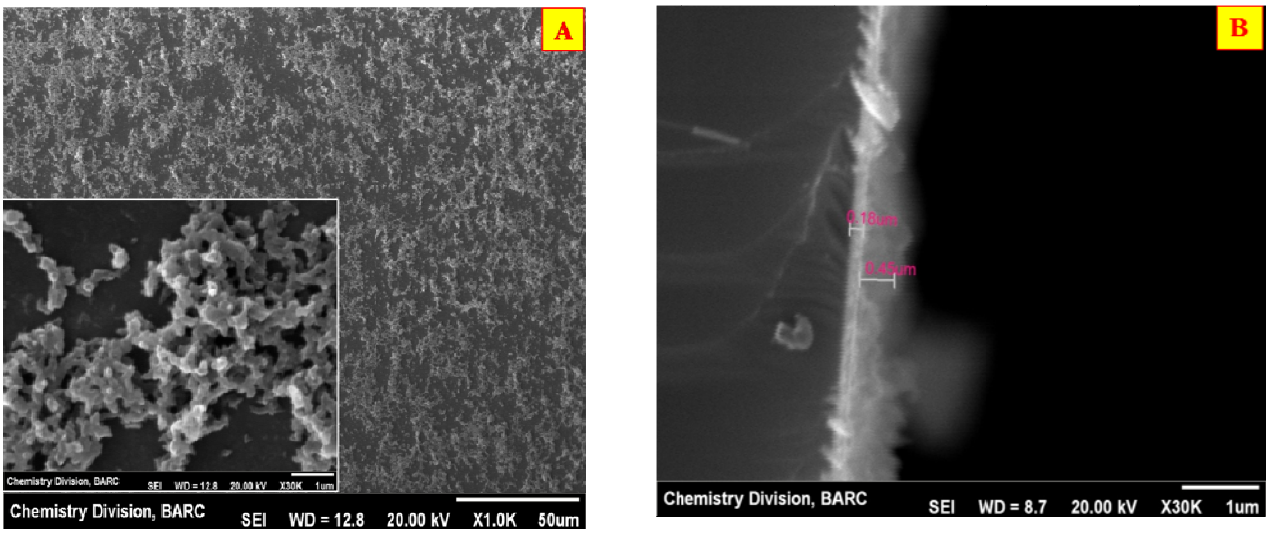

Fig. 4.12. *SEM images of the (A) top (inset shows higher magnification image) and (B) cross-sectional views of PANI/Pt.*

The cyclic voltammogram of 25 mM Pu(IV) in 1M H_2SO_4 solution on PANI-Pt electrode at a scan rate of 20 mV/s is shown in Fig. 4.13. The cyclic voltammogram of Pu(IV) recorded on Pt (which is already presented in Fig.4.11) was overlaid in the same scale in Fig.4.13 for comparison. The cathodic peak (1) at 0.460 V and the anodic peak (1') at 0.540 V observed on PANI-Pt correspond to the reduction of Pu(IV) to Pu(III) and vice-versa, respectively. The peak-to-peak potential separation (ΔE_p) is 80 mV, which is the lowest among the ΔE_p

values observed on bare Pt (266 mV) and on SWCNT-Pt (108 mV). This confirms that the redox reaction of Pu(IV)/Pu(III) couple became more reversible on PANI-Pt compared to SWCNT-Pt and bare Pt. One pair of additional peaks (3/3') at 0.032 V and 0.197 V, respectively, appeared in the voltammogram because of the redox transition between the fully reduced leucoemeraldine base (LB) and emeraldine salt (ES) forms of PANI.

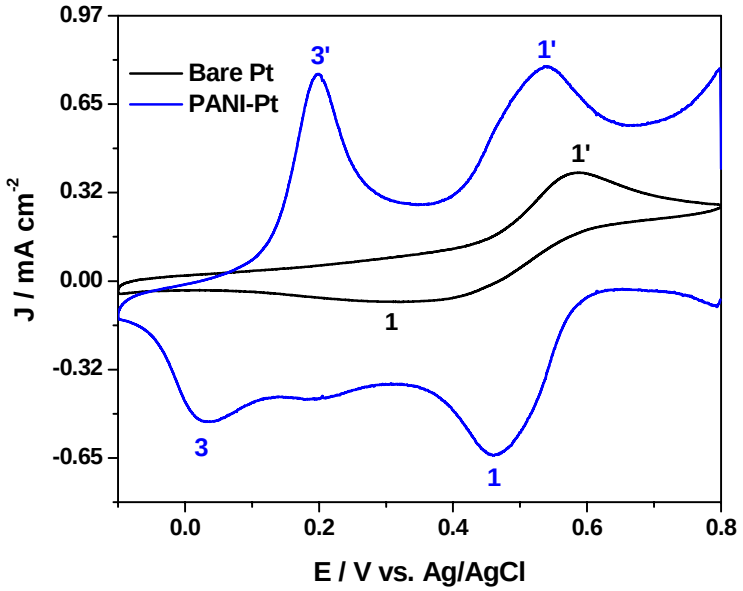

Fig. 4.13. *Cyclic voltammogram of 25 mM Pu(IV) in 1 M H_2SO_4 solution on Pt and PANI-Pt electrodes at scan rate of 20 mV/s.*

Fig. 4.14 shows cyclic voltammogram of the Pu(IV)/Pu(III) redox reaction at different scan rates (ν) in the range of 1-500 mV/s. The shape of the cyclic voltammograms changed progressively with increasing the scan rates. The cathodic and anodic peaks of ES/LB couple of PANI shifted towards more positive potentials with increasing scan rates. This suggests that insulating fraction of PANI matrix increased progressively with the increasing scan

rates. On the other hand, the cathodic peak of Pu(IV)/Pu(III) couple continuously shifted towards more negative potential with increasing scan rate, but the anodic peak initially shifted towards more positive potential till the scan rate of 40 mV/s and afterwards, it started shifting towards cathodic direction. Finally, the anodic peaks of Pu(IV)/Pu(III) and ES/LB couples got merged at scan rates higher than 300 mV/s.

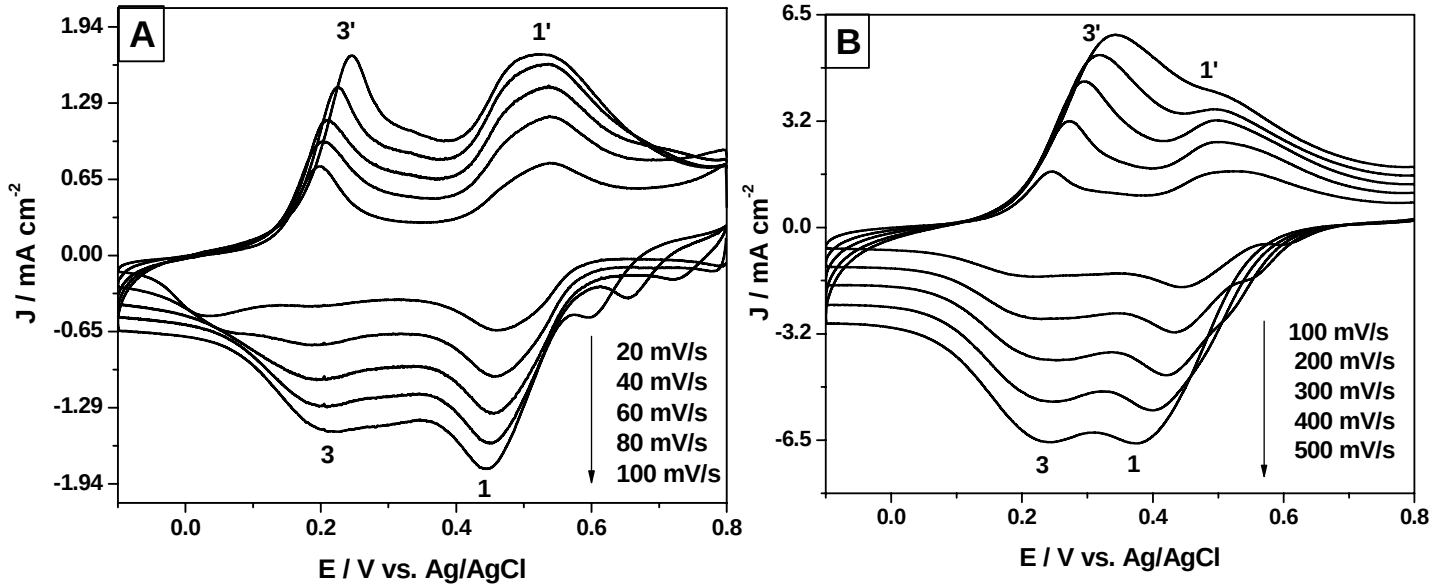

Fig. 4.14. *Cyclic voltammograms of 25 mM Pu(IV) in 1 M H_2SO_4 solution on PANI-Pt electrodes. Scan rates range : (A) 20-100 mV/s and (B) 100-500 mV/s.*

Fig. 4.15 shows a comparison of (A) cathodic and (B) anodic peak currents of Pu(IV)/Pu(III) redox reaction on Pt and PANI-Pt electrodes in the scan rate range of 10-100 mV/s. The catalytic efficiency (γ) of the cathodic reaction increased from ~150% at 10 mV/s to ~528% at 100 mV/s. However, the catalytic efficiency of the anodic reaction remained almost constant in between ~100% and 145% with increasing scan rates in the range of 10-100 mV/s.

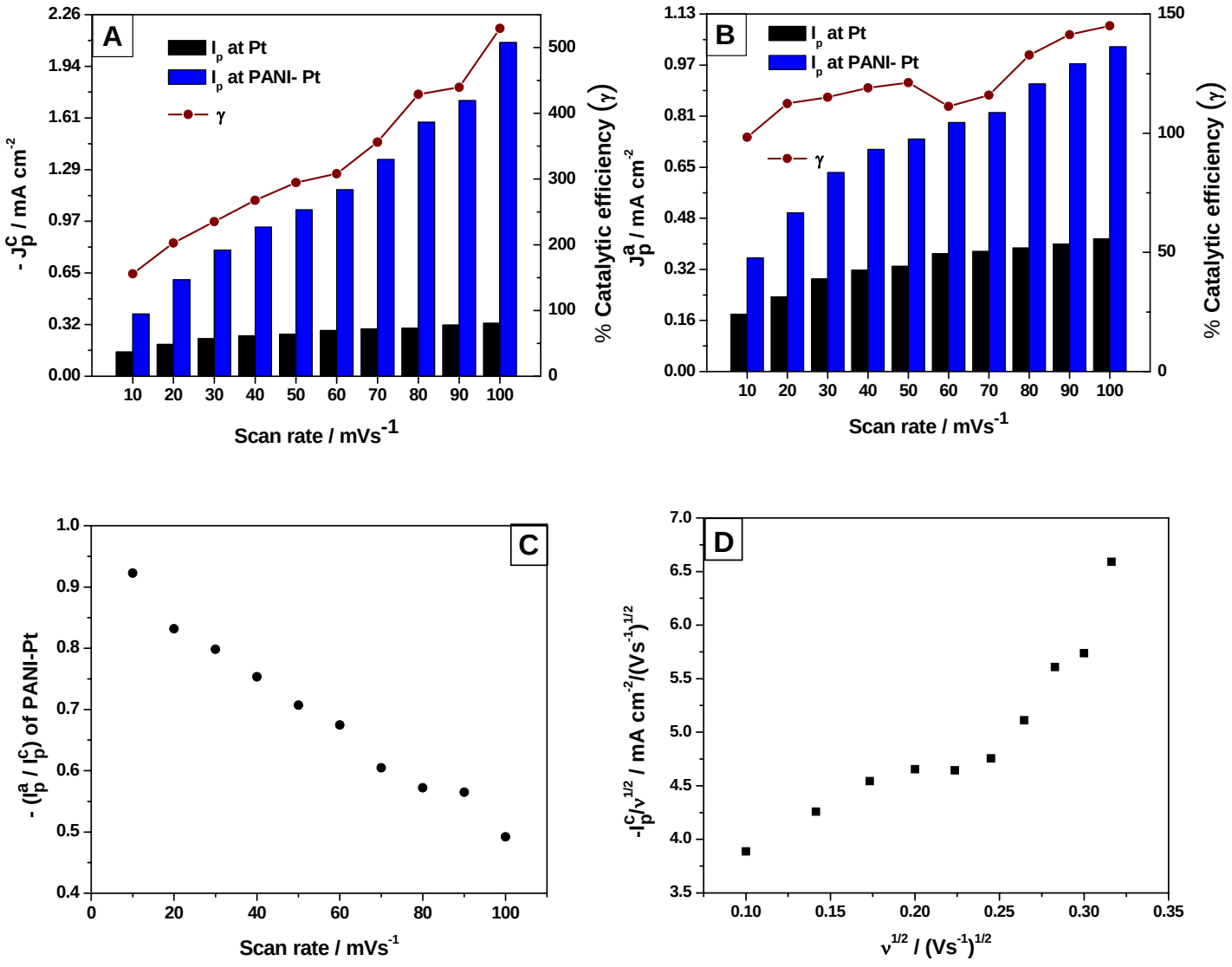

Fig.4.15. *The (A) cathodic and (B) anodic peak currents of Pu(IV)/Pu(III) redox reaction on Pt and PANI-Pt electrodes in the scan rate range of 10-100 mV/s. % catalytic efficiency of modified electrode as a function of scan rate is shown in the respective plots; (C) i_p^a/i_p^c of Pu(IV)/Pu(III) couple on PANI-Pt as a function of scan rate in range of 10-100 mV/s; (D) The plot of cathodic current function ($-i_p^c/v^{0.5}$) with respect to square root of scan rate (in V/s) in the range of 10-100 mV/s.*

The decrease inthe ratio i_p^a/i_p^c with increasing the scan rates (Fig. 4.15C) and the increase of the cathodic current function ($-i_p^c/\nu^{0.5}$) with increasing scan rates (in V/s) (Fig. 4.15D) suggest that redox reaction Pu(IV)/Pu(III) on PANI-Pt follows an electrochemical-chemical (EC) mechanism consisting of an electron transfer reaction followed by a chemical reaction.

The slopes of log $|Ip|$ versus log (ν) plots for both the cathodic and the anodic peaks were observed as 0.69 (R^2 = 0.986) and 0.43 (R^2 = 0.990), respectively, in the scan rate range of 10-200 mV/s. This illustrates that the cathodic reaction of Pu(IV)/Pu(III) couple in 1 M H_2SO_4 using PANI-Pt is governed by the mixed adsorption-diffusion controlled process. However, the reverse reaction {i.e., the oxidation of Pu(III)} is still governed by the diffusion controlled process. The charge transfer coefficient (α) and the heterogeneous rate constant (k_s) of Pu(IV) reduction in 1 M H_2SO_4 on PANI-Pt were calculated as 0.77 and 9.70×10^{-1} cm s^{-1}, respectively.

The results cumulatively illustrate the electrocatalysis of Pu(IV)/Pu(III) redox reaction on PANI-Pt. The anionic QSC complex is attracted by the positively charged PANI matrix (as ~ 50% of ES is protonated at the nitrogen centres in 1 M H_2SO_4) and finally gets adsorbed at the Lewis basic nitrogen centres. Hence the transition state energy level is reorganized and finally the electron transfer coefficient increases. Therefore, reversibility of Pu(IV)/Pu(III) redox reaction is significantly increased on PANI-Pt. However, this adsorption was completely absent during oxidation of Pu(III) due to lack of Donnan interaction between PANI and Pu(III)-species.

The cyclic voltammogram shown in Fig. 4.13 reveals that ES has stronger oxidizing ability than Pu(IV) in 1M H_2SO_4. Therefore, at the beginning of potential scan (0.8 V ≤ E ≤ ~0.65 V), QSC is adsorbed at the interface and then PANI (ES) only serves as an ordinary conducting polymer. At ~ 0.65 V, reduction of Pu(IV) to Pu(III) sets in by obeying the Nernst equation. As soon as Pu(III) appears at the PANI(ES)-electrolyte, a chemical reaction between Pu(III) and PANI(ES) is coupled with the electron transfer reaction. This chemical reaction regenerates Pu(IV) at the PANI-electrolyte interface. Therefore, the cathodic peak current was higher than the anodic peak current (notably, the cathodic peak current of Pu(IV)/Pu(III) redox reaction in 1 M H_2SO_4 on bare platinum electrode was observed as smaller than the anodic peak current). Here PANI acts as an electron mediator in the catalysis of Pu(IV)/Pu(III) redox reaction on PANI-Pt as shown in the following equations :

$$Pu(IV) = Pu(III) + e- \quad (7)$$

$$Pu(III) + PANI(ES) = Pu(IV) + PANI(LB) \quad (8)$$

It is well known that flux of the analyte ions increases with increasing scan rate. Hence the cathodic peak current of Pu(IV)/Pu(III) redox reaction increased with the increasing scan rate because of the catalytic regeneration of Pu(IV) at the electrode-electrolyte interface by the coupled chemical reaction. However, the coupled chemical reaction increases fully reduced LB form (which is insulating in nature) in PANI matrix. This induces the redox peaks of ES/LB couple to shift towards more positive potentials with increasing scan rates.

The electrocatalytic action of PANI-Pt on Pu(IV)/Pu(III) redox reaction is promising for electroanalytical applications. However, stability of the PANI-Pt electrode in Pu(IV) solution was poor for a prolonged electrochemical application. Fig. 4.16 shows cyclic voltammograms of Pu(IV)/Pu(III) in 1 M H_2SO_4 on PANI-Pt for multiple number of continuous potential scans at a rate of 20 mV/s. The peaks of Pu(IV)/Pu(III) redox couple were completely deformed from ~50 cycles onwards. This was attributed to the radiation damage of the soft organic PANI-matrix during the prolonged exposure to radioactive solution. Further studies are necessary to meet this goal.The shelf life was not studied because the fresh modification is recommended prior to each analysis.

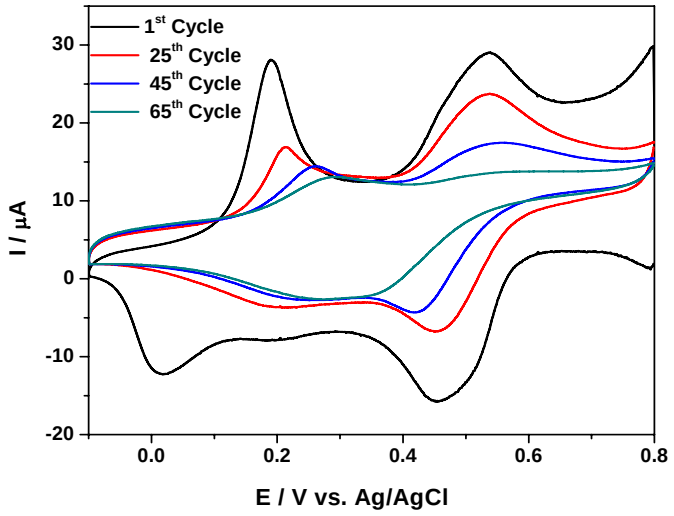

Fig. 4.16. *Cyclic voltammogram of 25 mM Pu(IV) in 1 M H_2SO_4 on PANI-Pt at a scan rate of 20 mV/s for 1st, 25th, 45th and 65th cycles under continuous operation.*

4.4. Conclusion

PANI/Pt electrode efficiently enhances the current response for Fe(III)/Fe(II) redox reaction compared to bare Pt electrode for all the three compositions viz. (i) $FeCl_3/FeCl_2$ in 1 M HCl, (ii) $FeCl_3$/ $FeCl_2$ in 0.5 M H_2SO_4 and (iii) $Fe_2(SO_4)_3/FeSO_4$ in 0.5 M H_2SO_4. Enhancement of peak current depends on thickness of porous PANI film as it provides total area of charge transfer at the polymer-solution interface, but reversibility of reaction is influenced greatly by polarity of charge on the ionic species as it influence the diffusion of analyte towards and throughout the polymer matrix. The desired polarity of diffusing species for the Fe(III)/Fe(II) redox couple can be obtained by judicious choice of the electrolytic composition (e.g. acid). Also PANI-Pt showed good electrocatalytic properties for Pu(IV)/Pu(III) redox reaction in 1 M H_2SO_4. The enhanced performance of PANI-Pt was attributed to the cumulative effects of Donnan interaction between PANI and Pu(IV)-QSC, specific adsorption of the analyte on the electron transfer centre, higher electron transfer rate constant and catalytic chemical reaction coupled with electron transfer reaction. This work provides a new opportunity to improve the quality of Pu determinations and shortens the analytical time for electroanalysis of actinides and other elements.

4.5. References

1. Y. Xian, F. Liu, L. Feng, F. Wu, L. Wang, L. Jin, Nanoelectrode ensembles based on conductive polyaniline/poly(acrylic acid) using porous sol–gel films as template, *Electrochem. Commun*. **9** (2007) 773.
2. J. Mathiyarasu, S. Senthilkumar, K. L. N. Phani, V. Yegnaraman, Selective detection of dopamine using a functionalised polyaniline composite electrode *J. Appl. Electrochem*. **35** (2005) 513.
3. N. Hamdi, J. Wang, H. G. Monbouquette, Polymer films as permselective coatings for H_2O_2-sensing electrodes, *J. Electroanal. Chem.* **581** (2005) 258.
4. Z. Matharu, G. Sumana, S. K. Arya, S. P. Singh, V. Gupta, B. D. Malhotra, Polyaniline Langmuir - Blodgett film based cholesterol biosensor, *Langmuir* **23** (2007) 13188.
5. S. Virji, R. B. Kaner, B. H. Weiller, Hydrazine detection by polyaniline using fluorinated alcohol additives, *Chem. Mater.* **17** (2005) 1256.
6. S. Virji, J. Huang, R. B. Kaner, B. H. Weiller, Polyaniline nanofiber gas sensors: Examination of response mechanisms, *Nano Lett.* **4** (2004) 491.
7. Q. Liu, F. Wang, Y. Qiao, S. Zhang, B. Ye, Polyaniline Langmuir–Blodgett film modified glassy carbon electrode as a voltammetric sensor for determination of Ag+ ion, *Electrochim. Acta*, **55** (2010) 1795.
8. A. P. Doherty, R. J. Forster, M. R. Smyth, J. G. Vos, Speciation of iron(II) and iron(III) using a dual electrode modified with electrocatalytic polymers, *Anal. Chem.* **64** (1992) 572.

9. Z. Mandic, L. Duic, Polyaniline as an electrocatalytic material, *J. Electroanal. Chem.* **403** (1996) 133.

10. R. Naujikas, A. Malinauskas, F. Ivanauskas, Modeling of electrocatalytic processes at conducting polymer modified electrodes, *J. Mathemat. Chem.* **42** (2007) 1069.

11. M. T. Ramirez, A. R. Hernandez, I. Gonzalez, Application of SQUAD to the refinement of formal potentials from coulometric steady-state and spectrophotometric measurements, *Talanta* **44** (1997) 31.

12. E. M. Genies, M. Lapkowski, J. F. Penneau, Cyclic voltammetry of polyaniline: interpretation of the middle peak, *J. Electroanal. Chem.* **249** (1988) 97.

13. D. E. Stiwell, S. –M. Park, Electrochemistry of Conductive Polymers II . Electrochemical Studies on Growth Properties of Polyaniline, *J. Electrochem. Soc.* **135** (1988) 2254.

14. P. L. Domingo, B. Garcia, J. M. Leal, Acid–base behaviour of the ferricyanide ion in perchloric acid media. Spectrophotometric and kinetic study, *Can.J. Chem.* **68** (1990) 228.

15. P. Marturano, L. Drozdova, G. D. Pirngruber, A. Kogelbauer, R. Prins, The mechanism of formation of the Fe species in Fe/ZSM-5 prepared by CVD, *Phys. Chem. Chem. Phys*. **3** (2001) 5585.

16. F. A. Cotton, G. Wilkinson, C. A. Murillo, M. Bochmann, Advanced Inorganic Chemistry (6^{th} ed.), John Wiley & Sons, Inc., NY, 1999, p.787.

17. P. J. Durrant, B. Durrant, Introduction to Advanced Inorganic Chemistry (1^{st} ed.), Longmans, London, 1962, p.1028.

18. M. Steiner, N. Lazaroff, Direct method for continuous determination of iron oxidation by autotrophic bacteria , *Appl. Microbiol.* **28** (1974) 872.

19. F. Rourke, J. A. Crayston, Cyclic voltammetry and morphology of polyaniline-coated electrodes containing $[Fe(CN)_6]^{3-/4-}$ ions, *J. Chem. Soc. Faraday Trans.* **89** (1993) 295.

20. N. G. Skinner, E. A. H. Hall, The relevance of an equivalent circuit for polyaniline using immittance spectroscopy, *Synth. Met*. **63** (1994) 133.

21. A. G. Macdiarmid, J. –C. Chiang, W. Huang, B. D. Humphrey, N. L. D. Somasiri, Polyaniline: protonic acid doping to the metallic regime, *Mol. Cryst. Liq. Cryst.* **125** (1985) 309.

22. M. Tagliazucchi, F. J. Williams, E. J. Calvo, Effect of acid-base equilibria on the donnan potential of layer-by-layer redox polyelectrolyte multilayers, *J. Phys. Chem. B* **111** (2007) 8105.

23. K.D. Singh Mudher and K. Krishnan, Crystal structure of $K_4Pu(SO_4)_4 \cdot 2H_2O$,*J. Alloys & Compounds,* **313** (2000) 65.

24. G.A. Planes, J.L. Rodriguez, M.C. Miras, G. Garcia, E. Pastor and C.A. Barbreo, Spectroscopic evidence for intermediate species formed during aniline polymerization and polyaniline degradation, *Phys. Chem. Chem. Phys*. **12** (2010) 10584.

25. C. Batchelor-McAuley, L.M. Goncalves, L. Xiong, A.A. Barros and R.G. Compton, Controlling voltammetric responses by electrode modification using adsorbed acetone

to switch graphite surfaces between adsorptive and diffusive modes , *Chem. Comm.* **46** (2010) 9037.

26. E. Laviron, A multilayer model for the study of space distributed redox modified electrodes: Part II. Theory and application of linear potential sweep voltammetry for a simple reaction, *J. Electroanal. Chem.* **112(**1980)11.

27. G. Gopu, P. Manisankar, B. Muralidharan and C. Vedhi, Stripping Voltammetric Determination of Analgesics in Their Pharmaceuticals Using Nano-Riboflavin-Modified Glassy Carbon Electrode, *Int. J. Electrochem. 2011, Article in press, Doi: 10.4061/2011/269452.*

28. F.S.M. Hassan, M.A. Ghandour, A.E. Mohamed and A.F.Al-Hossainy, Diphosphine Compounds: Part II. Synthesis and electrochemistry of (Ph2P)2C=CH2 and cis-Ph2PCH=CHPPh2 when chelated to M(CO)6(M=Cr, Mo, W) and $CuCl_2$, *Arabian J. Chem.* **1**(2008) 67.

29. E. Laviron, General expression of the linear potential sweep voltammogram in the case of diffusionless electrochemical systems, *J. Electroanal. Chem.* **101**(1979) 19.

30. D.K. Gosser Jr., *Cyclic voltammetry: Simulation and analysis of reaction mechanisms*; 1993, Wiley-VCH, Inc.: New York.

31. A. J. Bard and L.R. Faulkner, *Electrochemical methods: fundamentals and applications,* 2006, Wiley-India Ed.

32. L.V. Lipis, B.G. Pozharskii and V.V. Fomin, *Zhurnal Strukturnoi Khimii*, **1**(1959) 417.

33. G. Jerkiewicz, G. Vatankhah, J. Lessard, M.P. Soriaga and Y. Park, Surface-oxide growth at platinum electrodes in aqueous H_2SO_4: Reexamination of its mechanism through combined cyclic-voltammetry, electrochemical quartz-crystal nanobalance, and Auger electron spectroscopy measurements, *Electrochim. Acta*, **49**(2004) 1451.

34. D.G. Peters and W.D. Shults, Chronopotentiometry of plutonium in mineral acid media, *J. Electroanal. Chem,* **8**(1964) 200.

CHAPTER 5

Electrocatalytic Performance of Single Walled Carbon Nanotubes (SWCNT) Modified Electrode for U, Pu and Np

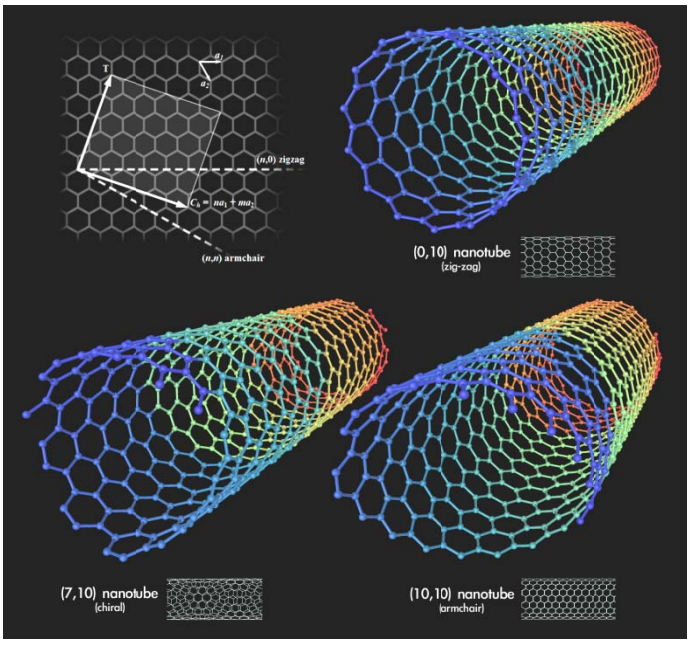

5.1 Introduction

Carbon nanotubes are interesting modifiers offering unique mechanical and electrical properties combined with good chemical stability. Single-walled carbon nanotube (SWCNTs) is a well defined system in terms of its electronic properties. The SWCNTs coated platinum electrodes may have the potential to improve electroanalytical behaviour of actinides by virtue of its higher surface to volume ratio and unique electronic properties. In this Chapter, the investigations carried out on the chemistry of Pu, U and Np redox reactions on platinum, gold and glassy carbon electrodes modified with SWCNTs are reported. Detailed experiments ere carried out to understand the electrocatalytic mechanism of the three redox couples at the modified electrodes. The motivation behind this work was that till date, no other research group has studied the electrocatalysis of actinides on SWCNT modified electrodes along with the detailed investigations of their electrocatalytic mechanism.

5.2 A Mechanistic Study on the Electrocatalysis of Pu(IV)/Pu(III) Redox Reaction at Platinum Electrode modified with Single-Walled Carbon Nanotubes (SWCNTs)

5.2.1. Experimental

All chemicals like nafion (sulfonated tetrafluoroethylene based fluoropolymer -copolymer) and sulphuric acid (H_2SO_4) were of G. R. (Guaranteed Reagent) grade and were used as received. Single walled carbon nanotubes (SWCNTs) of purity greater than 98% (along with characterization certificate) were used as received from Nanoshell USA. The diameter and the length of SWCNTs was in the range of 0.7 – 2 nm and 3 – 8 μm, respectively All the solutions were prepared in Millipore Milli-Q water (~ 18 MΩ cm).

Working reference potassium plutonium sulphate dihydrate {$K_4Pu(SO_4)_4$, $2H_2O$} was prepared in our laboratory as described elsewhere [1]. ^{239}Pu is an α-active nuclide with a half-life of 2.4×10^4 years. This corresponds to the production of 138×10^6 α-particles/min/mg of Pu. This radioactive material must be handled carefully in the radiological facilities with appropriate equipments to avoid any health risk caused by the radiation exposure. Therefore, all the experiments were performed with great care in a suitable place under safe conditions. Electrochemical measurements were performed using CHI 440A electrochemical workstation with a three electrode voltammetric cell having platinum disk working electrode (area, A = 0.031 cm^2), platinum wire counter electrode and Ag/AgCl reference electrode. All the potentials are quoted with respect to Ag/AgCl (3 M KCl) reference electrode. All experiments were carried out at room temperature (25 ± 1^0C). All solutions were deoxygenated using high purity nitrogen prior to electrochemical experiments. Each measurement was repeated thrice and the average numerical value of each parameter is quoted for discussion (relative error < ± 0.1%). Electrochemical impedance spectroscopy (EIS) was performed using Autolab PGSTAT20 with FRA2 (Eco-Chimie) software. Impedance was recorded at open circuit potentials with single sine excitation signal of 0.005 V for the frequency range 10^6 Hz to10^{-2} Hz. Impedance spectra were fitted to electrical equivalent circuits (EEC) and the fits had $\chi^2 \leq 10^{-2}$. Errors of all calculated parameters were within 5% of the reported values. The morphology of SWCNT-Pt was recorded by Seron Incorporation AIS 2100 scanning electron microscope. EDXRF spectrum was recorded using Jordan Valley EX-3600-TEC spectrometer having Rh target and Ge secondary target operated at 40 kV and 500 μA. The stable colloidal dispersions of both the

functionalized and non-functionalized SWCNTs were separately prepared by sonicating ~1 mg of SWCNTs for one hour in a 1:4 mixture of nafion and water. The SWCNT-Pt electrode was prepared by dropping a known volume (1-20 μL) of the SWCNT suspension on the platinum electrode followed by drying. The preparation conditions were optimized by recording the cyclic voltammograms of 25 mM Pu(IV) in 1M H_2SO_4 at a scan rate of 20 mV/s on each modified electrode (Fig. 5.1).

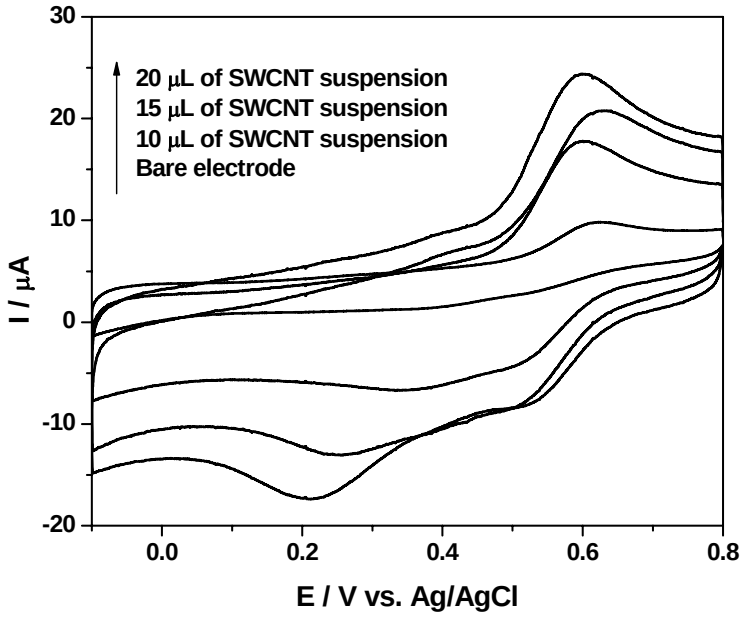

Fig. 5.1 *Cyclic voltammograms of 25 mM Pu(IV) in 1 M H_2SO_4 at a scan rate of 20 mV/s on SWCNT-Pt prepared by 1,10,15 and 20 μL of SWCNT suspension in 1:4 mixture of nafion and water.*

The redox peak currents of Pu(IV)/Pu(III) couple increased by increasing the volume of the SWCNT suspension on the platinum electrode, but maximum peak current was observed for 20 μL of SWCNT suspension. A part of the suspension fell down from the electrode surface

for suspension volumes higher than 20 µL. Therefore, platinum electrode was modified with 20 µL of SWCNT suspension for all further experiments.

5.2.2 Results and Discussion

5.2.2 a. Electrochemistry of Pu(IV)/Pu(III) in 1 M H_2SO_4 on SWCNT-Pt

Cyclic voltammogram of 25 mM Pu(IV) in 1M H_2SO_4 solution on SWCNT-Pt electrode at the scan rate of 20 mV/sec is shown in Fig.5.2. The cyclic voltammogram of Pu(IV) recorded on bare Pt was overlaid in the same scale in Fig. 5.2 for comparison.

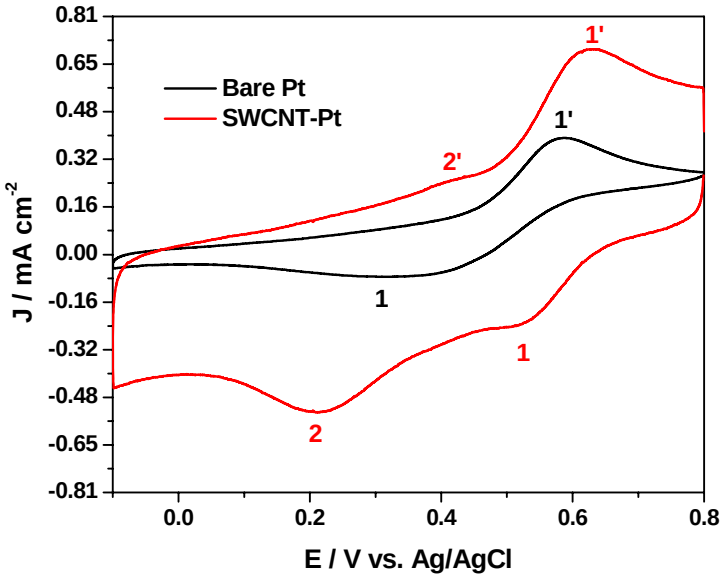

Fig.5.2 *Cyclic voltammogram of 25 mM Pu(IV) in 1 M H_2SO_4 solution on bare Pt and SWCNT-Pt electrodes at scan rate of 20 mV/s.*

The cathodic peak (1) at 0.520 V and the anodic peak (1') at 0.628 V observed on SWCNT-Pt correspond to the reduction of Pu(IV) to Pu(III) and vice-versa, respectively. The peak-to-peak potential separation (ΔE_p) is 108 mV, which is much smaller than the ΔE_p value 266 mV observed on bare platinum electrode. It indicates that Pu(IV)/Pu(III) couple still exhibits a quasi-reversible electron transfer behavior on SWCNT-Pt. One pair of additional redox peaks (2/2') appeared in the voltammogram due to the presence of trace impurities in the SWCNT [2,3]. The EDXRF spectrum of SWCNT and the cyclic voltammogram of SWCNT-Pt in 1M H_2SO_4 at the scan rate of 20 mV/s are shown in Fig. 5.3 and 5.4, respectively.

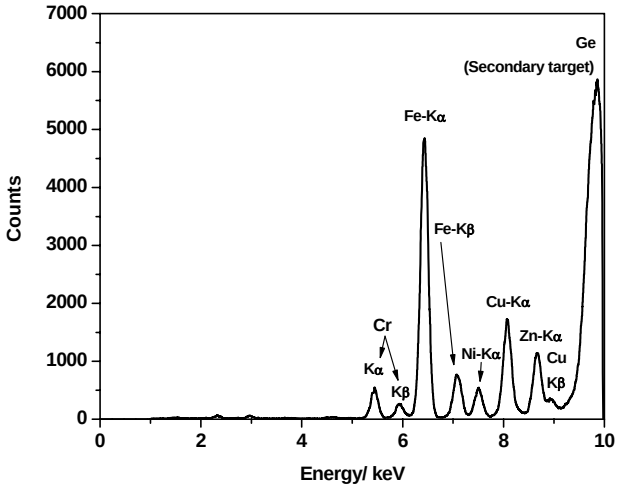

Fig.5.3. *EDXRF spectrum of SWCNTs as received from the supplier.*

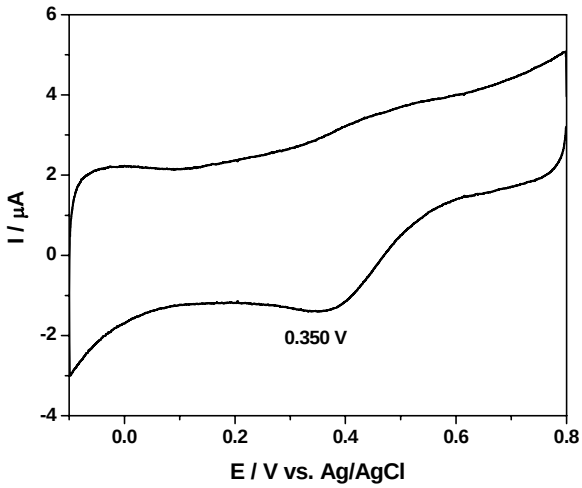

Fig. 5.4. *Cyclic voltammogram of SWCNT-Pt in 1 M H_2SO_4 at a scan rate of 20 mV/s.*

The increase in the redox peak current along with the significant improvement in the electrochemical reversibility suggest electrocatalytic action of SWCNT-Pt for the Pu(IV)/Pu(III) redox reaction. Fig. 5.5 shows a comparison of (A) cathodic and (B) anodic peak currents of Pu(IV)/Pu(III) redox reaction for Pt and SWCNT-Pt electrodes in the scan

rate range of 10-100 mV/s. Catalytic action of the modified electrode was quantified with the parameter named as catalytic efficiency (γ) which was defined as:

$$\gamma(\%) = 100 \times \frac{[I_p^M - I_p^{Pt}]}{I_p^{Pt}} \qquad (1)$$

where, I_p^M and I_p^{Pt} are the peak currents at the modified electrode and at bare Pt, respectively. As can be seen from Fig. 5.5, the catalytic efficiency of SWCNT-Pt for the cathodic reaction increased with increasing the scan rate, whereas the reverse phenomenon was observed for the anodic reaction. This could be attributed to electrostatic interaction between the functionalized SWCNT and plutonium ionic species in the electrolyte medium.

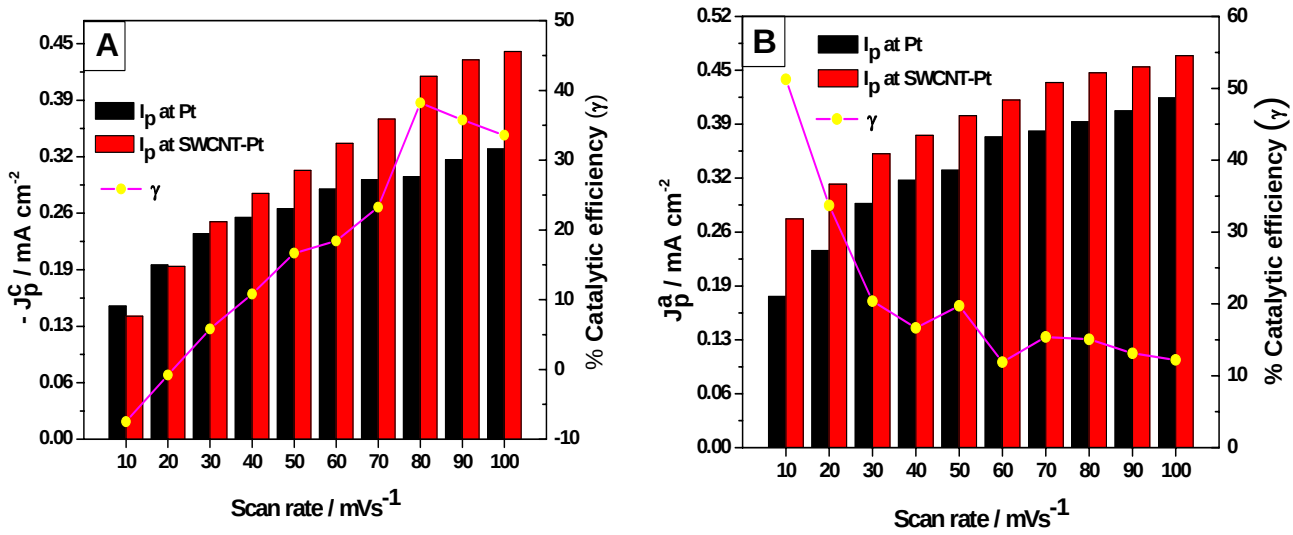

Fig. 5.5. *The (A) cathodic and (B) anodic peak currents of Pu(IV)/Pu(III) redox reaction on Pt and SWCNT-Pt electrodes in the scan rate range of 10-100 mV/s. The % catalytic efficiency of the modified electrode as a function of scan rate is shown in the respective plots.*

The pK_a of the carboxylic acid functionalized SWCNTs is ~4.5 as determined by the force titration method [4,5]. Thus the carboxylic group will be protonated in 2 M [H^+] and an additional proton may be attached with the electronegative oxygen atom of the carbonyl

group{as like (HO)(C)C=Oδ$^-$...H$^+$} resulting in a positively polarized SWCNT surface [6]. On the other hand, Pu(IV) forms an anionic QSC complex in 1M H_2SO_4. However, no anionic complex of Pu(III) is known to exist below 16 M H_2SO_4 [7]. The slopes of log | Ip | versus log (ν) plots for both the cathodic and the anodic peaks were observed as 0.50 (R^2 = 0.991) and 0.23 (R^2 = 0.989), respectively, in the scan rate range of 10-200 mV/s. This clearly indicates that the electrochemical reaction of Pu(IV)/Pu(III) couple in 1 M H_2SO_4 onto SWCNT-Pt is also governed by the diffusion controlled process. Fig.5.6 shows SEM image of SWCNT-Pt. It shows a rougher surface of SWCNT-Pt compared to bare Pt. Thus it may be stated that this rougher SWCNT-Pt surface played a major role in the calculated current efficiency values. The roughness of SWCNT-Pt is caused by the presence of two components viz. SWCNTs (conductive) and nafion (insulating) matrix. Thus, the catalytic efficiency in current mainly originated from the conductive area provided by the SWCNTs. Here, nafion was used only as a dispersing medium for SWCNTs.

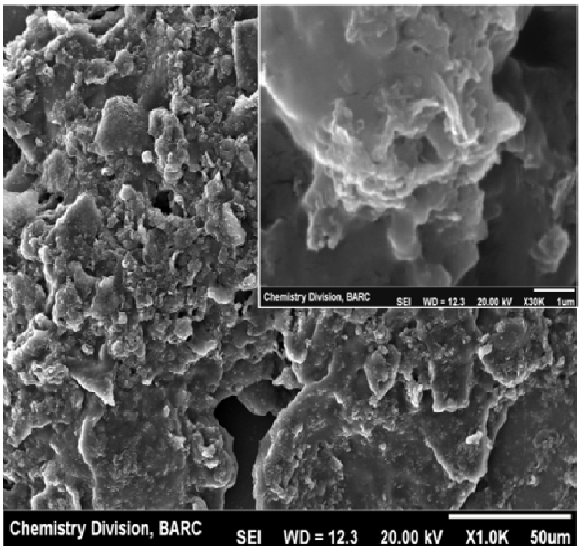

Fig. 5.6. *SEM image of SWCNT-Pt. Inset shows the higher magnification image.*

The charge transfer coefficient (α) and the heterogeneous rate constant (k_s) (calculated from Laviron equations 2 and 3) of Pu(IV) reduction on SWCNT-Pt in 1 M H_2SO_4 were calculated as 0.63 and 4.75×10^{-1}cm s^{-1}, respectively.

$$E_p^c = E_0' - \frac{2.303RT}{\alpha nF}\log(\frac{\alpha nF}{k_s RT}) - \frac{2.303RT}{\alpha nF}\log(\nu) \quad (2)$$

$$E_p^a = E_0' + \frac{2.303RT}{(1-\alpha)nF}\log(\frac{(1-\alpha)nF}{k_s RT}) + \frac{2.303RT}{(1-\alpha)nF}\log(\nu) \quad (3)$$

This suggests that the modification of platinum surface with SWCNT catalyzed the Pu(IV)/Pu(III) redox reaction. SEM image of SWCNT-Pt shown in Fig. 5.6 can be used to understand the role of surface modification on the electrochemical behaviour of Pu(IV)/Pu(III) couple.The platinum surface gets fully covered by the SWCNTs dispersed in nafion matrix. Hence direct contact between the electrolyte solution and platinum surface is restricted and as a result, the spontaneous galvanic reaction between platinum and Pu(IV) is sufficiently suppressed. Therefore, the quasi-reversible redox reaction of Pu(IV)/Pu(III) couple on Pt transformed to a more reversible redox reaction on SWCNT-Pt. The cyclic voltammograms of 25 mM Pu(IV) in 1M H_2SO_4 solution on (a) functionalized and (b) non-functionalized SWCNT-Pt electrodes at a scan rate of 20 mV/s are shown in Fig. 5.7.

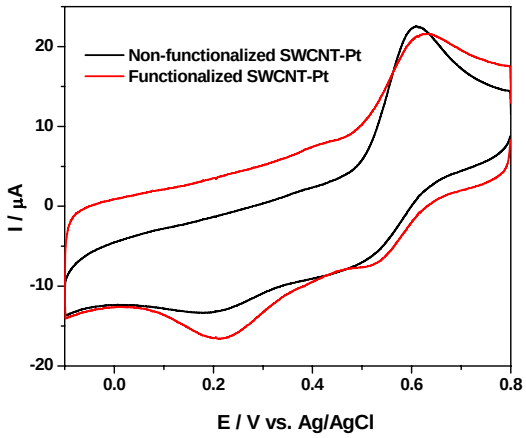

Fig. 5.7. *Cyclic voltammograms of 25 mM Pu(IV) in 1 M H_2SO_4 on functionalized and non-functionalized SWCNT-Pt at a scan rate of 20 mV/s.*

The reduction peak of Pu(IV) became more prominent on the functionalized SWCNT-Pt, but the functionalization also introduced higher capacitive current in the voltammogram. But for these, no significant difference was observed between the two voltammograms obtained on the functionalized and non-functionalized SWCNT-Pt.

5.2.2 (b) Comparison of Electrocatalysis of Pu(IV)/Pu(III)redox couple in 1 M H_2SO_4 on PANI-Pt and SWCNT-Pt

Fig. 5.8A shows the Nyquist plots of Pt, SWCNT-Pt and PANI-Pt electrodes in 25 mM $K_3[Fe(CN)_6]/K_4[Fe(CN)_6]$ + 0.1 M KCl at the open circuit potential (OCP) with an amplitude of 5 mV in the frequency range 10^6 Hz to 10^{-2} Hz. Each plot presents a well defined and depressed semicircle arc in the high frequency region (Inset of Fig. 5.8A) and a straight line in the low frequency region. The impedance spectra were best fitted with the electrical equivalent circuit (EEC) as presented in Fig. 5.8B. The standard notation of the fitted EEC is $R_s(Q[R_{Ct}W])$, where R_s and R_{Ct} correspond to the solution ohmic resistance and the charge transfer resistance across the interface, respectively. W is the Warburg impedance resulting from the diffusion of ions across the electrode-electrolyte interface. Q (Y_0,n) is the constant phase element (CPE) defined as :

(4)

where, Y_0 is the CPE constant, ω is the angular frequency in radians/s, j (=√ -1) is the imaginary number and φ is the CPE exponent. Depending on the value of φ ($0 \leq \varphi \leq 1$), the CPE is considered to be a pure resistor (φ = 0) or a pure capacitor (φ = 1) or Warburg impedance (φ = 0.5).

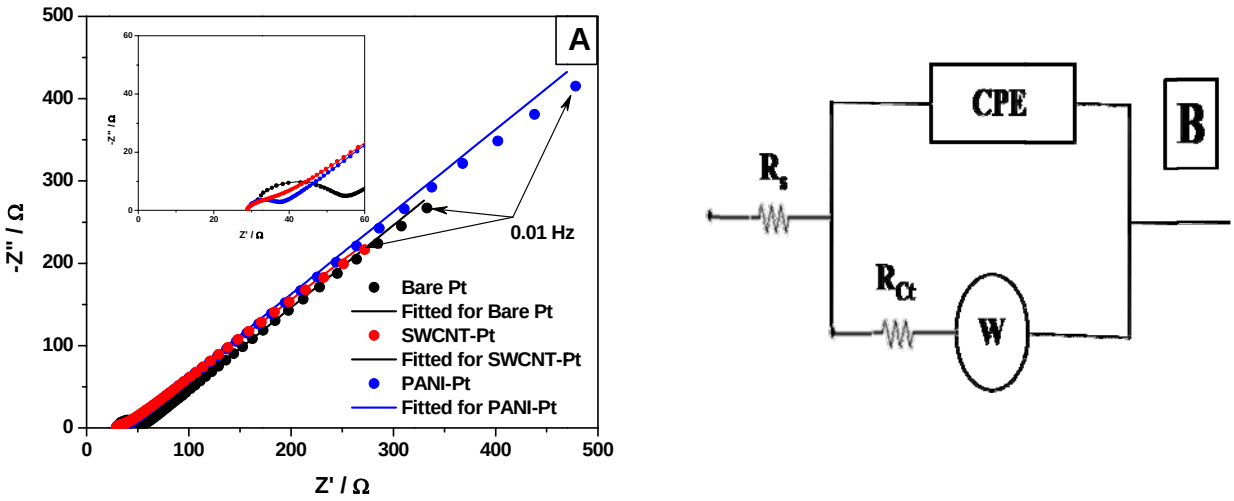

Fig5.8. ***(A)*** *Nyquist plots of Pt, SWCNT-Pt and PANI-Pt electrodes in 25 mM $K_3[Fe(CN)_6]/K_4[Fe(CN)_6]$ + 0.1 M KCl at the open circuit potential (OCP) with an amplitude of 5 mV in the frequency range 10^6 Hz–10^{-2} Hz. Inset shows the zoomed image of the same in the higher frequency region.* ***(B)*** *The best fitted EEC of the impedance spectra.*

Table 5.1 *The best fitted parameters of the impedance spectra of Pt, SWCNT-Pt and PANI-Pt as shown in Fig. 5.8(A).*

Electrode	**R_s / Ω**	**CPE**		**R_{ct} / Ω**	**W / m $\Omega^{-1}s^{1/2}$**	**χ^2**
		Y_0	**n**			
Pt	29.9	0.28	0.9	24.1	4.0	8.3×10^{-3}
SWCNT-Pt	27.3	1.6×10^{-3}	0.5	21.4	2.8	3.7×10^{-3}
PANI-Pt	28.5	1.3×10^{-5}	0.8	9.5	4.1	1.0×10^{-2}

The values of the fitted parameters for the three electrodes are presented in Table 5.1. It can be seen that the charge transfer resistance (R_{ct}) of PANI-Pt is 9.5 Ω, which is much smaller than those of SWCNT-Pt (21.4 Ω) and bare platinum electrode (24.1 Ω). The charge transfer resistance of an electrode is inversely proportional to the rate of electron transfer across the electrode-electrolyte interface. The impedance data i.e. $R_{Ct}^{PANI\text{-}Pt} \leq R_{Ct}^{SWCNT\text{-}Pt} \leq R_{Ct}^{Pt}$ support the trends of the heterogeneous rate constants calculated from the cyclic voltammetry experiments i.e. $k_s^{PANI\text{-}Pt} \geq k_s^{SWCNT\text{-}Pt} \geq k_s^{Pt}$. This is the signature of the best electrocatalytic behavior of PANI-Pt among the three electrode surfaces for Pu(IV)/Pu(III) redox reaction.

5.3 Electrochemical studies of U(VI)/U(IV) redox reaction in 1 M H_2SO_4 at Single-Walled Carbon Nanotubes (SWCNTs) modified gold (Au) electrode

5.3.1 Experimental

All the chemicals like uranyl nitrate, DMF (N,N-dimethyl formamide) and sulphuric acid (H_2SO_4) were of G. R. (Guaranteed Reagent) grade. Single walled carbon nanotubes (SWCNTs) of purity greater than 98% received from nanoshell USA were used. The diameter and the length of SWCNTs were in the range of 0.7 to 2 nm and 3 to 8 μm, respectively. All solutions were prepared in Millipore Milli-Q water (~18 MΩ cm). Cyclic voltammetry and differential pulse voltammetry were performed using CHI 440A electrochemical workstation with a three electrode voltammetric cell having gold disk working electrode (area, A = 0.031 cm^2), platinum wire counter electrode and Ag/AgCl reference electrode. All the potentials are quoted with respect to Ag/AgCl reference electrode. All experiments were carried out at room temperature (25 ± 1^0C). All solutions

were deoxygenated using high purity nitrogen prior to electrochemical experiments. Each measurement was repeated thrice and the average numerical value of each parameter is quoted for discussion (relative error < ± 0.1%). Electrochemical impedance spectroscopy (EIS) was performed using Autolab PGSTAT20 with FRA2 (Eco-Chimie) software. Impedance was recorded at the open circuit potential with single sine excitation signal of 0.005 V for the frequency range 10^6 Hz to 10^{-2} Hz. Impedance spectra were fitted to the electrical equivalent circuits (EEC) and the fits had $\chi^2 \leq 10^{-2}$. Errors of all the calculated parameters were within 5% of the reported values. The morphology of SWCNT-Au was recorded by Seron Incorporation AIS 2000 scanning electron microscope. The stable colloidal dispersion of SWCNTs was separately prepared by sonicating ~2 mg of SWCNTs for one hour in 4 mL of DMF solution. The SWCNT-Au electrode was prepared by dropping 20 μL of the SWCNT suspension on the gold electrode followed by drying.

5.3.2. Results and discussion

5.3.2 a. Electrochemistry of U(VI)/U(IV) in 1 M H_2SO_4 on Au disk electrode

Fig. 5.9 shows cyclic voltammogram of 25 mM U(VI) in 1M H_2SO_4 on gold electrode at a scan rate of 10 mV/s. The cathodic peak (1) at -0.233 V corresponds to the reduction of U(VI) to U(IV). The cyclic voltammograms of the same redox reaction were obtained by varying the scan rate (v) in the range of 10 to 500 mV/s.

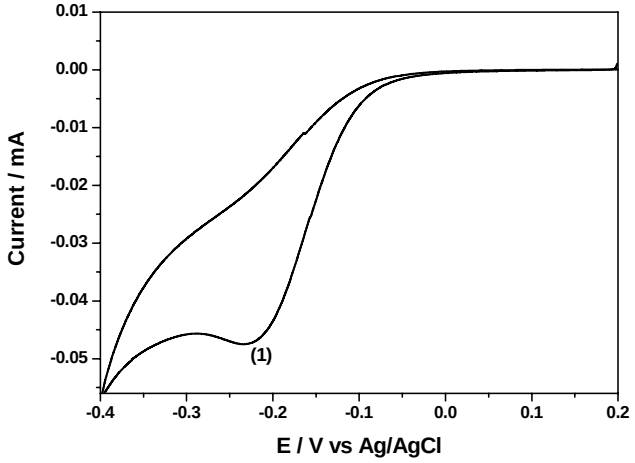

Fig. 5.9. *Cyclic voltammogram of 25 mM U(VI) in 1 M H_2SO_4 on gold electrode at a scan rate of 10 mV/s.*

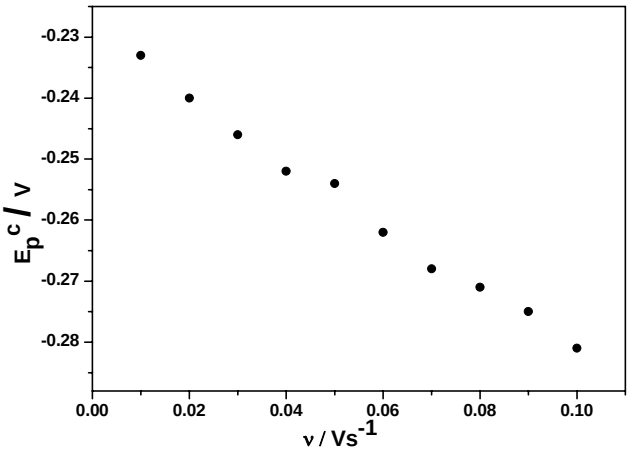

Fig. 5.10. *Variation of cathodic potential (E_p^c) as a function of scan rate.*

It was also noted that the cathodic (E_p^c) peak potential shifted towards more negative value with the increasing scan rate (Fig. 5.10). The ΔE_p i.e. ($E_p^c - E_0'$) also increased with increase in scan rate and showed linear dependence at higher scan rates (150 to 500 mV/s). The linear part of the plot obeys the Laviron equation (given in equation 2) [8] where E_0' value can be deduced from the intercept of E_p^c vs. ν plot on the ordinate by extrapolating the line to ν =0 [9]. The value of αn calculated from the slope was 0.32. The apparent heterogeneous rate constant (k_s) of U(VI)/U(IV) reduction was calculated as 1.59×10^{-3}cm s^{-1}. U(VI)/U(IV) couple is expected to exhibit irreversible electron transfer process because it involves uranium–oxygen bond formation reaction.

5.3.2.b. Electrochemistry of U(VI)/U(IV) in 1 M H_2SO_4 on SWCNT-Au

Cyclic voltammogram of 25 mM U(VI) in 1M H_2SO_4 solution on SWCNT-Au electrode at a scan rate of 10 mV/s is shown in Fig. 5.11. The CV of U(VI) recorded on bare Au is also

included in this figure for comparison. The cathodic peak at -0.140 V observed on SWCNT-Pt corresponds to the reduction of U(VI) to U(IV). The peak potential is having an anodic shift of 93 mV at SWCNT-Au electrode with respect to the bare Au electrode. Enhancement of the redox peak current along with significant anodic shift i.e. decrease in overpotential suggests electrocatalytic action of SWCNT-Au for the U(VI)/U(IV) redox reaction. Fig. 5.12 gives a comparison of the cathodic peak currents (Ip^c) of U(VI)/U(IV) redox reaction for Au and SWCNT-Au electrodes for the scan rates ranging from 10 to 100 mV/s. Fig. 5.13 shows the plot of cathodic peak current (Ip^c) vs square root of the scan rate ($\nu^{1/2}$). Ip^c was found to increase linearly with the square root of the scan rate suggesting that the electrochemical reaction of U(VI)/U(IV) couple in 1 M H_2SO_4 on SWCNT-Au is governed by the diffusion controlled process. The values of αn and the heterogeneous rate constant (k_s) of U(VI) reduction on SWCNT-Au in 1 M H_2SO_4 were calculated as 0.56 and 4.26×10^{-3}cm s^{-1}, respectively which is almost double the value obtained for the bare Au electrode. This suggests that the modification of gold surface with the SWCNT catalyzed the U(VI)/U(IV) redox reaction.

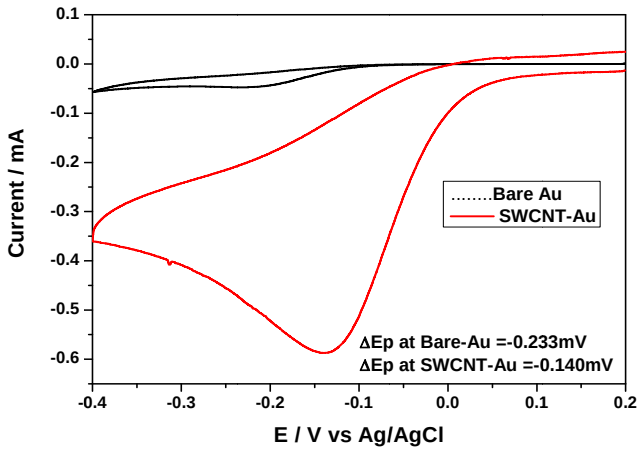

Fig. 5.11. *Cyclic voltammogram of 25 mM U(VI) in 1M H_2SO_4 solution on Au and SWCNT-Au electrodes at a scan rate of 10 mV/s.*

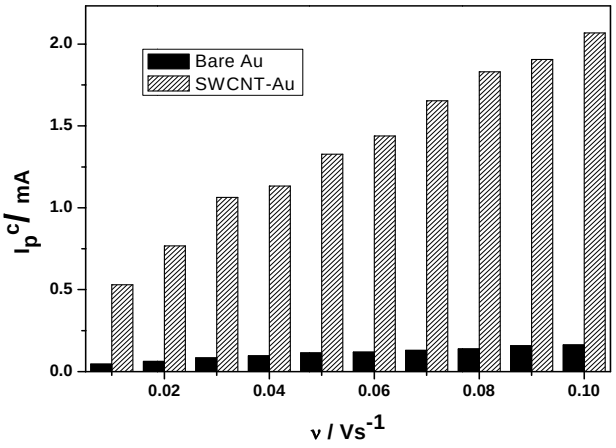

Fig. 5.12. *The cathodic peak currents of U(VI)/U(IV) redox reaction on Au and SWCNT-Au electrodes for scan rates ranging from 10 to 100 mV/s.*

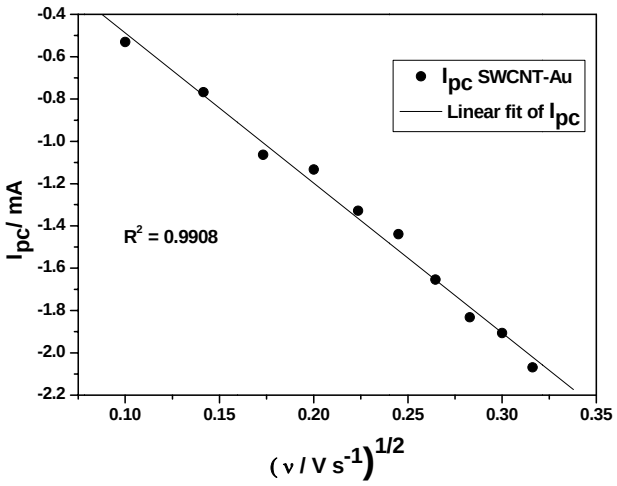

Fig. 5.13. *Cathodic peak current (Ip^c) vs. square root of scan rate ($v^{1/2}$) for SWCNT-Au electrode.*

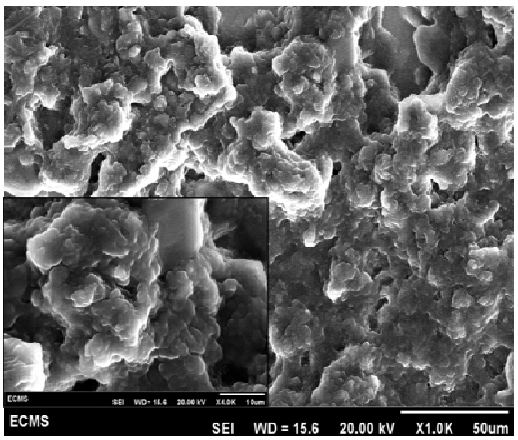

Fig.5.14. *SEM image of SWCNT-Au. Inset shows the higher magnification image.*

Fig. 5.14 presents the SEM image of SWCNT-Au electrode and it is seen that the SWCNTs are uniformly coated on the electrode surface leading to a mushroom like porous reticular formation. The special surface morphology provided a much larger real surface area than the

apparent geometric area. Differential pulse voltammograms (DPV) of bare Au and SWCNT-Au electrodes in 25 mM U(VI) in 1M H_2SO_4 solution are shown in Fig.5.15. On SWCNT-Au, the current values corresponding to U(VI) reduction increased significantly. The reduction waves were also well defined in the case of SWCNT-Au electrode as compared to that with bare Au electrode. Hence the CV and DPV studies prove that the modification of the gold surface with SWCNT results in a better redox behavior of U(VI)/U(IV) couple. In DPV, the peak current was found to increase with increase in the uranium concentration suggesting the potential application of SWCNT-Au electrode for uranium determination.

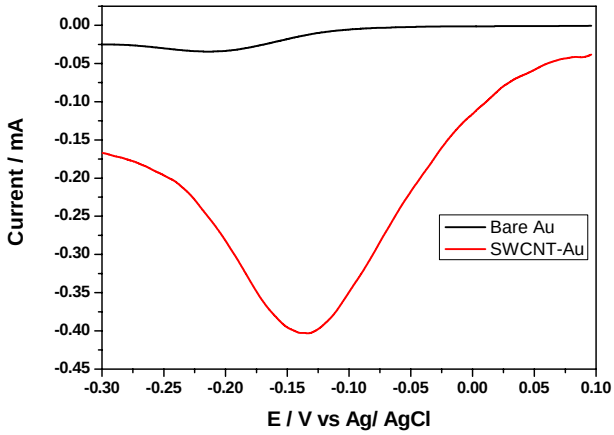

Fig.5.15. *DPV of 25 mM U(VI) in 1M H_2SO_4 on bare Au and SWCNT-Au electrodes.*

Fig. 5.16 shows the Nyquist plots of Au and SWCNT-Au electrodes in 25 mM $K_3[Fe(CN)_6]/K_4[Fe(CN)_6]$ + 0.1 M KCl at the open circuit potential (OCP) with an amplitude of 5 mV in the frequency range 10^6 Hz–10^{-2} Hz. Each of the two plots showed a well defined and depressed semicircular arc in the high frequency region and a straight line in the low frequency region.

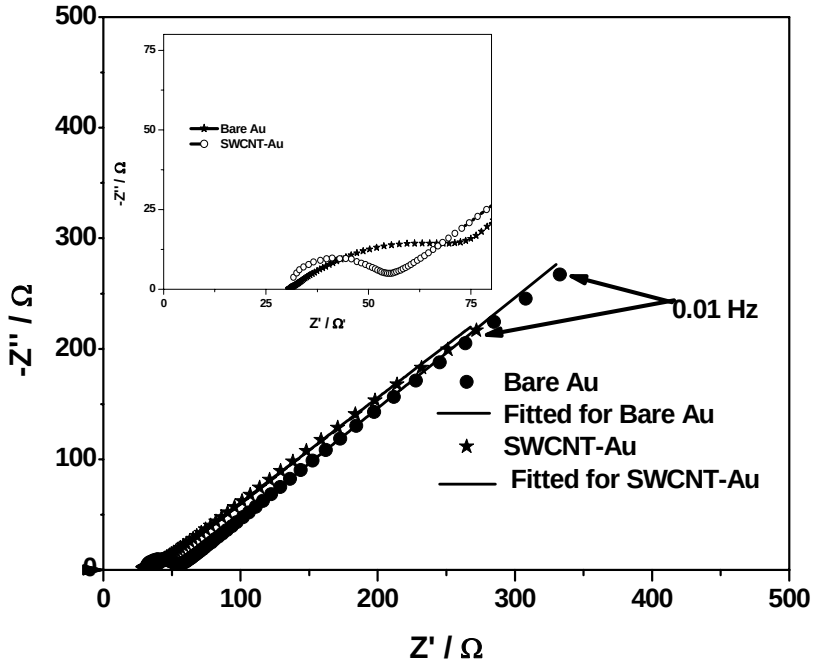

Fig.5.16. *Nyquist plots of bare Au and SWCNT-Au electrodes in 25 mM $K_3[Fe(CN)_6]/K_4[Fe(CN)_6]$ + 0.1 M KCl at the open circuit potential (OCP) with an amplitude of 5 mV in the frequency range 10^6 Hz–10^{-2} Hz.*

It was seen that the charge transfer resistance (R_{ct}) of SWCNT-Au was 12.3 Ω, which was much smaller than that of bare gold electrode (32.6 Ω). The charge transfer resistance of an electrode is inversely proportional to the rate of electron transfer across the electrode-electrolyte interface. The impedance data i.e. $R_{ct}^{SWCNT\text{-}Au} < R_{ct}^{Au}$ supported the trends of the heterogeneous rate constants calculated from the cyclic voltammetry experiments i.e. $k_s^{SWCNT\text{-}Au} > k_s^{Au}$. This confirms the electrocatalytic behavior of SWCNT-Au for the U(VI)/U(IV) redox reaction.

5.4. Single-Walled Carbon Nanotubes (SWCNTs) modified gold (Au) electrode for Simultaneous Determination of Plutonium and Uranium

5.4.1 Experimental

All the experimental conditions were same as those discussed in Section 5.3.1.

5.4.2. Results and discussion

5.4.2 a. Electrochemical behavior of uranium and plutonium

Initial experiments showed that the electrochemical detection of U and Pu simultaneously on untreated ordinary electrodes is difficult. Firstly; hydrogen evolution takes place at high overpotential required for the reduction of uranium. Secondly, very low peak currents are obtained due to the absence of electrocatalytic behavior at bare electrode for Pu and U determination. To confirm this at the SWCNT-Au electrode, the electrochemical behavior of Pu(IV)/Pu(III) and U(VI)/U(IV) redox couples on the surface of the bare Au were investigated.

Fig. 5.17A depicts cyclic voltammograms (CVs) of bare Au without (curve 1) and in presence of (curve 2) 10 mM Pu in 1M H_2SO_4 solution. Fig. 5.17B shows CV of bare Au in absence (curve 1) and presence (curve 2) of 10 mM U in 1M H_2SO_4 solution. The CVs in Fig 5.17 were recorded at a scan rate of 10 mV s^{-1}. Fig. 5.17A shows that the CV of H_2SO_4 solution at bare Au in the potential range from 0 to 0.8 V has no oxidation and reduction peaks. On the other hand, Pu(IV)/Pu(III) redox couple shows a quasi-reversible wave with an oxidative peak at E_{pa} = 0.695 V and a cathodic peak at E_{pc} = 0.124 V (curve 2). The separation between anodic and cathodic peak potentials is approximately 0.571 V for Pu(IV)/Pu(III)couple. Similarly, U(VI)/U(IV) redox couple demonstrates only a broad reduction peak at -0.233 V (Fig 5.17 B). As can be seen from Fig. 5.17B, the CV of U(VI)/U(IV) couple has a cathodic peak without any anodic wave. Moreover, the peak

currents of the two redox couples are quite small indicating the sluggish electron transfer kinetics of these redox couples at the bare Au.

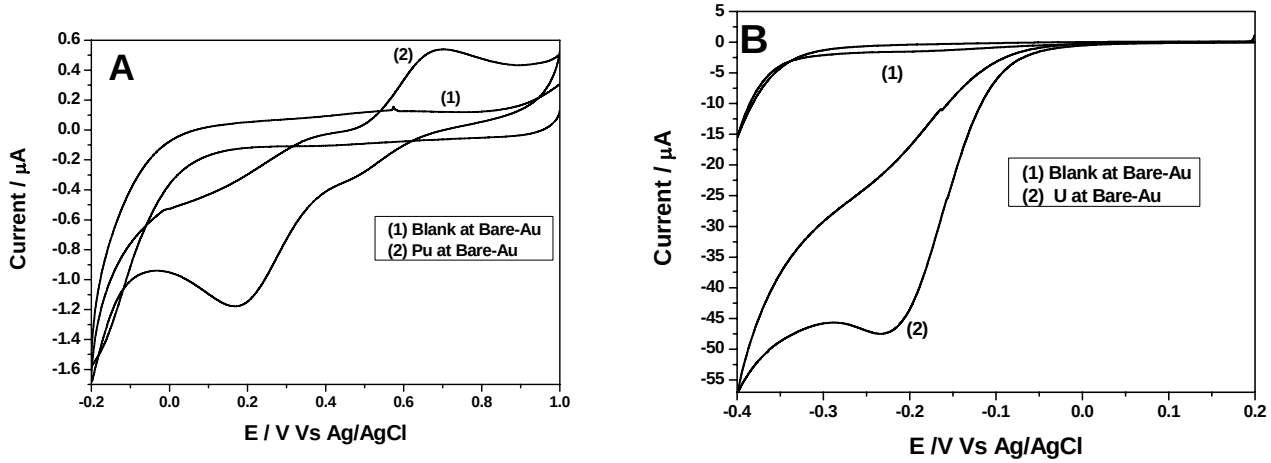

Fig. 5.17. *Cyclic voltammograms recorded (A) at bare Au in the absence (1), in the presence of 10 mM Pu (2) (B) absence (1), in the presence of 10 mM U(2) in 1 M H_2SO_4 solution at a scan rate of 10mV $s^{-1.}$*

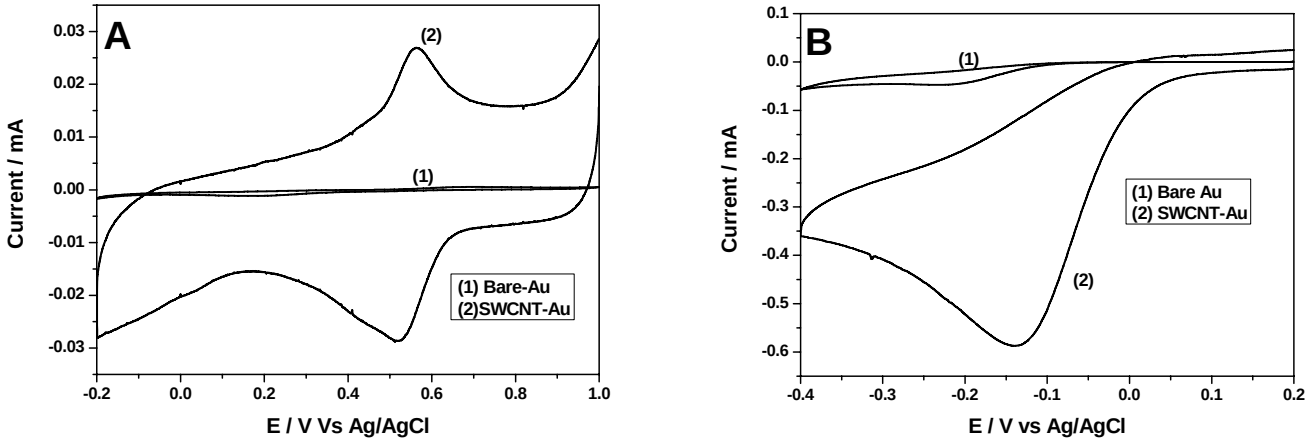

Fig. 5.18. *Cyclic voltammograms of (A)10 mM Pu in 1 M H_2SO_4 solution on Au (1) and SWCNT-Au (2) electrodes, (B) 10 mM U in 1 M H_2SO_4 solution on Au (1) and SWCNT-Au (2) electrodes at a scan rate of 10 mV/s.*

Fig. 5.18A shows the CV of Pu(IV)/Pu(III)couple on SWCNT-Au electrode. The cyclic voltammogram of Pu(IV) recorded on bare Au (which is already presented as Fig.5.17A) was

overlaid in same scale in Fig. 5.18A for comparison. SWCNT-Au electrode shows a pair of well-defined redox transitions with anodic and cathodic peak potentials at 0.574 V and 0.512 V, respectively. Furthermore, the cathodic peak potential of Pu(IV)/Pu(III) couple shifts from 0.124 V at the bare Au to 0.512 V at SWCNT/Au, and the peak current increased approximately 3-fold in comparison to that on bare Au. Fig. 5.18B shows CV of U(VI)/U(IV) couple on SWCNT-Au. The cyclic voltammogram of U(VI)/U(IV) recorded on bare Au is overlaid in the same scale. The cathodic peak potential for the reduction of U(VI)/U(IV) occurs at -0.132 V, which is approximately 0.101 V more positive than that at the bare Au, and the cathodic peak current is also enhanced significantly. The decrease of reduction overpotential, accompanied by a significant increase in the reduction current of U(VI)/U(IV) couple and a pair of symmetric redox peaks with smaller peak separation for Pu(IV)/Pu(III)couple, strongly indicates excellent catalytic ability of SWCNTs on the redox reaction of these couples. These observations demonstrate that SWCNTs accelerate the reduction of U(VI)/U(IV) and Pu(IV)/Pu(III) couples.

To study the effect of potential sweep rate (ν) on the peak current, cyclic voltammetric studies were carried out in the range of 10 to 500 mV s^{-1} in 1M H_2SO_4 solution containing 10 mM Pu and 10 mM U at the SWCNT-Au electrode (Fig. 5.19).

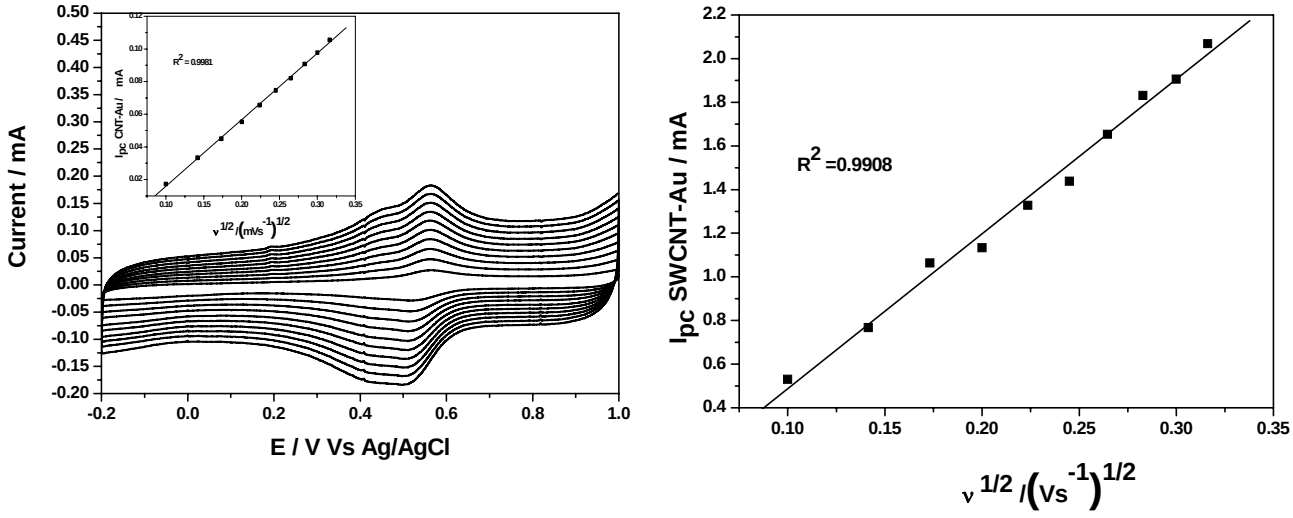

Fig. 5.19. *(A) Cyclic voltammogram of 10 mM Pu in 1 M H_2SO_4 solution on SWCNT-Au electrode. Scan rate range: 0.01-0.1 V $s^{-1.}$ Inset shows the variation of cathodic peak current i_p^c with square root of the scan rate (in V/s) in the range of 10-100 mV/s. (B) Variation of cathodic current i_p^c of 10 mM U solution with square root of the scan rate (in V/s) in the range of 10-100 mV/s*

The results showed that the cathodic peak currents vary linearly with the square root of the scan rate ($\nu^{1/2}$) for both U and Pu confirming the diffusion-controlled process for reduction of Pu(IV) and U(VI) on the surface of the SWCNT-Au in the studied range of potential sweep rates according the following equations:

Pu: i_{pc} (μA) = -0.248 $\nu^{1/2}$ (V s^{-1}) + 0.407 (R^2 =0.9981) (5)

U: i_{pc} (μA) = -0.220 $\nu^{1/2}$ (V s^{-1}) + 0.007 (R^2 =0.9908) (6)

5.4.2b. Electrochemical behavior of uranium and plutonium mixtures

Fig. 5.20A shows the CVs of a solution containing mixture of Pu(IV)/Pu(III) and U(VI)/U(IV) redox couple at the bare Au (Curve 1) and SWCNT/ Au (Curve 2). At the

bare Au, two broad cathodic peaks were obtained with very small currents. Therefore, it is impossible to determine the individual concentration of each element from the broad voltammetric peak on the surface of Au. At the SWCNT/Au, the voltammetric peaks of Pu(IV)/Pu(III) couple and U(VI)/U(IV) couple appeared at 0.512 V and -0.132 V, respectively, in 1M H_2SO_4. (curve 2). Fig 5.20B shows DPV of a mixture of Pu(IV)/Pu(III) and U(VI)/U(IV) redox couples at SWCNT-Au. The results show that the peak potential separation of 0.687 V and the appreciable peak currents of Pu and U in presence of each other permit simultaneous differential pulse voltammetric determination of Pu and U. The above obtained results demonstrate that SWCNTs accelerate the reduction of Pu(IV)/Pu(III) couple and U(VI)/U(IV) reactions because of many edge plane graphite and many defects.

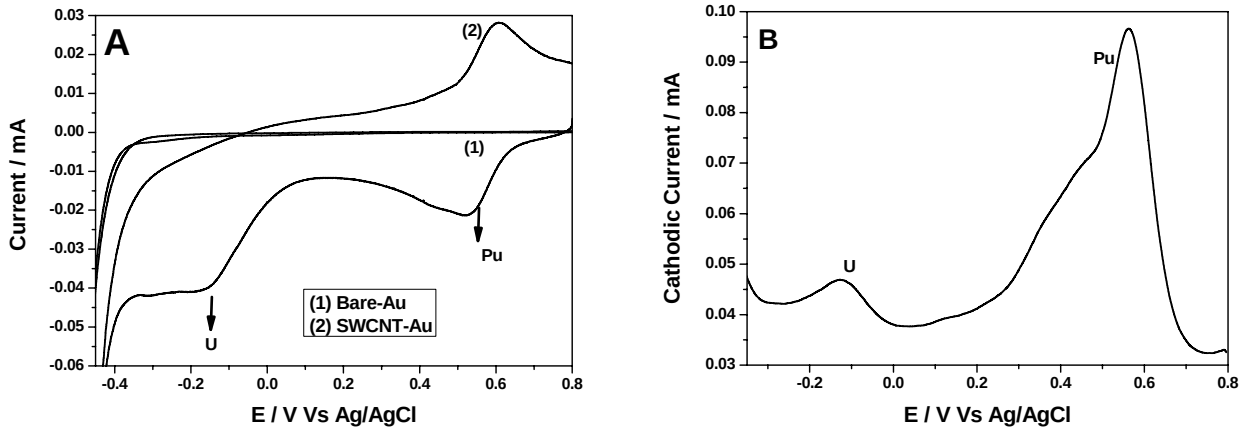

Fig.5.20. (A) *Cyclic voltammogram of a mixture of Pu and U in 1 M H_2SO_4 solution on Au (1) and SWCNT-Au (2) electrodes at a scan rate of 0.01 Vs^{-1}* ***(B)*** *DPV of SWCNT-Au in 1 M H_2SO_4 solution containing mixture of Pu and U. DPV conditions: amplitude,50 mV; pulse width, 50 ms; pulse period, 200 ms.*

On the other hand, the remarkable peak current enhancement and the decrease in reduction overpotentials undoubtedly testifies to the electrocatalytic properties of the SWCNT-Au for

the reduction of Pu(IV) and U(VI). Indeed, the SWCNT/Au electrode presents an interlinked highly mesoporous three-dimensional structure with a relatively higher electrochemically accessible surface area and easier charge transfer at the electrode/electrolyte interface [2]. Therefore, the SWCNT/Au greatly holds the potential of simultaneous determination of Pu and U on account of unusual structure and properties of SWCNTs (i.e., subtle electronic properties). It should be noted that the calculated electroactive surface area for the SWCNT/Au via application of $Fe(CN)6^{3-/4-}$ as an electroactive probe ions was $1.8x10^{-3}$ cm^2, which is 3 orders of magnitude higher than that of bare Au electrode. The significant increase in the electroactive surface area suggests that SWCNT/Au is promising for electrocatalytic reduction and electrochemical sensing.

5.4.2c. Individual Determination of Pu and U

Differential pulse voltammogram recorded for Pu (Fig. 5.21A) and U (Fig. 5.21B) show well defined peaks with E_p = 0.56 V and -0.13 V, respectively. The calibration graphs constructed over concentration range 10 to 100 μM (R^2 = 0.990) for Pu (Inset of 5.21A) and 3 to 10 μM (R^2 = 0.987) for U (Inset of Fig. 5.21B) are linear. The linear equations of the calibration plots are given below:

SWCNT-Au (Pu) : I_p (μA) = 3.4 μA + 4.661 μA / μM; (R^2 = 0.9904) (7)

SWCNT-Au (U) : I_p (μA) = 6.76 μA + 26.3581 μA / μM; (R^2 = 0.9878) (8)

The detection limit was calculated using the formula 3σ/slope where σ is the standard deviation of the blank which was taken from five replicates. The detection limits were found to be 8.2 μM for Pu and 2.4 μM for U at S/N = 3.

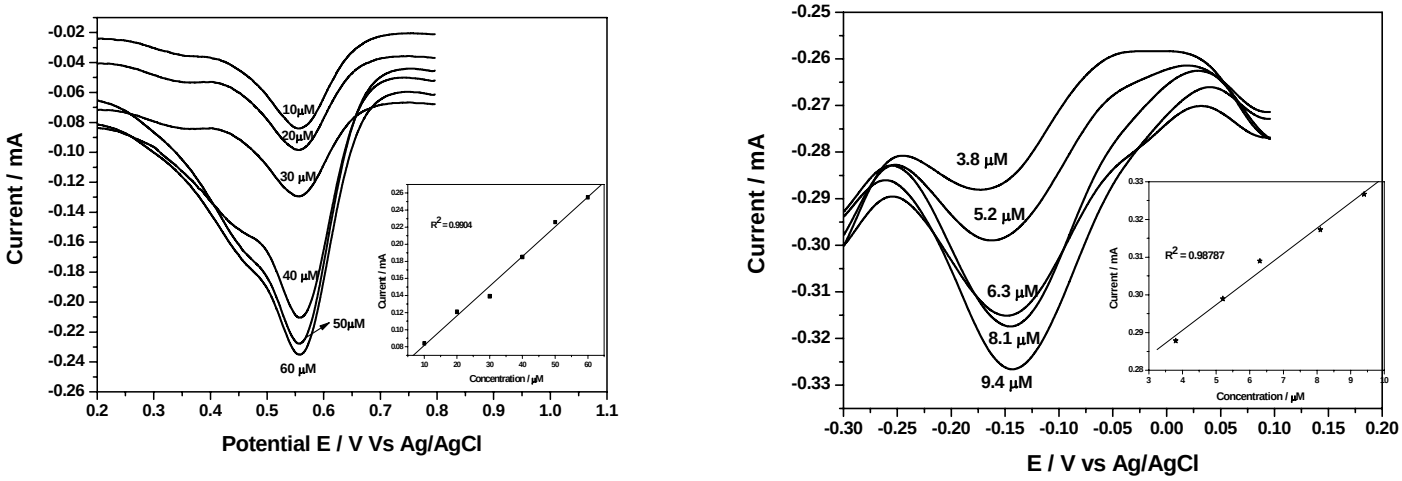

Fig. 5.21. (A) *DPV of various concentrations of Pu from 10 to 60 μM in 1 M H_2SO_4 solution. Inset: plot of cathodic peak current for Pu vs. Pu concentration.* ***(B)*** *DPV of various concentration of U from 3.8 to 9.4 μM in 1 M H_2SO_4 solution. Inset: plot of cathodic peak current for U, vs. U concentration*

5.4.2d. Simultaneous Determination of Pu and U

To verify the feasibility of the simultaneous determination of Pu and U at SWCNT-Au electrode, DPV measurements were carried out in their mixture of different concentrations. This study was carried out using Fast Breeder Test Reactor (FBTR) fuel samples. The calculated concentrations of Pu and U in FBTR fuel samples are in good agreement with the concentrations of Pu and U in these samples determined by Biamperometry. (Table 5.2)

Table 5. 2 *Simultaneous determination of Pu and U in FBTR fuel samples*

Analyte (Pu,U) Carbide	Concentration of Pu(mg/g)		Concentration of U(mg/g)	
	DPV (n=3)	Biamperometry(n=2)	DPV (n=3)	Biamperometry(n=2)
Sample 1	2.346(±0.92)	2.427(±0.02)	1.085(±0.63)	1.014(±0.05)
Sample 2	3.151(±0.53)	3.148(±0.09)	1.32(±0.85)	1.283(±0.03)
Sample 3	4.435(±0.23)	4.447(±0.04)	1.98(±0.96)	1.902(±0.18)
Sample 4	5.120(±0.21)	5.105 (±0.05)	2.102(±1.3)	2.112(±0.00)

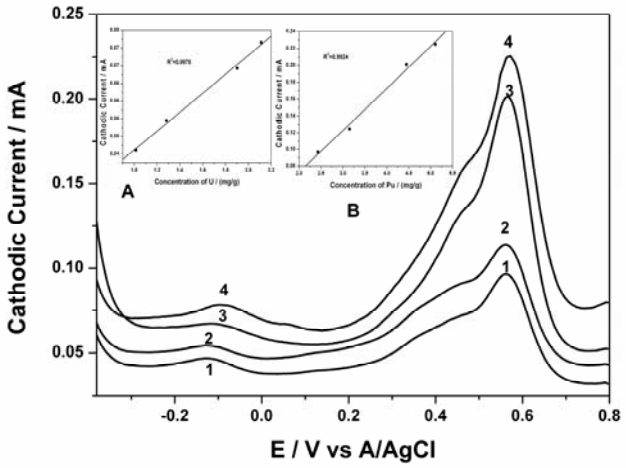

Fig.5.22. *DPV of various FBTR fuel samples containing different amount of Pu and U given in Table 2.Inset (1) shows the calibration plot for U, Inset(2) shows calibration plot of Pu.*

Fig. 5.22 shows DP voltammograms of the solutions having the mixture of Pu and U with different concentrations at SWCNT-Au electrode. As can be seen from Figure 5.22, two well defined reduction peaks of Pu and U at about 0.562 V and -0.125 V, respectively, were observed. The results show that the peak potential separation of 0.687 V between Pu(IV)/Pu(III) and U(VI)/(IV) couples and the appreciable peak currents of Pu and U in the presence of each other permit the simultaneous differential pulse voltammetric determination

of Pu and U. This confirms that the simultaneous determination of the two actinide elements is possible in a mixture, using the SWCNT-Au electrode.

5.5 Electrochemical Investigations on Np(VI)/Np(V) redox couple using Single walled carbon nanotube modified glassy carbon electrode (SWCNT-GC)

5.5.1. Results and discussion

5.5.1a. Electrochemistry of Np(VI)/Np(V) in 1 M H_2SO_4 on glassy carbon disk electrode

Fig. 5.23 shows cyclic voltammogram of 50 mM Np solution in 1M H_2SO_4 on glassy carbon electrode at a scan rate of 50 mV/s. Cathodic peak (1) at 0.624 V and anodic peak (1') at 1.076V correspond to the reduction of Np(VI) to Np(V) and vice-versa, respectively. The peak-to-peak potential separation (ΔE_p) of 452 mV was attributed to the quasi-reversible electron transfer reaction of Np(VI)/Np(V) couple. The cyclic voltammetry of this redox reaction was studied by varying the scan rate (ν) in the range of 10-500 mV/s. The plots of I_p versus $\nu^{1/2}$ for both the cathodic and the anodic peaks gave straight lines (Inset of Fig.5.23). This clearly suggests that the electrochemical reaction of Np(VI)/Np(V) couple onto glassy carbon electrode in 1 M H_2SO_4 solution is governed by the diffusion process.

The cathodic (E_p^c) and anodic (E_p^a) peak potentials were found to shift towards more negative and positive directions, respectively, with increasing scan rate (Fig. 5.24). ΔE_p also increased with scan rate and showed linear dependence at higher scan rates (150-500 mV/s). The linear part of the plot obeys the Laviron equation (Equations 2 and 3). The values of α and n calculated from the two slopes were ca. 0.34 and 0.91. The apparent heterogeneous rate constant (k_s) of Np(VI)/Np(V) reduction was calculated as 0.98×10^{-1}cm s^{-1}. This suggests

that the redox reaction of Np(VI)/Np(V) couple in 1 M H_2SO_4 solution is a quasi-reversible

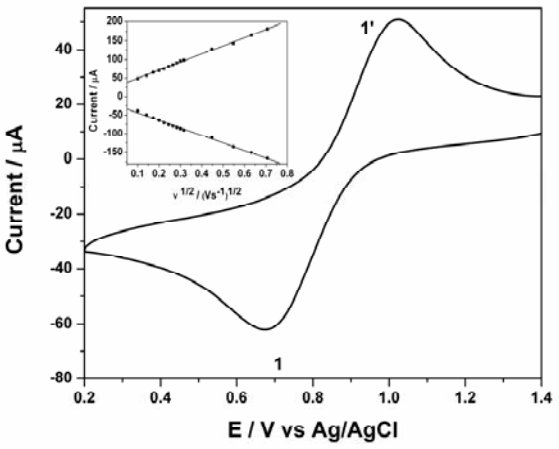

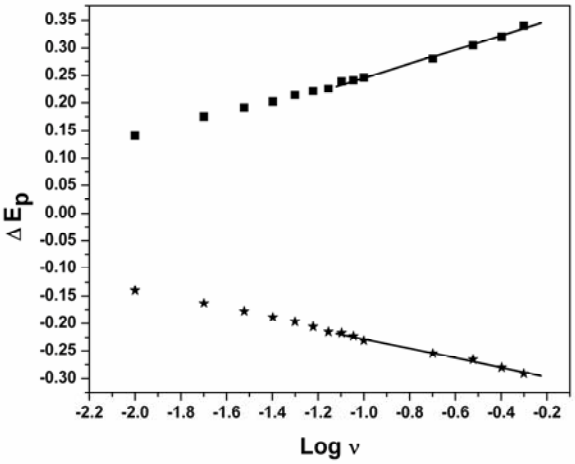

one-electron transfer process .

Fig. 5.23. *Cyclic voltammogram of 50 mM Np solution in 1 M H_2SO_4 on glassy carbon electrode at a scan rate of 20 mV/s. Inset shows the variation of the cathodic and anodic peak currents as a function of square root of scan rate at glassy carbon electrode.*

Fig.5.24. *Variation of cathodic and anodic peak potentials (ΔE_p) with respect to E_0' as a function of logarithm of scan rate.*

5.5.1b. Electrochemistry of Np(VI)/Np(V) in 1 M H_2SO_4 on SWCNT-GC

Cyclic voltammogram of 50 mM Np solution in 1M H_2SO_4 on SWCNT-GC electrode at a scan rate of 50 mV/s is shown in Fig. 5.25. The cyclic voltammogram of Np recorded on GC (presented as Fig.5.23) was overlaid in the same scale in Fig. 5.25 for the sake of comparison.

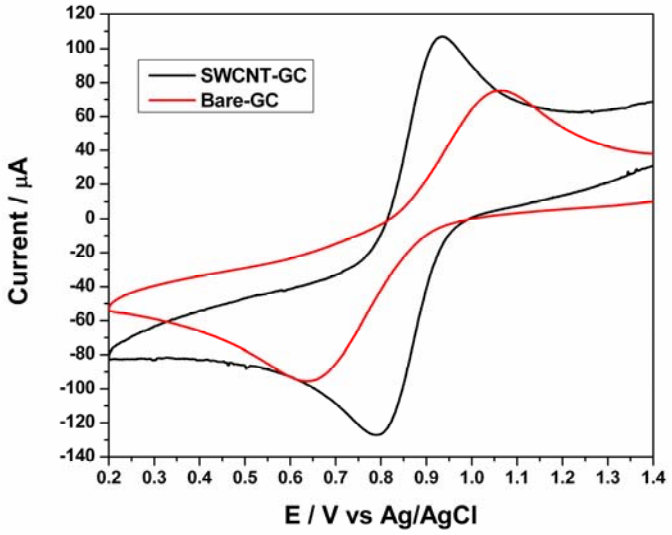

Fig.5.25. *Cyclic voltammograms of 50 mM Np solution in 1 M H_2SO_4 solution on GC and SWCNT-GC electrodes at a scan rate of 20 mV/s.*

The cathodic peak (1) at 0.792 V and the anodic peak (1') at 0.934 V observed on SWCNT-GC correspond to the reduction of Np(VI) to Np(V) and vice-versa, respectively. The peak-to-peak potential separation (ΔE_p) is 142 mV, which is much smaller than the ΔE_p value of 452 mV observed on bare glassy carbon electrode. It indicates that the Np(VI)/Np(V) couple exhibits a quasi-reversible electron transfer behavior on SWCNT-GC. The increase of the redox peak current along with the significant enhancement in the electrochemical reversibility suggest the electrocatalytic action of SWCNT-GC for the Np(VI)/Np(V) redox reaction. The plots of Ip versus $\nu^{1/2}$ for both the cathodic and the anodic peaks yield straight lines (Fig.5.26.). This suggests that the electrochemical reaction of Np(VI)/Np(V) couple onto SWCNT-GC in 1 M H_2SO_4 solution is also governed by the diffusion process.

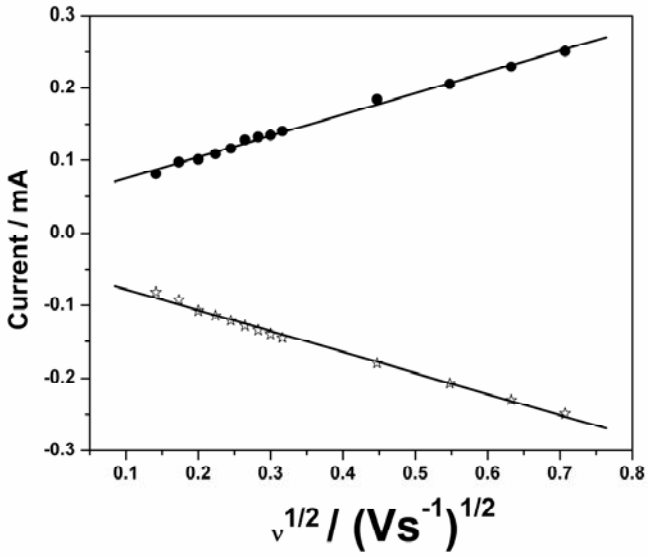

Fig.5.26. V*ariation of the cathodic and anodic peak currents as a function of square root of scan rate at SWCNT-GC electrode.*

The charge transfer coefficient (α) and the heterogeneous rate constant (k_s) of Np(VI) reduction on SWCNT-GC in 1 M H_2SO_4 were calculated as 0.83 and 5.25×10^{-1}cm s^{-1}, respectively. This shows that the modification of glassy carbon surface with SWCNT catalyzed the Np(VI)/Np(V) redox reaction. Indeed, the SWCNT/GC electrode presents an interlinked highly mesoporous three-dimensional structure with a relatively higher electrochemically accessible surface area and easier charge transfer at the electrode/electrolyte interface. Therefore, the quasi-reversible redox reaction of Np(VI)/Np(V) couple on GC transformed to a more reversible redox reaction on SWCNT-GC.

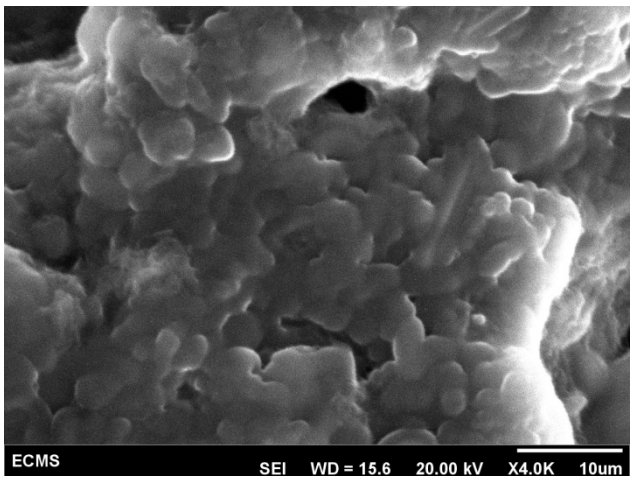

Fig. 5.27. SEM image of SWCNT-GC.

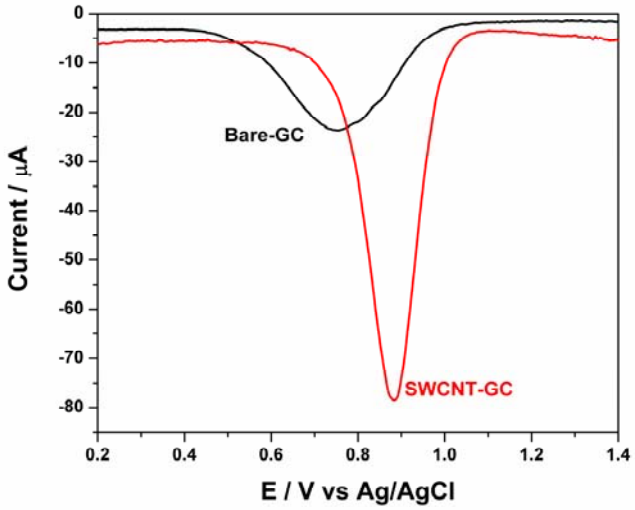

Fig.5.28.*Differential pulse voltammogram (DPV) of 50 mM Np solution in 1M H_2SO_4 on bare GC and SWCNT-GC electrodes.*

Fig. 5.27 presents the SEM image of SWCNT-GC electrode and it is seen that the SWCNTs are uniformly coated on the electrode surface leading to a mushroom like porous reticular formation. The special surface morphology provided a much larger real surface area than the apparent geometric area. Differential pulse voltammograms (DPV) of bare GC and SWCNT-GC electrodes in 50 mM Np solution in 1M H_2SO_4 are shown in Fig.5.28. On SWCNT-GC, the current values corresponding to Np(VI) reduction increased significantly. The reduction wave was also well defined in the case of SWCNT-GC electrode as compared to that with bare GC electrode. Hence the CV and DPV studies prove that the modification of the glassy carbon surface with SWCNT results in a better redox behavior of Np(VI)/Np(V) couple.

Fig.5.29 shows Nyquist plots of bare GC and SWCNT-GC electrodes in 25 mM $K_3[Fe(CN)_6]/K_4[Fe(CN)_6]$ + 0.1 M KCl at the open circuit potential (OCP) with an amplitude of 5 mV in the frequency range 10^6 Hz–10^{-2} Hz. Each of the two plots showed a well defined and depressed semicircular arc in the high frequency region and a straight line in the low frequency region.

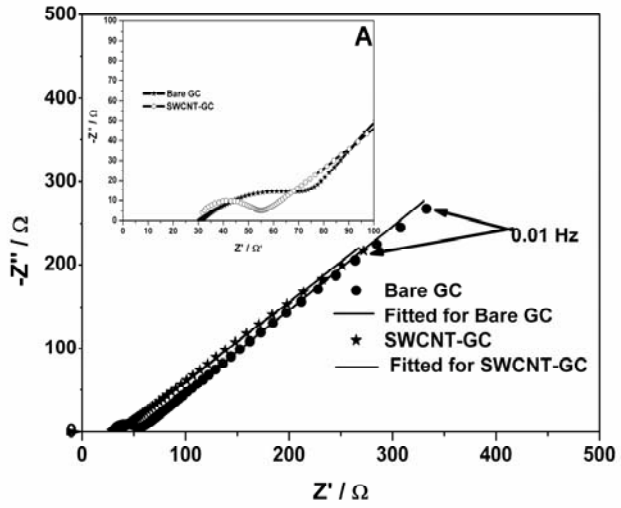

Fig.5.29. *Nyquist plots of GC and SWCNT-GC electrodes in 25 mM $K_3[Fe(CN)_6]/K_4[Fe(CN)_6]$ + 0.1 M KCl at the open circuit potential (OCP) with an amplitude of 5 mV in the frequency range 10^6 Hz–10^{-2} Hz.*

It was seen that the charge transfer resistance (R_{ct}) of SWCNT-GC was 16.2 Ω, which was much smaller than that of the bare glassy carbon electrode (41.3 Ω). The charge transfer resistance of an electrode is inversely proportional to the rate of electron transfer across the electrode-electrolyte interface. The impedance data i.e. $R_{ct}^{SWCNT\text{-}GC} < R_{ct}^{GC}$ supported the trends of the heterogeneous rate constants calculated from the cyclic voltammetry experiments i.e. $k_s^{SWCNT\text{-}GC} > k_s^{GC}$. This confirms the electrocatalytic behavior of SWCNT-GC for the Np(VI)/Np(V) redox reaction.

5.6. Conclusion

The modified platinum, gold and glassy carbon electrodes prepared by the optimized procedures showed good electrocatalytic properties for Pu, U and Np redox reactions in 1 M H_2SO_4. The electrocatalysis of these three redox couples on SWCNT modified electrodes is driven by the increase in the rate constant of the electron transfer reaction at SWCNT modified electrodes compared to the bare electrodes. The SWCNT modified electrodes showed excellent sensitivity to the determination of U and Pu in FBTR fuel samples by differential pulse voltammetry. This not only provides a new opportunity to improve the quality of actinides analysis and shortens the analytical time for the electroanalysis of actinides and other elements in nuclear fuel samples; but also reveals the interesting electrochemistry of Pu, U and Np with the modifiers (SWCNTs) and its impact on the analytical response of these actinides.

5.7. References

1. K.D. Singh Mudher and K. Krishnan, Crystal structure of $K_4Pu(SO_4)_4 \cdot 2H_2O$ *J. Alloys & Compounds* **313** (2000) 65.
2. M. Pumera and H. Iwai, Metallic impurities within residual catalyst metallic nanoparticles are in some cases responsible for "Electrocatalytic" effect of carbon nanotubes *Chem. Asian J.*, **4 (**2009) 554.
3. M. Pumera and H. Iwai, Multicomponent metallic impurities and their influence upon the electrochemistry of carbon nanotubes *J. Phys. Chem. C* **113** (2009) 4401.
4. D.V. Vezenov, A. Noy, L.F. Rozsnyai and C. M. Lieber, Force titrations and ionization state sensitive imaging of functional groups in aqueous solutions by chemical force microscopy *J. Am. Chem. Soc*., **119** (1997) 2006.
5. S.S. Wong, E. Joselevvich, A.T. Woolley, C.L. Cheung and C.M. Lieber, Covalently functionalized nanotubes as nanometre sized probes in chemistry and biology *Letters to Nature*, **394** (1998) 52.
6. R. Stewart and K. Vates, *J. Am. Chem. Soc. The Position of Protonation of the Carboxyl Group1* **82**, (1960) 4059.
7. O.J. Wick (Ed.), *Plutonium Handbook : A Guide to the Technology*, **Vol. 1**, Gordon and Breach, Science Publishers,1967, London.
8. E. Laviron , General expression of the linear potential sweep voltammogram in the case of diffusionless electrochemical systems. *J. Electroanal. Chem.* **101** (1979)19 .

9. Umesh Chandra, Gilbert Ongera, B.E Kumara Swamy, D.B. Yadav and B.S Sherigara Electrochemical studies of eriochrome black T at carbon paste electrode and immobilized by SDS surfactant: A cyclic voltammetric study. *Int. J. Electrochem. Sci.* **3**, (2008) 1044.

Conclusions and future scope

Conclusions

The present dissertation focuses on electrodes modified with single walled carbon nanotubes and electrochemical behaviour of actinides at the modified electrode in aqueous solution.The main aim of this thesis was the preparation, characterization and applications of electrodes modified with metal nanoparticle, conducting polymer and carbon nanotubes. These were applied for electrocatalytic reactions such as formic acid and methanol oxidation and also for studying the redox behavior of actinides. The intention of these studies was to utilize the modified electrodes for determination of actinides in the nuclear fuel samples and to mitigate the effect of CO poisoning in direct formic acid fuel cells (DFAFC) and direct methanol fuel cells (DMFC).

Synthesis of palladium nanoparticles on platinum electrode was carried out by employing a potentiostatic pulse method of electrodeposition. The mechanism of electrocrystallization of PdNPs on Pt was investigated. Experimental results showed that Pd electrodeposition follows Volmer–Weber growth mechanism. The nucleation and growth phenomena in the initial stages of Pd deposition were investigated by potentiostatic transient measurements. Experimental current transients for 0.28V and 0.15V in a non-dimensional $(i/i_{max})^2$ vs. t/t_{max} plot were compared with the theoretical curves. The transient at 0.15V fits relatively well with the theoretical curve for instantaneous nucleation. The electrodeposited PdNPs were characterized by X-ray photoelectron spectroscopy and Field emmisision scanning electron microscopy. The results obtained suggested the presence of chemisorbed oxygen on the surface of PdNPs. The influence of time of deposition on the size and monodispersity of the deposited PdNPs was investigated. The studies revealed that, the size of PdNPs

increased with increase in the time of deposition. The effective catalytic surface area for the PdNPs/Pt was found to be 0.197 cm^2. The synthesized Pd nanoparticles modified Pt electrode displayed significantly different voltammetric behavior compared to bare Pt electrode and also showed high catalytic activity towards the electrooxidation of formic acid and methanol.

At polyaniline modified electrode, two systems were studied. Initially Influence of ionic speciation on electrocatalytic performance of polyaniline coated platinum electrode for Fe(III)/Fe(II) redox reaction was studied. Porous-polyaniline coated Pt electrode (PANI/Pt) was electro-synthesized potentiodynamically. Nature of predominant Fe-species in HCl and H_2SO_4 was checked by UV–vis spectrophotometry. Electrocatalysis of Fe(III)/Fe(II) reaction was studied by cyclic voltammetry (CV) and electrochemical impedance spectroscopy (EIS) for three different solution compositions viz. (i) $FeCl_3/FeCl_2$ in 1M HCl, (ii) $FeCl_3/FeCl_2$ in 0.5M H_2SO_4 and (iii) $Fe_2(SO_4)_3/FeSO_4$ in 0.5M H_2SO_4. The Donnan interaction of the polyaniline modified electrode for the three compositions was investigated with respect to $[Fe(CN)_6]^{3-}/H_2[Fe(CN)_6]^{2-}$ which are believed to be the predominant species present in $K_3[Fe(CN)_6]/K_4[Fe(CN)_6]$ solution in 0.5M H_2SO_4. The electrocatalytic performance of PANI/Pt for Fe(III)/Fe(II) redox reaction was found superior in HCl compared to that in H_2SO_4. Further, a mechanistic study on the electrocatalysis of the Pu(IV)/Pu(III) redox reaction at a platinum electrode modified with polyaniline (PANI) was carried out. In this, electrochemistry of Pu(IV)/Pu(III) couple in 1 M H_2SO_4 was studied on bare and modified platinum electrode by cyclic voltammetry and electrochemical impedance spectroscopy. The platinum electrode was modified with polyaniline. The modified electrode was characterized by scanning electron microscopy and energy dispersive X-ray fluorescence. Electrocatalysis of

Pu(IV)/Pu(III) redox reaction was observed on PANI-Pt. Pu(IV)/Pu(III) couple showed quasi-reversible electron transfer behavior on bare platinum electrode because of the PtO layer formation by Pu(IV) solution at the electrode-electrolyte interface. Electrocatalysis of Pu(IV)/Pu(III) couple on PANI-Pt was attributed to the cumulative effect of the Donnan interaction between PANI and Pu(IV) anionic complex, specific adsorption of Pu(IV) on the reactive centres, low charge transfer resistance across the electrode-electrolyte interface and a catalytic chemical reaction coupled with the electron transfer reaction. In Chapter 5, electrocatalytic performance of SWCNT modified electrode was explained. Three redox couples were studied at SWCNT modified electrode. Firstly, mechanistic study on the electrocatalysis of Pu(IV)/Pu(III) redox reaction at platinum electrode modified with single-walled Carbon nanotubes (SWCNTs) was carried out. Electrocatalysis of Pu(IV)/Pu(III) redox reaction was observed on SWCNT-Pt. Pu(IV)/Pu(III) couple showed quasi-reversible electron transfer behavior on bare platinum electrode because of the PtO layer formation by Pu(IV) solution at the electrode-electrolyte interface. In SWCNT-Pt, the direct interaction between Pu(IV) and platinum was blocked by SWCNTs and it diminished the oxide layer formation at the interface. The lower charge transfer resistance at SWCNT-Pt also promoted the rate of electron transfer reaction of Pu(IV)/Pu(III) couple. Electrochemical studies of U(VI)/U(IV) redox reaction in 1 M H_2SO_4 at single-walled carbon nanotubes (SWCNTs) modified gold (Au) electrode are also discussed in this chapter. A detailed investigation was done to determine the kinetic parameters at the modified electrode. It was found that the electrocatalysis of U(VI)/U(IV) couple on SWCNT-Au is driven by an increase in the rate constant of the electron transfer reaction compared to that with the bare gold electrode. Electrochemical impedance spectroscopy data confirmed the electrocatalytic activity

of SWCNT-Au electrode. After a detailed study on electrocatalytic mechanism of U(VI)/U(IV) couple and Pu(IV)/Pu(III) redox couple, studies were carried out to simultaneously determine Pu and U at SWCNT-Au electrode in the fuel samples. In the differential pulse voltammetry technique (DPV), both Pu and U gave sensitive reduction peaks at 564 mV and -128 mV, respectively, versus saturated Ag/AgCl electrode. Under the optimized experimental conditions, Pu and U gave linear responses over ranges of 10 to 100 μM (R^2 = 0.990) and 3 to 10 μM (R^2 = 0.987), respectively. The detection limits were found to be 8.2 μM for Pu and 2.4 μM for U.

This Chapter also explains the electrochemical investigations on Np(VI)/Np(V) redox couple using single walled carbon nanotube modified glassy carbon electrode (SWCNT-GC). The peak-to-peak potential separation (ΔE_p) was found to be 133 mV, which is much smaller than the ΔE_p value of 338 mV observed on bare glassy carbon electrode. It indicates that the Np(VI)/Np(V) couple still exhibits a quasi-reversible electron transfer behavior on SWCNT-GC. The increase of the redox peak current along with the significant enhancement in the electrochemical reversibility suggest the electrocatalytic action of SWCNT-GC for the Np(VI)/Np(V) redox reaction. The charge transfer coefficient (α) and the heterogeneous rate constant (k_s) of Np(VI) reduction on SWCNT-GC in 1 M H_2SO_4 were calculated as 0.83 and 5.25×10^{-1}cm s^{-1}, respectively. This shows that the modification of glassy carbon surface with SWCNT catalyzed the Np(VI)/Np(V) redox reaction. Indeed, the SWCNT/GC electrode presents an interlinked highly mesoporous three-dimensional structure with a relatively higher electrochemically accessible surface area and easier charge transfer at the electrode/electrolyte interface. Therefore, the quasi-reversible redox reaction of Np(VI)/Np(V) couple on GC transformed to a more reversible redox reaction on SWCNT-GC. The impedance data on charge transfer resistance (R_{ct}) i.e. $R_{ct}^{SWCNT-GC}$

$< R_{ct}^{GC}$ supported the trends of the heterogeneous rate constants calculated from the cyclic voltammetry experiments i.e. $k_s^{SWCNT-GC} > k_s^{GC}$. This confirms the electrocatalytic behavior of SWCNT-GC for the Np(VI)/Np(V) redox reaction.

Future scope

(1) Theoretical measurements to understand the electrocatalytic behaviour of carbon nanotubes

(2) Comapring the electrocatalytic performance of graphene and carbon nanotubes for actinides.

(3) Exploring carbon nanotubes from different origin to study actinides.